SISSA ISAS
SCUOLA INTERNAZIONALE SUPERIORE DI STUDI AVANZATI
INTERNATIONAL SCHOOL FOR ADVANCED STUDIES

Theoretical study of the structural, thermodynamic, and electronic properties of a quaternary semiconductor alloy: (Zn,Mg)(S,Se)

Thesis submitted for the degree of

"Doctor Philosophiæ"

CANDIDATE

Antonino Marco Saitta

SUPERVISORS

Dr. Stefano de Gironcoli

Prof. Stefano Baroni

October 1997

Table of Contents

1 Introduction

The purpose of this thesis is the theoretical study of the structural, thermodynamic and electronic properties of a II-VI substitutional semiconductor quaternary alloy.

Since when the first electronic devices, such as the diode and the transistor, were constructed in the 50's, semiconductor materials have attracted a wide experimental and theoretical interest, because of their enormous industrial importance. As a consequence, the semiconductor technology has made huge progresses, and much of the effort in the past few years has been devoted to the realization of electronic and opto-electronic devices which require the design of materials with *ad hoc* structural and optical properties. The range of realizable material properties can be greatly enlarged using not only pure materials, but also alloys and superlattices of these compounds, due to the possibility of modulating the lattice parameter and the fundamental band gap by acting on the alloy or superlattice compositions.

Modern opto-electronics is able to produce and commercialize, at low cost, very efficient laser diodes (LD) and light-emitting diodes (LED) based on solid IV and III-V semiconductors and operating in the low visible-light range (up to $2.0 - 2.2\ eV$). In the last decade the main effort of semiconductor technology has been focused on the feasibility of optical devices operating at shorter wavelength ($\lambda < 580\ nm$). The purpose of such research is to achieve LD's and LED's encompassing the entire visible-light window and, in perspective,

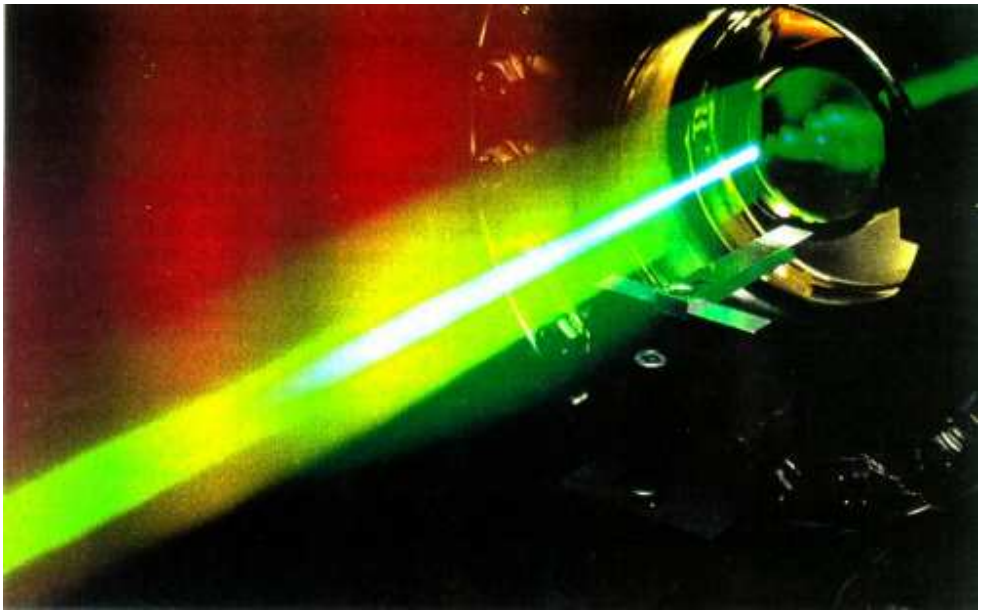

Figure 1.1 (color): Green laser device developed at the Trieste TASC-INFM Labs and based on a ZnCdSe alloy.

the industrial-scale production of high-density storage optical disks and light sources for full-color displays.

At the present day, blue-green devices research has been carried out on three main guidelines: *i)* the very promising GaN-based technology, which still has to face the lack of appropriate substrates for the molecular-beam epitaxial (MBE) growth, and the equilibrium structural properties of nitrides; *ii)* the research on SiC and related materials, that are however affected by an intrinsic inefficiency due to their indirect-gap nature; *iii)* the II-VI technology.

It is well known that II-VI semiconductors have large optical gaps, but only recently the feasibility of green-blue opto-electronic devices based on these materials has been demonstrated. An experimental group actively operating in this research field is the Trieste TASC-INFM group. In Fig. 1.1 a picture of a green laser realized in the TASC-INFM Labs is displayed [1]. The theoretical work presented in this thesis has been done in collaboration with this group [2]. A difficult problem that heavily limits the use of II-VI compounds arises

from their largely varying lattice parameters. It is in fact quite difficult to grow them on typical substrates, such as GaAs, without introducing crystal defects at the interface due to the large lattice-mismatch. Threading dislocations are especially harmful defects because propagate along the growth direction [3, 4] and are able to seriously damage II-VI devices, such as light-emitting diodes (LED) and lasers, dramatically shortening their operating life-time, or even breaking the samples [5].

A possible way to cope with this problem relies on considering quaternary solid solutions $A_xB_{1-x}C_yD_{1-y}$ with chemical disorder both on the cationic (A, B) and the anionic (C, D) sublattices. In this way it is possible, in principle, to optimize the lattice parameter, a_0, and the fundamental band-gap, E_g, of the alloy *independently*, by tuning the *two* cationic and anionic compositions x and y. However, for the large majority of II-VI and III-V alloys this additional "degree of freedom" is almost completely useless, because for these materials E_g and a_0 are related by a rough law of inverse proportionality (compounds with larger a_0 have usually smaller E_g and *vice versa*), and this behavior actually precludes the possibility of obtaining solid solutions with really independent values of those physical quantities, that are the most relevant from the applicative and technological point of view (see Fig. 1.2). For example, in $Zn_xCd_{1-x}S_ySe_{1-y}$, the band-gap is almost constant ($\Delta E_g \approx 0.2\ eV$) along the lattice-matching line [6].

The quaternary $Zn_xMg_{1-x}S_ySe_{1-y}$ solid solutions play a special role in this context for in this system the lattice parameter and the fundamental band-gap are almost independent functions of the concentrations. This feature is due to the unusual properties of $Mg-VI$ compounds that have both larger a_0 and larger E_g than the corresponding Zn chalcogenides. Such alloy has been proposed a few years ago [7], and widely studied [1–13] since then.

In the alloy the lattice parameter grows going from ZnS towards MgSe, while the fundamental band gap grows along the other diagonal (roughly lattice-matched to GaAs) of the

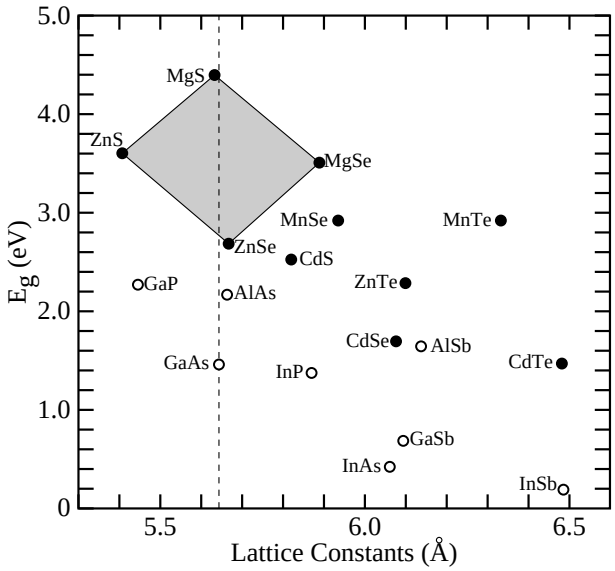

Figure 1.2: Bandgap (eV) vs. lattice parameter (Å) for cubic II-VI wide bandgap semiconductors (full dots). The connection by the solid lines indicates the presently studied alloy. Selected choice for III-V buffer layers and substrates are indicated with empty dots. The dashed line corresponds to the lattice matching to GaAs.

quadrangle of compositions, from ZnSe ($E_g = 2.8\ eV$) to MgS, whose estimated gap is about 4.5 eV. The value of the band gap varies of about 1.7 eV along the line of lattice-matching to GaAs, and this peculiarity is very promising from the technological point of view.

The large difference among the lattice parameters of the pure materials that constitute $(Zn, Mg)(S, Se)$ solid solutions is however a source of problems, since it induces local clusterizations that—while reducing the stress of the system—also reduce the randomness and the homogeneity of the alloy. Moreover, the possible existence of miscibility gaps [9] may hinder the growth of a homogeneous solution.

To better control material quality, the growth of short-period superlattices (SL) of the ternary $Zn_xMg_{1-x}Se$ and ZnS_xSe_{1-x} alloys [3] or of the pure constituents [4], rather than the random quaternary alloy, has been recently suggested. In particular, the latter technique seems to have two advantages. First of all, by growing layers of pure materials (in the

sequence MgSe/ZnSe/ZnS/ZnSe) the composition of any single layer is better controlled and it is not necessary to solve the difficult experimental problem of determining the exact concentration of the alloy. More importantly, the alternation of layers subject to tensile stress (ZnS) and layers subject to compressive stress (MgSe) at the lattice parameter of the GaAs substrate generate strong strain fields that block threading dislocations thus avoiding the propagation of defects in the growth direction. The defect density decreases by one order of magnitude and, as a consequence, a better color purity and much longer operating life-times of the resulting optical devices—thus extended to a few or even tens of hours [4, 11]—are obtained.

Another problem that $Zn_xMg_{1-x}S_ySe_{1-y}$ technology has to deal with, concerns the stability in the Mg-rich region: Mg chalcogenides are not stable in the zincblende (ZB) phase, being both the wurtzite and, even more, the rocksalt structures energetically favored [7]. For this reason huge experimental uncertainties are present in the Mg-rich phase-diagram of the alloy where the properties of zincblende polytypes are poorly known. Up to now, the most relevant region of compositions, from the technological point of view, has been the Zn-rich region, and in particular the region close to ZnSe, where the system is stable and more easily controlled. Also in that region, however, the alloy shows a tendency to generate stacking faults, that are extended planar defects due to a deviation of the atomic stacking sequence along the [111] direction from the zincblende (ABCABCA...) to the wurtzite (ABABABA...) sequence [14, 15].

In spite of the large experimental effort devoted to this system, many difficulties arise in obtaining even the most basic information about the properties of this quaternary alloy. As shown in Ref. [7], the knowledge of the exact concentrations cannot be easily determined and the dependence of the lattice parameter and of the fundamental band gap upon them is poorly known. Furthermore, the typical MBE growth processes occur far from thermo-

dynamic equilibrium and in such processes kinetics effects may play a very important role. As a consequence, equilibrium properties are hardly accessible and the relevant information on miscibility gaps and thermodynamic stability are almost completely lacking [9].

In this thesis the equilibrium properties of the (Zn,Mg)(S,Se) alloy are studied using state-of-the-art first-principles techniques based on Density-Functional Theory (DFT). Our goal is to determine its thermodynamic stability with respect to the segregation in its constituents and/or in possible ordered structures or superlattices; this understanding is preliminary to any further investigation and provides the physical limits to the tunability of the alloy properties.

First-principles methods are widely and successfully used to determine the equilibrium properties of materials. The method is completely unbiased by external inputs, and the accuracy of the results is very satisfactory when compared to experiments. Numerical studies are thus predictive and particularly useful when experiments are lacking or do not allow to extract the desired physical information. At the present day, the class of physical systems that can be studied with reasonable computational effort is limited to relatively simple systems that can be described with periodically repeated large unit cells (supercells) containing a number of inequivalent atoms ranging from a few tens up to a couple of hundreds. The description of disorder would require the use of quite larger supercells, thus becoming computationally too demanding. In the present work, the effects of disorder are dealt with by a perturbative approach known as *computational alchemy*, which allows to map efficiently the energetics of the alloy onto a lattice-gas model and to simulate its finite-temperature properties by standard MonteCarlo (MC) sampling.

In Chapter 2 we will present the theoretical framework of this thesis. The Density Functional Theory [16, 17] will be shortly described, along with its simplest and most popular formulation, the Local Density Approximation (LDA), and its implementation in

a Plane-Wave Pseudopotential (PW-PP) scheme [18]. We will then introduce the Density-Functional Perturbation Theory (DFPT) [19], and the DFPT-based *computational alchemy* approach to the study of alloys. In Chapter 3 we will present the results on the structural, vibrational and electronic properties of the four pure compounds involved in the quaternary alloy: ZnS, ZnSe, MgS and MgSe. The accuracy of our perturbative expansion will be checked in Chapter 4, that is devoted to the structural and thermodynamic properties of the 4 pseudobinary alloys, $Zn_xMg_{1-x}S$, $Zn_xMg_{1-x}Se$, ZnS_xSe_{1-x} and MgS_xSe_{1-x}, and of the quaternary $Zn_xMg_{1-x}S_ySe_{1-y}$ alloy. We pay a special attention to the determination and the characterization of short-range order (SRO). In Chapter 5 we study the optical properties of the system. Short-range order effects are taken into account through a generalization of the Special Quasirandom Structures (SQS) [20] approach to the study of the electronic properties of alloys, which allows a rather precise account of the effects of disorder beyond the commonly adopted virtual-crystal approximation. Chapter 6 is finally devoted to the conclusions and the future developments of this work.

2 Theoretical tools

A random alloy in which the atomic positions determine a crystal lattice is called *substitutional*. This case is the most common for semiconductor solutions, whose coordination is usually tetrahedral and whose underlying lattice is usually the zincblende structure. For such systems any configuration is simply and fully identified by the distribution of the atoms on the crystal sites, and the disordered alloy problem may be mapped onto standard lattice-gas models.

In order to use the statistical mechanics techniques to obtain the desired *macroscopic* properties, in principle, the knowledge of all the *microscopic* states of the system of interest is necessary. Such microstates are identified by the possible different configurations of the atoms in the crystal lattice, and by the possible different equilibrium crystal structures for different values of the concentration(s), of the temperature and of pressure.

Given a microscopic configuration $\mathcal{C}$, the equilibrium properties of the system are given by:

$$\langle \mathcal{O} \rangle = \sum_{\mathcal{C}} \mathcal{O}(\mathcal{C}) P(\mathcal{C}), \tag{2.1}$$

where $\mathcal{O}(\mathcal{C})$ is the value of a macroscopic physical observable for that configuration, and $P(\mathcal{C})$ is the probability that such configuration occur. The statistical problem is thus twofold: *i)* to evaluate $\mathcal{O}(\mathcal{C})$; *ii)* to find the relevant configuration probability distribution $P(\mathcal{C})$. At thermal equilibrium such probability is proportional to a Boltzmann factor, and

Eq. 2.1 reads:

$$\langle \mathcal{O} \rangle = \frac{\sum_{\mathcal{C}} \mathcal{O}(\mathcal{C}) e^{-\beta E(\mathcal{C})}}{\sum_{\mathcal{C}} e^{-\beta E(\mathcal{C})}}, \tag{2.2}$$

where $E(\mathcal{C})$ the energy associated to such a configuration, and $\beta = (k_B T)^{-1}$, where T is the temperature and k_B is the Boltzmann constant. The problem of the statistical average is so reduced to the calculation of the energy $E(\mathcal{C})$ that is directly related to the occurrence probability of any microscopic configuration $\mathcal{C}$, if the system is in thermodynamic equilibrium.

The statistical problem can be dealt with by using MonteCarlo lattice simulations or other statistical mechanics techniques, such as the cluster variation method [21]. The calculations of the interaction constants, that enter the definition of the lattice-gas models, are performed in an *ab initio* scheme, and are developed in the framework of Density Functional Theory.

2.1 Density Functional Theory

Alloys, as well as ordered crystals, are systems of interacting ions and electrons whose properties could be in principle determined by solving a many-body Schrödinger equation. This task is impossible in practice and one has to resort to a number of approximations. The Born-Oppenheimer approximation allows to decouple the "fast" electronic variables from the "slow" ionic ones, by virtue of the large difference of masses. The system is thus divided in two subsystems (electrons and ions): the electrons move in the potential of the fixed nuclei, following adiabatically their slow motion and remaining always close to the quantum-mechanical ground state, while the ions are usually treated as classical particles in the effective potential determined by the electronic ground state.

Even in the Born-Oppenheimer approximation scheme, the electron-electron interaction is very difficult to deal with; DFT provides the appropriate mathematical framework for

determining self-consistently the ground state of the whole system that is the only required knowledge for the study of many physical properties.

Density-Functional Theory was developed in the mid 60's on the basis of the Hohenberg-Kohn theorem [16], which states that the external potential acting on the subsystem of the electrons is a unique functional of the electronic ground-state density $n(\mathbf{r})$. The energy of the electrons can be written as

$$E[n(\mathbf{r})] = F[n(\mathbf{r})] + \int V(\mathbf{r})n(\mathbf{r})d\mathbf{r}, \tag{2.3}$$

where $F[n]$ is a universal functional of the electronic density (*i.e.* it is independent of the external potential), and $V(\mathbf{r})$ is the "external" potential acting on the electrons and generated by the nuclei.

In principle, the ground-state of the system can be found via the minimization of this functional with respect to the electron density, under the constraint of normalization to the number N of electrons:

$$\int n(\mathbf{r})d\mathbf{r} = N. \tag{2.4}$$

The functional $F[n(\mathbf{r})]$ is not known explicitly. In order to apply this theory to actual calculations, Kohn and Sham proposed [17] to separate the functional $F[n]$ into three distinct contributes:

$$F[n(\mathbf{r})] = T_0[n(\mathbf{r})] + \frac{1}{2}\int \frac{n(\mathbf{r})n(\mathbf{r}')}{|\mathbf{r}-\mathbf{r}'|}d\mathbf{r}d\mathbf{r}' + E_{xc}[n(\mathbf{r})], \tag{2.5}$$

where $T_0[n(\mathbf{r})]$ is the kinetic energy of a system of noninteracting electrons whose ground state density is $n(\mathbf{r})$, the second term is their classical (Hartree) electrostatic energy. Eq. 2.5 is actually a definition of $E_{xc}[n(\mathbf{r})]$—known as the exchange and correlation energy functional—where all the complexity of the many-body interactions—as well as our ignorance—is hidden.

As shown in Ref. [17], the problem of constrained minimization may be reformulated into a set of *non-interacting* single particle equations to be solved with iterative self-consistent

procedures:

$$\underbrace{\left[-\frac{\nabla^2}{2}+V_{SCF}(\mathbf{r})\right]}_{H_{KS}}\psi_i(\mathbf{r})=\epsilon_i\psi_i(\mathbf{r}), \tag{2.6}$$

$$n(\mathbf{r})=\sum_i |\psi_i(\mathbf{r})|^2\,\theta(\epsilon_i-\epsilon_F). \tag{2.7}$$

$$V_{SCF}(\mathbf{r})=V(\mathbf{r})+\int\frac{n(\mathbf{r}')}{|\mathbf{r}-\mathbf{r}'|}d\mathbf{r}'+v_{xc}[n(\mathbf{r})], \tag{2.8}$$

These are the well known Kohn-Sham (KS) equations, where the Fermi energy, ϵ_F, is defined by the constraint on the number of electrons, the θ step function reflects the fact that N lowest energy eigenstates are occupied. The term $v_{xc}(\mathbf{r})=\delta E_{xc}[n]/\delta n(\mathbf{r})$ is the exchange-correlation potential and the single particle orbitals satisfy the orthonormality constraint $\int\psi_i^*(\mathbf{r})\psi_j(\mathbf{r})d\mathbf{r}=\delta_{ij}$.

In order to make use of this scheme in practice, it is necessary to have at one's disposal an approximation to the unknown exchange and correlation potential. The simplest such approximation is the local density approximation (LDA), in which the exchange-correlation energy of the system is assumed to have the form:

$$E_{xc}[n(\mathbf{r})]=\int n(\mathbf{r})\epsilon_{xc}(n(\mathbf{r}))d\mathbf{r}, \tag{2.9}$$

where $\epsilon_{xc}(n)$ is the exchange-correlation energy of a homogeneous electron gas at the same density. The corresponding potential is given by:

$$v_{xc}(\mathbf{r})=\frac{d}{dn}(n\epsilon_{xc}(n))\Big|_{n=n(\mathbf{r})}\equiv\mu_{xc}(n(\mathbf{r})). \tag{2.10}$$

In this approximation, the ground state energy of the system reads:

$$\begin{aligned}E^{tot} &= -\frac{1}{2}\sum_i\theta(\epsilon_i-\epsilon_F)\int\psi_i^*(\mathbf{r})\nabla^2\psi_i(\mathbf{r})d\mathbf{r}+\int V(\mathbf{r})n(\mathbf{r})d\mathbf{r}\\ &+ \frac{1}{2}\int\frac{n(\mathbf{r})n(\mathbf{r}')}{|\mathbf{r}-\mathbf{r}'|}d\mathbf{r}d\mathbf{r}'+\int n(\mathbf{r})\epsilon_{xc}(n(\mathbf{r}))d\mathbf{r}\\ &+ {\sum_{\mathbf{R},s,s'}}'\frac{Z_sZ_s'}{|\mathbf{R}+\tau_s-\tau_{s'}|}\,.\end{aligned} \tag{2.11}$$

By construction, the LDA is exact in the limit of slowly varying electron density, but it works surprisingly well for a large variety of systems [18, 22]. It is however known that the LDA tends to fail in the description of weak atomic bonds. In the last decade, many generalizations of the LDA have been proposed [23, 24], in which the functional F depends not only on the electronic density, but also on its gradient, and, more generally, on higher derivatives. For this reason they are commonly known as generalized gradient approximations (GGA).

DFT is nowadays the most popular and successful framework for the computational description of structural and vibrational properties of materials. It is strictly speaking a ground-state theory that cannot be used for the study of excited-states properties such as electronic band-structure and optical gaps. However, it is known that DFT-LDA is able to give qualitatively good results also for these properties, for example describing very well the band-structure shape of most semiconductors.

2.2 The plane-wave pseudopotential method

In a solid, the KS equations are more easily dealt with in reciprocal space, where the differential eigenvalue problem is mapped onto an algebraic linear system. In the study of infinite solids it is necessary to exploit the crystal symmetry in order to circumvent the problem of the infinite number of electronic degrees of freedom and, as a consequence, of infinite linear equations. The Bloch theorem states that in a periodic crystal the electronic wavefunctions are given by the product of a function having the same periodicity times a phase factor. This property allows to map the problem onto a single cell, repeated in space through the so-called periodic boundary conditions (PBC), having a small number of atoms and thus, of electrons. The solution of this problem would require the knowledge of the electronic wavefunctions in the infinite number of reciprocal-space points of the Brillouin

zone (BZ). A very good approximation that overcomes this difficulty consists in the choice of small sets of "special points" [25] that are taken as representative of the entire zone.

In order to solve numerically the KS equations the wavefunctions are expanded on a basis set. A standard choice is that of expanding on plane waves (PW), which have the great advantage of being translationally invariant:

$$\psi_i(\mathbf{r}) = \psi_{n,\mathbf{k}}(\mathbf{r}) = \sum_{\mathbf{G}} e^{i(\mathbf{k}+\mathbf{G})\mathbf{r}} c_n(\mathbf{k}+\mathbf{G}), \tag{2.12}$$

where $\mathbf{k}$ belongs to the first Brillouin zone of the crystal, $\mathbf{G}$ is a reciprocal lattice vector and n is the band index. The solution of the secular equations is obtained through a diagonalization of the Hamiltonian. This is a natural choice for periodic solids: plane waves are in fact the exact solutions for zero potential. Furthermore, PW are a complete set of orthonormalized wavefunctions, the matrix elements of the Hamiltonian can be rather easily evaluated, and the convergence can be systematically improved by controlling one single parameter. The PW basis set is in fact infinite and it is usually truncated by choosing a kinetic energy cutoff, and including in the basis set the PW satisfying the condition:

$$|\mathbf{k}+\mathbf{G}|^2 \leq E_{cut}. \tag{2.13}$$

To treat explicitly all the electrons it would be necessary to include a very large number of PW in order to describe accurately their behavior near the nucleus. Lowest-energy wavefunctions are in fact strongly peaked; higher-levels functions rapidly oscillate for the constraint of orthogonalization. This would require a very heavy computational effort for the calculation. It is possible to avoid this problem by freezing the core electrons in the atomic configuration around the ions, and considering only the valence electrons.

Smooth angular-momentum-dependent *pseudopotentials* are introduced in order to describe the interactions between valence electrons and the *pseudoions* (ions+ core electrons). The valence-electron wavefunctions do not need to be orthogonalized to the core-electrons

wavefunctions, and thus they are considerably smoother near the nucleus, but they are identical to the "true" wavefunctions outside the core region. This pseudopotential *frozen-core* approximation is widely used in the study of solids, being usually the core-electrons contribution to the solid materials properties not very important, and in this case core-electrons eigenfunctions are not included in the calculations.

The norm-conserving pseudopotentials, in their original formulation [26], consist of a local contribution for the radial function and a non-local one for the angular part:

$$v_s(\mathbf{r},\mathbf{r}') = v_s^{loc}(r)\delta(\mathbf{r}-\mathbf{r}') + \sum_{l=0}^{l_{max}} v_{s,l}(r)\delta(r-r')P_l(\hat{\mathbf{r}},\hat{\mathbf{r}}'), \tag{2.14}$$

where P_l is the projector on the angular momentum l.

It is worth noting that a computationally more convenient, fully non-local, form of the pseudopotentials has been introduced by Kleinman and Bylander (KB), in which also the radial part of the potential is non-local [27, 28]:

$$v_s^{(NL)}(\mathbf{r},\mathbf{r}') = v_s^{loc}(r)\delta(\mathbf{r}-\mathbf{r}') + \sum_{l=0}^{l_{max}} v_{s,l}^{(NL)}(\mathbf{r},\mathbf{r}'), \tag{2.15}$$

where

$$v_{s,l}^{(NL)}(\mathbf{r},\mathbf{r}') = \sum_{m=-l}^{l} |f_{l,m}^s(r)\rangle \frac{1}{v_{s,l}} \langle f_{l,m}^s(r')|, \tag{2.16}$$

where $f_{l,m}^s(r) = v_{s,l}(r)R_{s,l}(r)Y_l^m(\hat{\mathbf{r}})$. This form of the potential allows a very efficient computation of its matrix elements, and the KS equations may be more easily solved.

The description of cases in which the crystal symmetry is broken, as in surfaces, quantum-confined-systems, amorphous solids and so on, needs the construction of larger cells ("supercells") that introduce a fictitious periodicity in the system. The computational cost of DFT *ab-initio* calculations grows approximately with the third power of the number of electrons. At present, systems containing up to a few tens of inequivalent atoms can be simulated on big workstations, while larger supercells with a couple of hundreds of particles are dealt with by using parallel supercomputers.

2.3 Theoretical approaches to the alloy problem

Through DFT it is possible to calculate the ground-state energy of a given microscopic configuration in a disordered system. This choice is however not of practical use: in the theoretical study of disordered alloys, one should consider several supercells containing thousands of atoms, in order to cope with disorder, and to take into account different configurations. For this reason, such "direct" approach has always been considered well beyond the reachable numerical power. The typical approaches to the study of alloys are based on approximations in which all the possible, inequivalent, microscopical configurations are averaged into an effective medium having the same crystal structure of the underlying lattice, in order to recover the translational symmetry.

The simplest of these historical approaches is the so-called virtual crystal approximation (VCA) [29], in which the real, disordered, alloy is modeled with a crystalline solid of "virtual" atoms which are given by an average, weighted by the composition, of the "real" atoms, and whose chemical properties are intermediate between the pure constituents ones. A refinement of this method is the coherent potential approximation (CPA) [30], where the potential is modified with respect to VCA only on sites, hence all the like atoms are separately considered equivalent and each is embedded in a uniform medium. CPA is also able to capture effects associated with the existence in the alloy of statistical distributions of sites. These theories are all *nonstructural* in the sense that they consider only the average occupations of lattice sites, retaining the topology, but removing all the informations associated with the geometrical arrangements of atoms around such sites.

The range of validity of such approximations is limited to those properties that are associated with symmetry-preserving, uniform volume changes, and that for typical semiconductors are simple functions of the composition, and do not depend but weakly on the local environment of atoms. These theories are therefore inadequate for the study of prop-

erties, such as the vibrational or electronic properties, that in many cases strongly depend on the substitutional disorder for which it is necessary to consider different approaches, more recently developed.

If one considers the substitutional alloy A_xB_{1-x}, it is possible to attach to each lattice site a spin-like variable σ that is equal to ± 1 if the site is occupied by an A- or B-type atom respectively. In this way, the problem is mapped onto a standard lattice-gas model and it is possible to apply the statistical mechanics methods to solve it. The internal energy of the alloy may be expanded in a series of volume-dependent multiatom interaction energies.

In the method proposed by Connolly and Williams [31, 32] for the *structural* study of disordered alloys, one considers clusters of spins whose contribution to the internal energy of the alloy is given by a geometrical part that depends on the shape of the cluster and on the number of vertices, and a configurational part given by the product of the spins that identify the cluster. The expansion of the energy $E(\{\sigma\}, V)$ is performed on clusters f consisting of k vertices and up to m neighbors. Denoting by $J_f(V)$ the simultaneous interaction energy of a figure $f = (k, m)$ and by $\Pi_f(l_f, \sigma)$ the product of the spin variables at the vertices of the figure f located at l, the expansion reads:

$$E(\{\sigma\}, V) = \sum_f \sum_{l_f} J_f(V) \Pi_f(l_f, \sigma) \tag{2.17}$$

The expansion is exact, holding a biunivocal correspondence between $E(\{\sigma\}, V)$ and $J_f(V)$. In fact, for a lattice with N sites, there are 2^N different spin configurations on the lattice, and one has 2^N interaction constants J_f. A few years ago Zunger and co-workers [33] proposed the so-called renormalized-interaction method (RIM). Eq. 2.17 may be inverted, and the multiatom interaction constants $J_f(V)$ be determined from self-consistent total-energy calculations on periodic compounds described within the local-density formalism. Approximate solution to the general Ising model, using the cluster variation method [21], underlying these effective interactions provides the excess enthalpy and hence the phase

diagram.

2.4 Density Functional Perturbation Theory

An alternative possible solution to the problem of studying disordered alloys in a first-principles scheme is given by a very efficient approach to the perturbation theory in the DFT framework, the Density Functional Perturbation Theory (DFPT) [19], that in the last decade has been very successfully applied to the study of structural [34], dielectric [35], and vibrational properties of fullerenes [36], semiconductors [37], alloys [38–42] and metals [43], as well as to describe phonon-induced structural phase transitions [44].

Once solved the problem for a given potential $V(\mathbf{r})$, let us consider a set of parameters $\boldsymbol{\lambda} \equiv \{\lambda_i\}$ and a perturbed potential $V(\mathbf{r}) + \boldsymbol{\lambda}\Delta V(\mathbf{r})$, that for $\boldsymbol{\lambda} = 0$ corresponds to the unperturbed potential of the reference system. The ground-state energy of the perturbed system is:

$$E_{\boldsymbol{\lambda}} = \int n_{\boldsymbol{\lambda}}(\mathbf{r}) V_{\boldsymbol{\lambda}}(\mathbf{r}) d\mathbf{r} + F[n_{\boldsymbol{\lambda}}]. \tag{2.18}$$

The celebrated Hellman-Feynman theorem [45] states that the generalized force associated to a perturbation is given by:

$$\frac{\partial E_{\boldsymbol{\lambda}}}{\partial \lambda_i} = \int n_{\boldsymbol{\lambda}}(\mathbf{r}) \frac{\partial V_{\boldsymbol{\lambda}}(\mathbf{r})}{\partial \lambda_i} d\mathbf{r}. \tag{2.19}$$

The energy variation $E_{\boldsymbol{\lambda}} - E_0$ due to the perturbation within a second-order error can be obtained by integration:

$$\frac{\partial E_{\boldsymbol{\lambda}}}{\partial \lambda_i} = \int \left(n_0(\mathbf{r}) \frac{\partial V_{\boldsymbol{\lambda}}(\mathbf{r})}{\partial \lambda_i}\bigg|_0 + \sum_j \lambda_j \frac{\partial n_{\boldsymbol{\lambda}}(\mathbf{r})}{\partial \lambda_j}\bigg|_0 \frac{\partial V_{\boldsymbol{\lambda}}(\mathbf{r})}{\partial \lambda_i}\bigg|_0 + \right.$$

$$\left. + n_0(\mathbf{r}) \sum_j \lambda_j \frac{\partial^2 V_{\boldsymbol{\lambda}}(\mathbf{r})}{\partial \lambda_i \partial \lambda_j}\bigg|_0 \right) d\mathbf{r} + \mathcal{O}(\boldsymbol{\lambda}^2), \tag{2.20}$$

obtaining therefore:

$$E_{\boldsymbol{\lambda}} = E_0 + \sum_i \lambda_i \int n_0(\mathbf{r}) \frac{\partial V_{\boldsymbol{\lambda}}(\mathbf{r})}{\partial \lambda_i}\bigg|_0 d\mathbf{r} +$$

$$+ \frac{1}{2}\sum_{i,j} \lambda_i \lambda_j \int \left(\frac{\partial n_{\boldsymbol{\lambda}}(\mathbf{r})}{\partial \lambda_j}\bigg|_0 \frac{\partial V_{\boldsymbol{\lambda}}(\ bfr)}{\partial \lambda_i}\bigg|_0 + n_0(\mathbf{r}) \frac{\partial^2 V_{\boldsymbol{\lambda}}(\mathbf{r})}{\partial \lambda_i \partial \lambda_j}\bigg|_0 \right) d\mathbf{r} + \mathcal{O}(\boldsymbol{\lambda}^3). \quad (2.21)$$

Eq. 2.21 shows that the linear response of the system—*i.e.* the first-order variation of the electronic density due to the perturbation—is sufficient to compute energy up to the second order. Actually, the so-called "$2n+1$" theorem [46] states that the knowledge of the linear response of the system gives access to the correct energy up to the *third* order in the strength of the perturbation.

The calculation of the first-order variation of the electronic density may be carried on by linearizing the set of equations 2.6-2.8:

$$\left[-\frac{\nabla^2}{2} + V_{SCF}(\mathbf{r}) - \epsilon_i \right] \Delta\psi_i(\mathbf{r}) = -\Big[\Delta V_{SCF}(\mathbf{r}) - \langle \psi_i | \Delta V_{SCF} | \psi_i \rangle \Big] \psi_i(\mathbf{r}), \quad (2.22)$$

$$\Delta V_{SCF}(\mathbf{r}) = \Delta V(\mathbf{r}) + \int \frac{\Delta n(\mathbf{r}')}{|\mathbf{r} - \mathbf{r}'| d\mathbf{r}'} + \frac{d\mu_{xc}(n(\mathbf{r}))}{dn} \Delta n(\mathbf{r}), \quad (2.23)$$

$$\Delta n(\mathbf{r}) = 2 \sum_i \psi_i^*(\mathbf{r}) \Delta\psi_i(\mathbf{r}) \theta(\epsilon_i - \epsilon_F), \quad (2.24)$$

that are solved with the same iterative procedure mentioned above.

This approach to the calculation of the response function of the system is very efficient and has the great advantage of being easily applicable to external perturbations of *any* periodicity. In the linear regime, in fact, the variation of the electronic density has the same wavevector $\mathbf{q}$ as the perturbing potential. The computational demand of the calculation for each value of such wavevector is thus of the same order of magnitude as the effort needed for a self-consistent calculation for the unperturbed system. This allows, in particular, to calculate the response also to long-wavelength ($\mathbf{q} \to 0$) perturbations, that are related to the macroscopic response functions of the material.

2.4.1 Lattice dynamics

Density Functional Perturbation Theory offers an efficient scheme to study the vibrational properties of a crystal in the adiabatic approximation. In the harmonic approximation the total potential energy of the ions can be expanded in a Taylor series in the atomic displacements $\mathbf{u}$ around the equilibrium positions:

$$E^{tot}[\mathbf{u}] = E_0^{tot} + \frac{1}{2} \sum_{\substack{\mathbf{R},\mathbf{R}' \\ s,s'}} \frac{\partial^2 E^{tot}}{\partial \mathbf{u}_{\mathbf{R}s} \partial \mathbf{u}_{\mathbf{R}'s'}} \mathbf{u}_{\mathbf{R}s} \mathbf{u}_{\mathbf{R}'s'} + \mathcal{O}(\mathbf{u}^3), \tag{2.25}$$

where $\mathbf{u}_{\mathbf{R}s}$ is the displacement of the s-th atom in the unit cell in $\mathbf{R}$. The classical equations of motion for the ions are:

$$M_s \ddot{u}^{\alpha}_{\mathbf{R}s}(\mathbf{R}) = - \sum_{\substack{\mathbf{R}',s' \\ \beta}} C_{\substack{\alpha\beta \\ ss'}}(\mathbf{R} - \mathbf{R}') u^{\beta}_{\mathbf{R}'s'}, \tag{2.26}$$

where α and β are the polarizations of the modes, $\ddot{u}^{\alpha}_{\mathbf{R}s}$ are the second derivatives of the ionic positions with respect to time and $C_{\substack{\alpha\beta \\ ss'}}(\mathbf{R} - \mathbf{R}') = \frac{\partial^2 E^{tot}}{\partial \mathbf{u}_{\mathbf{R}s} \partial \mathbf{u}_{\mathbf{R}'s'}}$ are the interatomic force constants which, thanks to the translational invariance of the crystal, depend just on $(\mathbf{R} - \mathbf{R}')$, rather than on $\mathbf{R}$ and $\mathbf{R}'$ separately.

The solution of Eqs. 2.26 can be written in Bloch form:

$$\mathbf{u}_{\mathbf{R}s} = \frac{1}{\sqrt{M_s}} \mathbf{u}_{\mathbf{q}s} e^{i(\mathbf{q}\cdot\mathbf{R} - \omega t)}, \tag{2.27}$$

where the wave vector $\mathbf{q}$ belongs to the BZ. Substituting in the equations of motion, we obtain the eigenvalue problem:

$$\omega^2 \mathbf{u}_{\mathbf{q}s} = \sum_{s'} \mathbf{D}_{ss'}(\mathbf{q}) \mathbf{u}_{\mathbf{q}s'} \tag{2.28}$$

where $\mathbf{D}_{ss'}(\mathbf{q})$ is called the *dynamical matrix* of the system and is simply proportional to the Fourier transform of the interatomic force constants matrix $C_{\substack{\alpha\beta \\ ss'}}$. From the diagonalization of this matrix one obtains the dispersion relations $\omega = \omega(\mathbf{q})$ of the system.

2.5 Computational alchemy

The fundamental hypothesis of the DFPT-based approach to the study of solid solutions is that the compositional disorder among chemically similar atoms can be treated perturbatively. Any configuration of the system can thus be considered as a perturbation of an ideal reference system, that is chosen to be the virtual crystal previously mentioned. As already discussed, such a system has the complete translational symmetry of its crystal lattice, and can therefore be studied easily with the present *ab-initio* numerical methods.

Let us consider first the simpler case in which lattice relaxations due to the different atomic sizes may be neglected. Any microscopic configuration in a substitutional binary alloy A_xB_{1-x} is completely specified by a set of Ising-like variables $\sigma_{\mathbf{R}s}$ that are equal to ± 1 when the s-th particle, in the unit cell identified by the lattice vector $\mathbf{R}$, is an A- or B-type atom respectively. In the calculation, we can think of σ as the variable that describes the transformation of a virtual atom ($\sigma = 0$) into a real one ($\sigma = \pm 1$).

In a pseudopotential scheme only the valence-shell electrons, that are the relevant ones for the chemical bonding, are explicitly included in the calculation and atoms belonging to the same group, that have similar chemical properties, are usually well described by similar pseudopotentials. A perturbative approach is therefore likely to be justified.

In the generic binary alloy A_xB_{1-x} the external potential acting on the electrons is:

$$V_{ext}(\mathbf{r}) = \sum_{\mathbf{R}s} \left(\frac{1+\sigma_{\mathbf{R}s}}{2} v_A^s(\mathbf{r}-\mathbf{R}) + \frac{1-\sigma_{\mathbf{R}s}}{2} v_B^s(\mathbf{r}-\mathbf{R}) \right), \tag{2.29}$$

where $v_A^s(\mathbf{r}-\mathbf{R})$ and $v_B^s(\mathbf{r}-\mathbf{R})$ are the pseudopotentials of $A-$ and $B-$type atoms, $\mathbf{R}$ is the Bravais lattice vector and s runs over the particles in the elementary cell. This expression

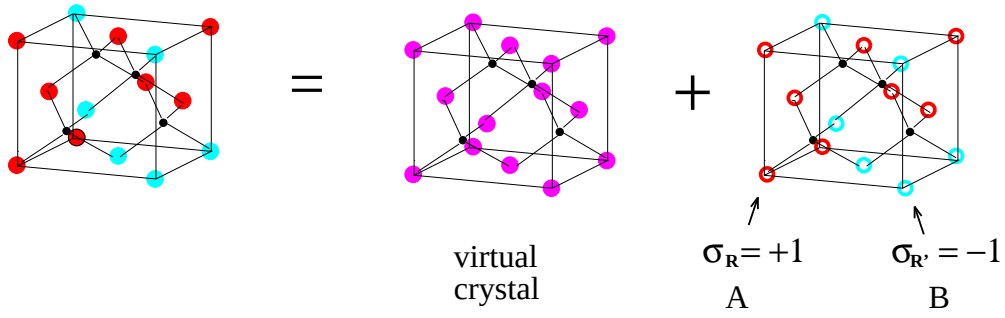

Figure 2.1 (color): Decomposition of a given disordered configuration in a superposition of an ideal system and a compositional perturbation.

can be recast as:

$$V_{ext}(\mathbf{r},\{\sigma_{\mathbf{R}s}\}) = \underbrace{\sum_{\mathbf{R}s}\frac{1}{2}\Big(v_A^s(\mathbf{r}-\mathbf{R})+v_B^s(\mathbf{r}-\mathbf{R})\Big)}_{V_0(\mathbf{r})}+ \\ + \underbrace{\sum_{\mathbf{R}s}\sigma_{\mathbf{R}s}\frac{1}{2}\Big(v_A^s(\mathbf{r}-\mathbf{R})-v_B^s(\mathbf{r}-\mathbf{R})\Big)}_{\Delta V(\mathbf{r},\{\sigma_{\mathbf{R}s}\})\equiv\sum_{\mathbf{R}s}\sigma_{\mathbf{R}s}\Delta v_\sigma^s(\mathbf{r}-\mathbf{R})}, \tag{2.30}$$

where the potential acting on electrons is given by the superposition of *i)* a reference system, the so-called *virtual crystal* — that have the same periodicity of the pure material and does *not* depend on the particular distribution of the atoms on the lattice — and *ii)* a configuration dependent part in which $\Delta v_\sigma^s(\mathbf{r}-\mathbf{R})$ describes the chemical difference between A and B atoms and corresponds to a perturbation that transforms the virtual atom into an A or B atom, according to the sign of $\sigma_{\mathbf{R}s}$ (see Fig. 2.1).

The energy of any configuration can then be expanded in the configurational variables

in a similar way as Ref. [33]:

$$E(\mathcal{C}) = E(\{\sigma_{\mathbf{R}s}\}) = J^{(0)} + \sum_{\mathbf{R}}\sum_{s} J_s^{(1)}(\mathbf{R})\sigma_{\mathbf{R}s} + \frac{1}{2!}\sum_{\substack{\mathbf{R},\mathbf{R}'\\ s,s'}} J_{ss'}^{(2)}(\mathbf{R}-\mathbf{R}')\sigma_{\mathbf{R}s}\sigma_{\mathbf{R}'s'} + \\ + \frac{1}{3!}\sum_{\substack{\mathbf{R},\mathbf{R}',\mathbf{R}''\\ s,s',s''}} J_{s,s',s''}^{(3)}(\mathbf{R}-\mathbf{R}',\mathbf{R}'-\mathbf{R}'',\mathbf{R}''-\mathbf{R})\sigma_{\mathbf{R}s}\sigma_{\mathbf{R}'s'}\sigma_{\mathbf{R}''s''} + \ldots \qquad (2.31)$$

where $J^{(n)}$ are the n-th order derivatives of the virtual crystal energy with respect to the alchemical perturbations. It is worth noting that such interaction constants are not the same J_f of the cluster expansion approach [31–33]: the second order of perturbation corresponds to two-body interactions, while two-body interactions include higher perturbative orders [47].

If the chemical difference between the A and B atoms is sufficiently small to be treated perturbatively, this expansion can be truncated to a certain order of interactions and/or to a certain distance. DFPT offers an efficient framework for the computation of two-body and infinite-range interaction constants, and can be applied to this problem in a very natural way: one can describe the reference system by DFT plane-wave total-energy techniques, with the same computational effort as needed for the calculation of any bulk material, and treat the second term along the lines expounded in Section 2.4.

The ground state electronic density of the given configuration can be expressed as:

$$n(\mathbf{r},\{\sigma_{\mathbf{R}s}\}) = n_0(\mathbf{r}) + \sum_{\mathbf{R}s}\sigma_{\mathbf{R}s}\Delta n_\sigma^s(\mathbf{r}-\mathbf{R}) + \mathcal{O}(\sigma^2), \qquad (2.32)$$

where $n_0(\mathbf{r})$ is the virtual crystal density, that also has the bulk periodicity, and $\Delta n_\sigma^s(\mathbf{r}-\mathbf{R})$ is the linear density-response to the alchemical perturbation $\Delta v_\sigma^s(\mathbf{r}-\mathbf{R})$. The expression of the total energy of the system (Eq. 2.31) is given, up to the second order in the perturbation strength, by:

$$E(\{\sigma_{\mathbf{R}s}\}) = E_0 + \sum_s K_s\sum_{\mathbf{R}}\sigma_{\mathbf{R}s} + \frac{1}{2}\sum_{\substack{\mathbf{R},\mathbf{R}'\\ s,s'}} J_{ss'}(\mathbf{R}-\mathbf{R}')\sigma_{\mathbf{R}s}\sigma_{\mathbf{R}'s'} + \mathcal{O}(\sigma^3), \qquad (2.33)$$

where E_0 is the total energy of the virtual crystal, while the first and second derivatives (see Section 2.4) are given by:

$$K_s = \int \Delta v_\sigma^s(\mathbf{r} - \mathbf{R}) n_0(\mathbf{r}) d\mathbf{r} + \frac{\partial E_{ion}}{\partial \sigma_{\mathbf{0}s}}, \tag{2.34}$$

$$J_{ss'}(\mathbf{R} - \mathbf{R}') = \int \Delta v_\sigma^s(\mathbf{r} - \mathbf{R}) \Delta n^{s'}(\mathbf{r} - \mathbf{R}') d\mathbf{r} + \frac{\partial^2 E_{ion}}{\partial \sigma_{\mathbf{R}s} \partial \sigma_{\mathbf{R}'s'}}. \tag{2.35}$$

Eqs. 2.33-2.35 show that the energy expansion up to the pair interactions depends just on the pseudopotential difference between the atoms that form the alloy and on the linear variation of the electronic density. As previously mentioned, it is actually possible to determine the energy up to the third order in the perturbation strength [46].

It is important to underline that, at variance with the RIM approach [33], where only short-range terms are taken into account, in the present approach the only approximation is given by the order of perturbation at which the expansion is truncated. The accuracy of this method, as well as the validity of the fundamental hypothesis of chemical similarity, will be shown in the next chapters of the thesis.

The condition of lattice-matching, considered up to now, is very well satisfied in some $III - V$ semiconductor alloys such as $Ga_xAl_{1-x}As$. In the general case, however, the system at equilibrium does not have the ideal geometry of the lattice, but is locally distorted from the ideal positions, in order to account for the different bond lengths of its constituents.

DFPT allows one to deal with atomic relaxation on the same footing, by including in the energy expansion of Eq. 2.31 terms which depend on the displacements $\{\mathbf{u}_{\mathbf{R}s}\}$ from the equilibrium position of the virtual crystal; it is worth noting that $\mathbf{u}_{\mathbf{R}s}$ are to leading order linear in ΔV. Taking into account all terms up to second order in the perturbation, the

new expression reads:

$$E(\{\sigma_{\mathbf{R}s}\},\{\mathbf{u}_{\mathbf{R}s}\}) = E_0 + \sum_s K_s \sum_{\mathbf{R}} \sigma_{\mathbf{R}s} + \frac{1}{2} \sum_{\substack{\mathbf{R},\mathbf{R}' \\ s,s'}} J_{ss'}(\mathbf{R}-\mathbf{R}')\sigma_{\mathbf{R}s}\sigma_{\mathbf{R}'s'} +$$

$$+\frac{1}{2} \sum_{\substack{\mathbf{R},\mathbf{R}' \\ s,s'}} \mathbf{u}_{\mathbf{R}s} \cdot \Phi_{ss'}(\mathbf{R}-\mathbf{R}') \cdot \mathbf{u}_{\mathbf{R}'s'} - \sum_{\substack{\mathbf{R},\mathbf{R}' \\ s,s'}} \mathbf{u}_{\mathbf{R}s} \cdot F_{ss'}(\mathbf{R}-\mathbf{R}')\sigma_{\mathbf{R}'s'} + \mathcal{O}(\sigma^3), \qquad (2.36)$$

where the linear term in the $\{\mathbf{u}_{\mathbf{R}s}\}$ vanishes being the atomic position of the reference system the equilibrium ones. The K_s and $J_{ss'}$ constants are the same previously defined; the term $\Phi_{ss'}(\mathbf{R}-\mathbf{R}')$ is the matrix of the second-order derivatives with respect to atomic displacements from the ideal positions, while $F_{ss'}(\mathbf{R}-\mathbf{R}')$ is the force acting on a virtual atom located in $(\mathbf{R},s)$ when the s'-th virtual atom of the unit cell located in $(\mathbf{R}',s')$ is replaced by a real one. It is usually referred to as *Kanzaki's force* [48]. All these terms can be obtained within DFPT and their expressions are:

$$\underset{\alpha\beta}{\Phi}_{ss'} = \int \Delta v^s_{\mathbf{u}^\alpha}(\mathbf{r}-\mathbf{R})\Delta n^{s'}_{\mathbf{u}^\beta}(\mathbf{r}-\mathbf{R}')d\mathbf{r} + \frac{\partial^2 E_{ion}}{\partial \mathbf{u}^\alpha_{\mathbf{R}s}\partial \mathbf{u}^\beta_{\mathbf{R}'s'}}, \qquad (2.37)$$

$$\begin{aligned} \underset{\alpha}{F}_{ss'} &= -\int \Delta v^s_{\mathbf{u}^\alpha}(\mathbf{r}-\mathbf{R})\Delta n^{s'}_{\sigma}(\mathbf{r}-\mathbf{R}')d\mathbf{r} + \frac{\partial^2 E_{ion}}{\partial \mathbf{u}^\alpha_{\mathbf{R}s}\partial \sigma_{\mathbf{R}'s'}} = \\ &= -\int \Delta v^{s'}_{\sigma}(\mathbf{r}-\mathbf{R}')\Delta n^{s}_{\mathbf{u}^\alpha}(\mathbf{r}-\mathbf{R})d\mathbf{r} + \frac{\partial^2 E_{ion}}{\partial \mathbf{u}^\alpha_{\mathbf{R}s}\partial \sigma_{\mathbf{R}'s'}}, \end{aligned} \qquad (2.38)$$

where $\Delta v^s_{\mathbf{u}^\alpha}(\mathbf{r}-\mathbf{R}')$ and $\Delta n^s_{\mathbf{u}^\alpha}(\mathbf{r}-\mathbf{R}')$ are the perturbing potential and the linear response of the electronic density associated to the displacement in the α direction of the atom located in $(\mathbf{R},s)$. The atomic displacements from ideal positions are not independent variable but, for any given configuration, are those that minimize the total energy. The condition that

the total forces acting on atoms vanish at the equilibrium reads:

$$0 = -\frac{\partial E(\{\sigma_{\mathbf{R}s}\},\{\mathbf{u}_{\mathbf{R}s}\})}{\partial \mathbf{u}_{\mathbf{R}s}} = -\sum_{\mathbf{R}',s'} \Phi_{ss'}(\mathbf{R}-\mathbf{R}')\cdot\mathbf{u}_{\mathbf{R}'s'} + \sum_{\mathbf{R}',s'} F_{ss'}(\mathbf{R}-\mathbf{R}')\sigma_{\mathbf{R}'s'}, \quad (2.39)$$

The solution of this equation is:

$$\mathbf{u}^{eq}_{\mathbf{R}s} = \sum_{\substack{\mathbf{R}',\mathbf{R}'' \\ s',s''}} \Phi^{-1}_{ss'}(\mathbf{R}-\mathbf{R}')\cdot F_{s's''}(\mathbf{R}'-\mathbf{R}'')\sigma_{\mathbf{R}''s''}. \quad (2.40)$$

Inserting this equation in the expression for the total energy one obtains:

$$E(\{\sigma_{\mathbf{R}s}\}) = E_0 + \sum_s K_s \sum_{\mathbf{R}} \sigma_{\mathbf{R}s} + \frac{1}{2}\sum_{\substack{\mathbf{R},\mathbf{R}' \\ s,s'}} \hat{J}_{ss'}(\mathbf{R}-\mathbf{R}')\sigma_{\mathbf{R}s}\sigma_{\mathbf{R}'s'} + \mathcal{O}(\sigma^3), \quad (2.41)$$

that is formally identical to equation 2.33, but that includes the relaxation effects via a renormalization of the two-body interaction constants:

$$\hat{J}_{ss'}(\mathbf{R}-\mathbf{R}') = J_{ss'}(\mathbf{R}-\mathbf{R}') - \sum_{\substack{\mathbf{R}'',\mathbf{R}''' \\ s'',s'''}} F_{ss''}(\mathbf{R}''-\mathbf{R})\cdot\Phi^{-1}_{s''s'''}(\mathbf{R}''-\mathbf{R}''')F_{s'''s'}(\mathbf{R}'''-\mathbf{R}'). \quad (2.42)$$

The translational invariance of the crystal makes all the interaction constants depend only on the *relative* positions of atoms; it is convenient to solve the obtained equations in reciprocal space, where the convolutions are replaced by simple multiplications:

$$\hat{J}_{ss'}(\mathbf{q}) = \tilde{J}_{ss'}(\mathbf{q}) - \sum_{s'',s'''} \tilde{F}_{ss''}(\mathbf{q})^{+}\cdot\tilde{\Phi}^{-1}_{s''s'''}(\mathbf{q})\cdot\tilde{F}_{s'''s'}(\mathbf{q}), \quad (2.43)$$

where $\tilde{f}(\mathbf{q}) = \sum_{\mathbf{R}} \mathrm{e}^{-\mathrm{i}\mathbf{q}\cdot\mathbf{R}} f(\mathbf{R})$ indicates the Fourier transform of the function $f(\mathbf{R})$. In this scheme we can deal both with *microscopic* relaxation of interatomic distances in the disordered alloy and with *macroscopic* elastic effects, coming from the dependence of the alloy equilibrium volume upon composition. This last term is in fact related to the long-wavelength limits ($\mathbf{q}\to\mathbf{0}$) of $\Phi_{ss'}(\mathbf{q})$ and $F_{ss'}(\mathbf{q})$ that are related to the elastic constants and to the macroscopic stress. However, it is both simpler and more accurate to deal with the macroscopic elastic effects by an *ad hoc* procedure.

The binary alloy A_xB_{1-x} formation energy is the difference between the total energy of a particular configuration at a given molar volume Ω and the appropriate average of the energies of the pure components at their respective equilibrium volumes:

$$\Delta E(\{\sigma_{\mathbf{R}s}\},\Omega) = E(\{\sigma_{\mathbf{R}s}\},\Omega) - xE_A(\Omega_A) - (1-x)E_B(\Omega_B), \tag{2.44}$$

where $E_{A,B}$ and $\Omega_{A,B}$ are the energy and the equilibrium volumes of the pure compounds.

It is convenient to split ΔE into an elastic and a configurational term. We define the elastic contribution as the energy needed to vary the pure materials volumes from their equilibrium values, $\Omega_{A,B}$, to the volume of the alloy, Ω:

$$\Delta E_{\text{elast}}(x,\Omega) = x(E_A(\Omega) - E_A(\Omega_A)) + (1-x)(E_B(\Omega) - E_B(\Omega_B)). \tag{2.45}$$

The configurational term coincides with the formation energy of the alloy at the fixed volume Ω:

$$\Delta E_{\text{config}}(\{\sigma_{\mathbf{R}s}\},\Omega) = E(\{\sigma_{\mathbf{R}s}\},\Omega) - xE_A(\Omega) - (1-x)E_B(\Omega). \tag{2.46}$$

In this way the elastic term is computed exactly from the knowledge of the equation of state of the constituents, and the perturbative expansion enters only the definition of the configurational term:

$$\Delta E_{\text{config}}(\{\sigma_{\mathbf{R}s}\},\Omega) = \frac{1}{2}\Big(\sum_{s,s'}\sum_{\mathbf{R},\mathbf{R}'} \hat{J}^{(\Omega)}_{ss'}(\mathbf{R}-\mathbf{R}')\sigma_{\mathbf{R}s}\sigma_{\mathbf{R}'s'} - N\sum_{s,s'}\sum_{\mathbf{R}} \hat{J}^{(\Omega)}_{ss'}(\mathbf{R})\Big). \tag{2.47}$$

It is important to notice that the $J(\mathbf{q}=\mathbf{0})$ has not to be renormalized, being the macroscopic relaxation already accounted for exactly in the elastic term. The interaction constants are calculated for different volumes in the range of interest, and this dependence describes some of the anharmonic effects also in the $\mathbf{q} \neq \mathbf{0}$ terms.

In the case of a binary or pseudobinary alloy, the molar fractions of the pure constituents needed for the formation of the alloy with a given composition, x, is uniquely determined by it. In the case of quaternary $A_xB_{1-x}C_yD_{1-y}$ alloys, the definition is not unique. The

two compositions are not sufficient to fix in a univocal way the correspondence between the compositions and the molar fractions and there are different possible choices due to such additional degree of freedom.

The simplest generalization of Eq. 2.44 to the quaternary alloy case consists in a bilinear form:

$$\begin{aligned}\Delta E(\{\sigma_{\mathbf{R}s}\},\Omega) &= E(\{\sigma_{\mathbf{R}s}\},\Omega) - xyE_{AC}(\Omega_{AC}) - (1-x)yE_{BC}(\Omega_{BC}) + \\ &- x(1-y)E_{AD}(\Omega_{AD}) - (1-x)(1-y)E_{BD}(\Omega_{BD}). \end{aligned} \tag{2.48}$$

However different choices are more convenient and will be adopted in the following; for instance, the elastic strain is minimized, and the perturbative error lowered in (Zn,Mg)(S,Se), if the following recipe is chosen:

$$\begin{aligned}\Delta E(\{\sigma_{\mathbf{R}s}\},\Omega) &= E(\{\sigma_{\mathbf{R}s}\},\Omega) - xE_{\mathrm{ZnSe}}(\Omega_{\mathrm{ZnSe}}) - yE_{\mathrm{MgS}}(\Omega_{\mathrm{MgS}}) + \\ &- (1-x-y)E_{\mathrm{MgSe}}(\Omega_{\mathrm{MgSe}}) \end{aligned} \tag{2.49}$$

if $x + y \leq 1$, and:

$$\begin{aligned}\Delta E(\{\sigma_{\mathbf{R}s}\},\Omega) &= E(\{\sigma_{\mathbf{R}s}\},\Omega) - (1-y)E_{\mathrm{ZnSe}}(\Omega_{\mathrm{ZnSe}}) - (1-x)E_{\mathrm{MgS}}(\Omega_{\mathrm{MgS}}) + \\ &- (x+y-1)E_{\mathrm{ZnS}}(\Omega_{\mathrm{ZnS}}) \end{aligned} \tag{2.50}$$

if $x + y \geq 1$.

2.6 Electronic structure

It is well known that energy gaps are systematically underestimated in *ab-initio* calculations and that this is an intrinsic feature of DFT-LDA [49–52], being density-functional theory a ground-state theory not suitable to describe excited states properties, such as the energy gap. Other approaches based on quasi-particle description of electronic excitations in the

GW approximation [53] have been developed in the last decade, and applied also to the case of II – VI semiconductors [54]. However it is widely accepted that LDA electronic band structures are qualitatively in good agreement with experiments in what concerns the ordering of the energy levels and the shape of the bands. In many cases it is even possible to superpose LDA electronic bands to the experimental ones simply with a rigid upwards shift of the theoretical conduction bands, using the so-called *scissor operator*, whose amount is roughly inversely proportional to the high-frequency static dielectric constant, ϵ_∞, of the system [51].

The direct *ab-initio* calculations of the electronic properties of a disordered system is computationally too demanding, as previously discussed. It is thus necessary to adopt a different strategy also for the determination of the band structure of the alloy. In this work we will follow the approach of Special Quasi-random Structures (SQS) [20], that are rather small supercells containing up to a few tens of atoms, and still are representative of the alloy. They are in fact constructed in such a way as to have short-range correlations as similar to the "real" alloy as possible. This approach allows application of first-principles methods to the calculation of the optical properties of solid solutions.

In the original work, SQS's were constructed for the simple case of $A_{0.5}B_{0.5}C$ pseudobinary *perfectly random* alloys. In this cases the off-site terms of the correlation functions vanish. This ideal situation allows to obtain good SQS's with $8 \div 16$ particles. In our case the purpose of studying the random and the "true" short-range-ordered alloy, in the presence of chemical disorder in both sublattices, and for different concentrations, implies the choice of larger superlattices, from 64 up to 216 atoms, for which *ab-initio* electronic structure calculations are still possible with reasonable computational effort. The electronic levels of the alloy are then obtained with an ensemble average of the results obtained for a few fully relaxed SQS's.

Describing alloys by short-period supercells clearly introduces spurious correlations beyond a certain distance. However, for many physical properties interactions between distant neighbors are generally much less important than those between close neighbors, and it will be shown that this condition is satisfactorily fulfilled for the electronic properties of $Zn_xMg_{1-x}S_ySe_{1-y}$.

3 Properties of the pure materials

ZnS, ZnSe, MgS and MgSe are the basic constituents, in correspondence of $x = 0, 1$ and $y = 0, 1$, of the quaternary $Zn_xMg_{1-x}S_ySe_{1-y}$ alloy. The calculation of the structural properties of such materials is straightforward within DFT. The comparison of our theoretical predictions with the experimental structural parameters and phase stability obtained in these simpler cases is a necessary step in order to determine the degree of accuracy that we can expect for the alloy.

In this chapter we present the results of the DFT calculations on the energetics and on the structural and electronic properties of the pure constituents, and we compare them to the experimental data, where available. As a byproduct, we report on the first *ab-initio* theoretical calculations of the vibrational properties of the Mg chalcogenides.

The ground state properties of our systems are computed by using the plane-wave pseudopotential scheme previously discussed in Section 2.2. The *frozen-core* approximation, that is at the basis of pseudopotential theory, holds when the energies of the core electrons are much lower than the valence electrons energies. In such a case, the overlap between the core and the valence charge is negligible and it is possible to separate the non-linear exchange-correlation term as $\epsilon_{xc}(n_c(\mathbf{r}) + n_v(\mathbf{r})) \approx \epsilon_{xc}(n_c(\mathbf{r})) + \epsilon_{xc}(n_v(\mathbf{r}))$, including the core part in the pseudopotential.

The case of zinc atoms is however more difficult to deal with, because the closed-shell

of $3d$ orbitals is quite close in energy to the $4s$ and $4p$ electrons energy and higher than the anion s band energy in the compounds presently considered. This fact suggests the possibility of a failure of the frozen-core approximation: in the solid there is a core relaxation which is completely neglected in the pseudopotential picture. Furthermore, there is a large overlap between the core and the valence charges. In principle one may consider also d electrons as valence electrons, but this would require the use of a very large PW basis set with the standard norm-conserving pseudopotential technique or of the more cumbersome *ultra-soft* pseudopotential scheme [55]. The error associated with the core relaxation is almost unavoidable with PW, but it is possible to improve the transferability of the pseudopotential by following the von Barth and Car (VBC) recipe [56], in which they have the analytical form:

$$v^{\rm loc}(r) = \frac{-Z_v}{r}{\rm erf}(r\sqrt{\alpha_c}), \quad v_l(r) = (a_l + b_l r^2){\rm exp}(-\alpha_l r^2), \tag{3.1}$$

and by fitting them to *several* different configurations, rather than to the atomic ground state only [57].

It is possible to correct the large error due to the charge overlap by adopting the Non-Linear Core-Corrections (NLCC) scheme [57, 58]. The NLCC solution consists in including the *total* charge rather than the *valence* only in the dependence of the exchange-correlation term:

$$E_{xc} = \int \epsilon_{xc}(n_c(\mathbf{r}) + n_v(\mathbf{r}))(n_c(\mathbf{r}) + n_v(\mathbf{r}))\, d\mathbf{r}, \tag{3.2}$$

where n_c is the core charge calculated once for all on the atomic configuration, and then added to the valence charge when needed. In our calculations, the core charge is parameterized as:

$$n_c(\mathbf{r}) = (a_{cc} + b_{cc} r^2) e^{-\alpha_{cc} r^2} \tag{3.3}$$

which is easily computed both in direct and reciprocal space. This correction improves the results also for the magnesium pseudopotential; we describe the Se atoms in the VBC

scheme, while for sulphur atoms we adopt the standard Bachelet-Hamann-Schlüter parameterization [26].

3.1 Energetics and structural properties

We have calculated the structural properties of the four pure materials in three different crystal structures, *i.e.* in the zincblende, wurtzite and rocksalt (cubic $B1$) structures. The wurtzite phase has an hexagonal unit cell with a four-atom basis. It is determined by its lattice constant, a, by the $\frac{c}{a}$ ratio, and by an internal parameter u that refers to the relative distance of the planes in the c direction; in the ideal close-packed case $\frac{c}{a} = \sqrt{\frac{8}{3}} \approx 1.633$ while $u = 0$.

The electron-gas exchange-correlation energy and potential used in our LDA scheme are those determined by Ceperley-Alder quantum MonteCarlo simulations [59], in the Perdew-Zunger [60] parameterization. Our results are well converged using a kinetic-energy cutoff of 15 Ry and a BZ sampling of 10 special $\mathbf{k}$ points [25] for the fcc-based structures and an equivalent set of points for the wurtzite phase.

The common procedure for the determination of the structural properties near equilibrium consists in computing the total energy at different values of the lattice parameter and in fitting the results to a semi-empirical equation of state. In this work we use the Murnaghan equation [61]:

$$P(V) = \frac{B_0}{B_0'}\left[\left(\frac{V}{V_0}\right)^{-B_0'} - 1\right], \tag{3.4}$$

where P is the pressure, V the volume, B_0 is the bulk modulus and B_0' its first derivative with respect to volume. For the wurtzite structure calculations, the pressures entering Eq. 3.4 are determined for those configurations which minimize the total energy with respect to variations of both u and $\frac{c}{a}$. In Table 3.1 we display for each of the 4 pure materials the difference in energy with respect to the most stable phase. In agreement with exper-

	Zincblende		Wurtzite				Rocksalt	
	ΔE(meV)	a_0(Å)	ΔE(meV)	a_0(Å)	$\frac{c}{a}$	Δu	ΔE(meV)	a_0(Å)
ZnS	0.0	5.34 (5.41)	2.6	3.78 (3.82)	1.64 (1.64)	0.2%	439.7	4.99 (5.06)
ZnSe	0.0	5.59 (5.67)	8.7	3.96 (4.00)	1.64 (1.63)	0.1%	524.6	5.22 (5.28)
MgS	142.0	5.71 (5.62)	129.3	4.05	1.63	0.5%	0.0	5.24 (5.19)
MgSe	69.9	5.99 (5.89)	59.9	4.24 (4.15)	1.63 (1.62)	0.4%	0.0	5.51 (5.45)

Table 3.1: Relative total energies and structural parameters of the 4 pure materials in three different structures, at the respective equilibrium lattice parameters, compared to experimental data, when available. Energies are expressed in meV/atom-pair.

iments, the zincblende structure is energetically favored for the Zn compounds, while Mg chalcogenides are more stable in the rocksalt phase. For all the compounds the wurtzite phase is the intermediate one, and its energy is always very close to that of the zincblende structure. In particular, for ZnS the two structures appear to be almost degenerate.

In the same Table 3.1, the calculated lattice constants, in the different structures, are compared with experimental data, when available. The theoretical predictions agree within 2% with experimental results, an accuracy typical of LDA calculations. LDA usually underestimates structural parameters and this is the case for what concerns Zn chalcogenides, while the lattice parameters of Mg compounds are, quite unusually, overestimated.

We note however that for the latter materials experimental data are not directly measured in the zincblende phase, but extrapolated from the Zn-rich regions of the ternary alloys [7, 10], being the pure materials unstable in that phase. The few *ab-initio* theoretical

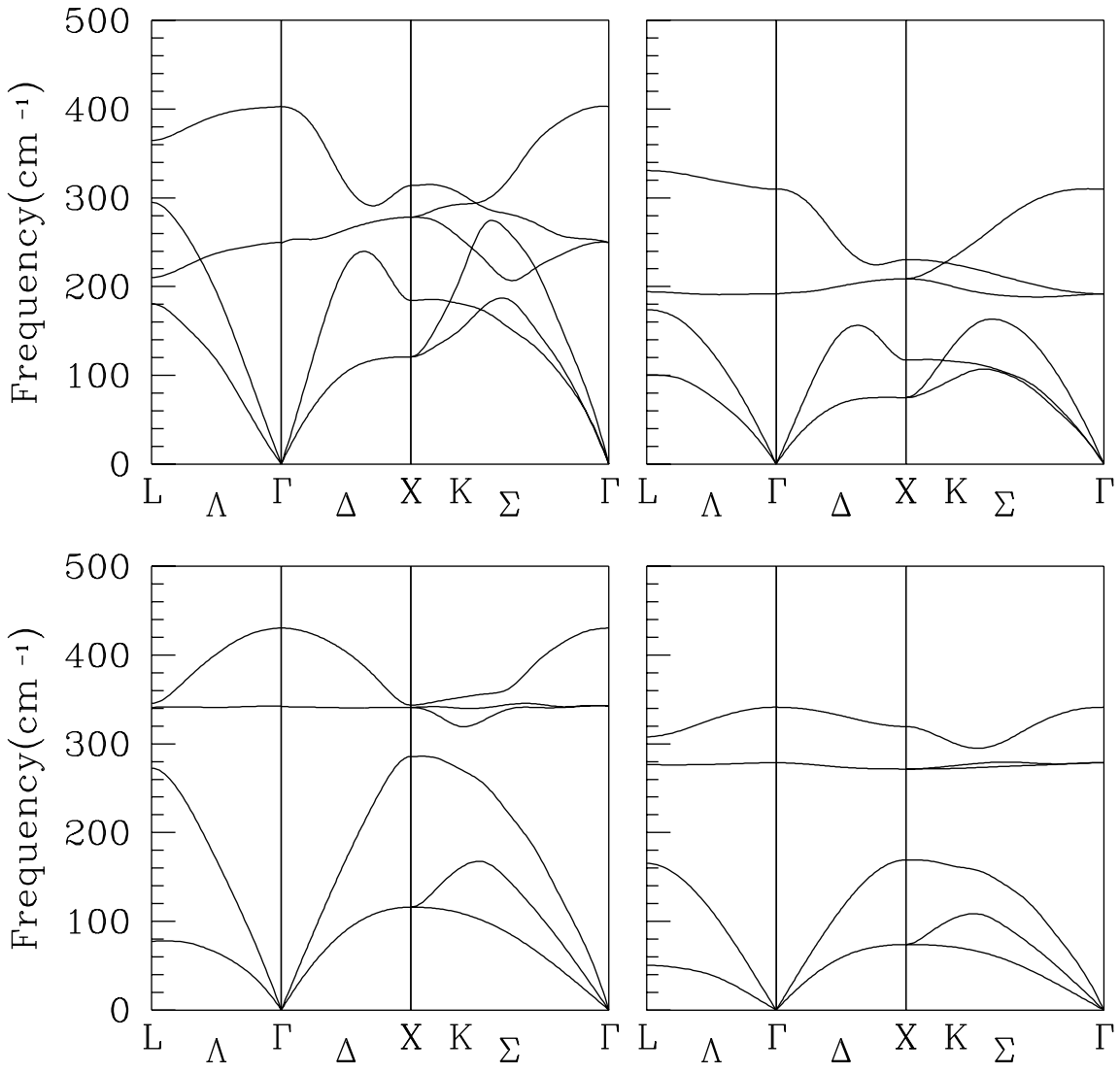

Figure 3.1: MgS (left panel) and MgSe (right panel) phonon dispersions in the rocksalt structure.

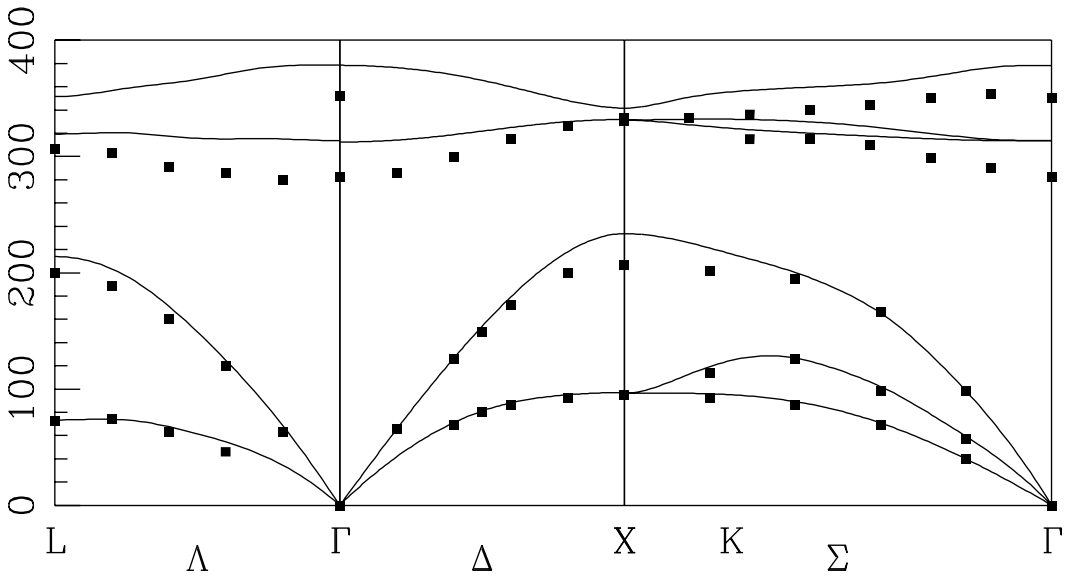

Figure 3.2: Theoretical (full lines) and experimental (squares) ZnS phonon dispersions in the zincblende structure.

results [62] for zincblende MgSe show different equilibrium lattice constants, from $a_0 = 5.87$ Åto $a_0 = 6.07$ Å, and our result falls in this range.

3.2 Vibrational properties

As a byproduct of our calculations based on DFPT, we have computed the vibrational spectra of the four materials. We display the results for MgS and MgSe both in the rock-salt and in the zincblende structures, and the phonon dispersions of ZnS in the zincblende phase. Only for the latter case, to our knowledge, experimental data are available for comparison [63]. The calculations have been performed at the theoretical equilibrium lattice constant. The agreement is very good for the acoustic branches, while the optical frequencies are somewhat overestimated by about 5%, because of the underestimation of the equilibrium lattice parameter. Analogous calculations performed on ZnSe and other II – VI semiconductors at lattice constants closer to the experimental ones had in fact given a better

	ZnS		ZnSe		MgS		MgSe	
	th.	exp.	th.	exp.	th.	exp.	th.	exp.
$E(\Gamma_{1v})$	-12.5	-13.5(4)	-12.7	-15.2(6)	-11.0	-	-11.2	-
$E(L_{1v})$	-11.1	-12.4(3)	-11.5	-13.1(3)	-10.2	-	-10.6	-
$E(X_{1v})$	-10.6	-12.0(3)	-11.1	-12.5(4)	-10.0	-	-10.4	-
$E(L_{1v})$	-5.0	-5.5(2)	-5.1	-5.6(3)	-3.3	-	-3.3	-
$E(X_{3v})$	-4.7	-5.5(2)	-4.9	-5.3(3)	-2.9	-	-3.1	-
$E(X_{5v})$	-1.9	-2.5(3)	-2.0	-2.1(3)	-1.2	-	-1.2	-
$E(L_{3v})$	-0.7	-1.4(4)	-0.8	-1.0(3)	-0.4	-	-0.4	-
$E(\Gamma_{1c})$	3.1	3.8(1)	2.5	2.8(1)	3.1	(4.5)	2.7	(3.6)
$E(X_{1c})$	3.6	4.1(2)	3.1	3.4(3)	3.8	-	3.3	-
$E(L_{1c})$	4.0	4.4(3)	3.2	3.8(3)	4.8	-	4.1	-

Table 3.2: Theoretical and experimental band energies at different high-symmetry points. The values in parentheses are estimated by extrapolation from ternary alloys.

agreement [57].

3.3 Electronic structure

In spite of the well known failure of LDA in the quantitative description of the electronic properties of materials, the agreement of LDA-predicted band-structure shape with experiments is satisfactory in many cases.

The band structures of the 4 constituents have been calculated at the *theoretical* equilibrium lattice constant, rather than at the experimental one. This choice appears to be more consistent with the structural calculations, and the comparison with experimental

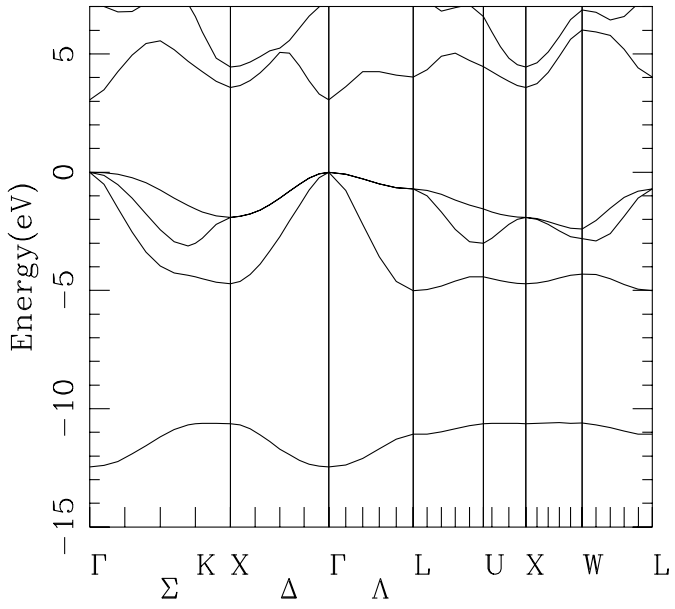

Figure 3.3: LDA electronic bands of ZnS.

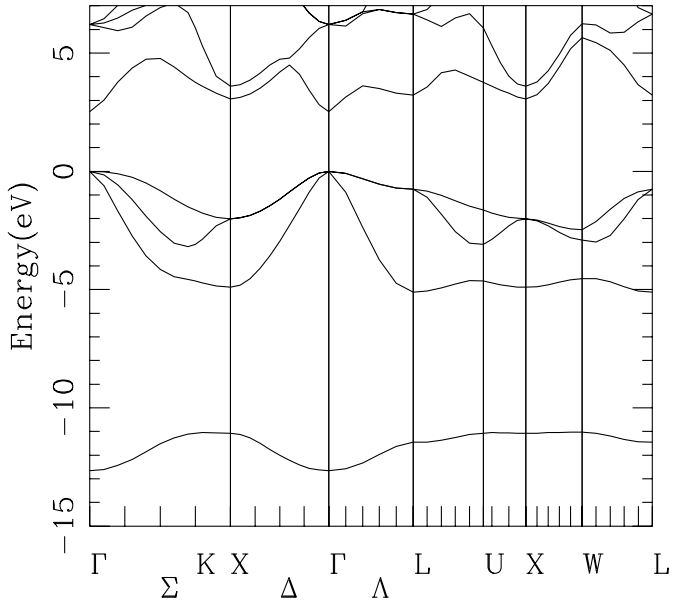

Figure 3.4: LDA electronic bands of ZnSe.

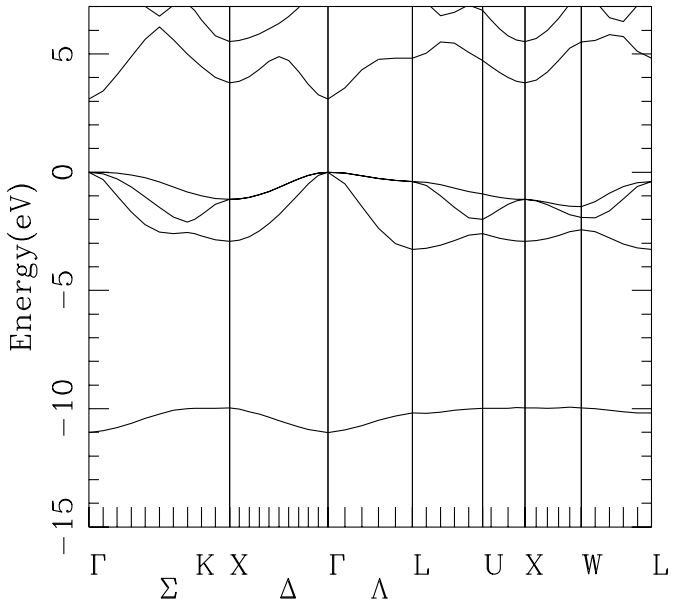

Figure 3.5: LDA electronic bands of MgS.

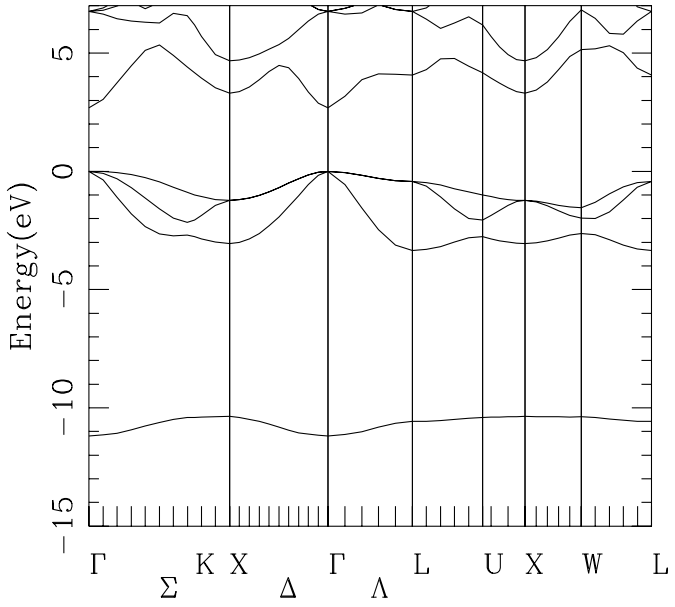

Figure 3.6: LDA electronic bands of MgSe.

data yields better results both qualitatively and quantitatively [51, 52].

The resulting high-symmetry points energies are compared in Table. 3.2 to experimental findings [64, 65]. The latter are almost completely lacking for the Mg compounds, whose fundamental band gaps are extrapolated from pseudobinary alloys. The complete electronic band structures are shown for ZnS, ZnSe, MgS, andMgSe (Figs. 3.3, 3.4, 3.5, and 3.6 respectively).

DFT-derived fundamental band gaps are, as usual, underestimated, but a precise determination of the error is not possible, as previously discussed, for the Mg chalcogenides. In the zinc compounds the difference between theoretical and experimental gaps is lower than expected. This is probably due to the freezing of $3d$ electrons in the pseudo-ion. The energy difference between $3d$ zinc electrons and the p anion bands is rather small ($\approx 3\ eV$), and the coupling with $3d$ states, not included in our calculations, would shift upwards the p-based bands and the top of the valence band, thus reducing the fundamental gap [54].

4 Structure and thermodynamics of $Zn_xMg_{1-x}S_ySe_{1-y}$

Semiconductor alloys usually behave as regular solutions, being characterized by a tendency to segregate in the pure constituents rather than to form ordered structures or superlattices. The latter behavior is generally observed only in epitaxially grown alloys [66] in which the system is far from thermodynamic equilibrium and the growth-induced atomic configurations persist due to the low diffusivity of particles. The energetically most stable phase for bulk solutions, in the limit of slow growth processes, is in most cases the segregated alloy.

As explained in the previous chapters, the present theoretical approach to the study of substitutional alloys is based on the assumption of the chemical similarity of the atomic species present in the solution, and on a perturbative expansion of the relevant physical quantities on such chemical difference. The perturbation strength, as discussed in Section 2.5, is measured by the pseudopotential difference $\Delta v^s_\sigma(\mathbf{r} - \mathbf{R})$. The convergence of such an expansion has been checked by comparing the formation energies of a few ordered structures with full DFT self-consistent calculations. In such structures the particles are not constrained by symmetry—as in pure compounds—to occupy the ideal crystal sites and in these DFT, *non-perturbative*, calculations, the atomic positions were fully *relaxed* from the ideal lattice positions as to minimize the energy of the system.

We then present our results for the structural properties and the phase diagrams of the

4 pseudobinary alloys, *i.e.* $Zn_xMg_{1-x}S$, $Zn_xMg_{1-x}Se$, ZnS_xSe_{1-x} and MgS_xSe_{1-x}, and of the quaternary $Zn_xMg_{1-x}S_ySe_{1-y}$ alloy.

4.1 Accuracy of the expansion

A preliminary step to the study of the thermodynamic properties of the alloy is the check of the convergence of the perturbative expansion with respect to the pseudopotential differences between the atomic species, that has been discussed in the previous chapter.

The interaction constants $J_{ss'}$, $\Phi_{ss'}$ and $F_{ss'}$ defined in Eq. 2.35, Eq. 2.37, and Eq. 2.38 respectively, have been calculated for the virtual crystal $Zn_{\frac{1}{2}}Mg_{\frac{1}{2}}S_{\frac{1}{2}}Se_{\frac{1}{2}}$ on a regular grid of 64 points in reciprocal space, for five different, uniformly spaced, values of the lattice parameter, from the theoretical ZnS constant (10.09 a.u.) to the MgSe lattice parameter (11.32 a.u.). The study of an infinite solid on a discrete, rather than continuous, grid in the reciprocal space is equivalent to the supercell approximation mentioned in Section 2.2; the equivalent supercell size is inversely proportional to the separation of the **q**-points in the grid.

The **q**-space grid we have chosen to calculate the force constants would correspond to the calculation of all real-space interactions in a supercell of 128 atoms; we thus include in our calculations force constants up to the 9^{th} neighbor. The advantage of our reciprocal-space approach relies on the fact that the computational effort scales linearly with the number of **q**-points, rather than with the third power of the number of atoms in the "equivalent" supercell. The interaction constants for arbitrary **q** are obtained using Fourier interpolation: the **q**-space grid is Fourier-transformed in real space, and the arbitrary **q** force constants are obtained by transforming such real-space constants. The procedure is exact for interaction constants that vanish beyond the 9^{th} shell. The $J_{ss'}$'s, Fss''s, and $\Phi ss'$'s are short-ranged; the renormalization through Eq. 2.42 makes the interaction constants rather

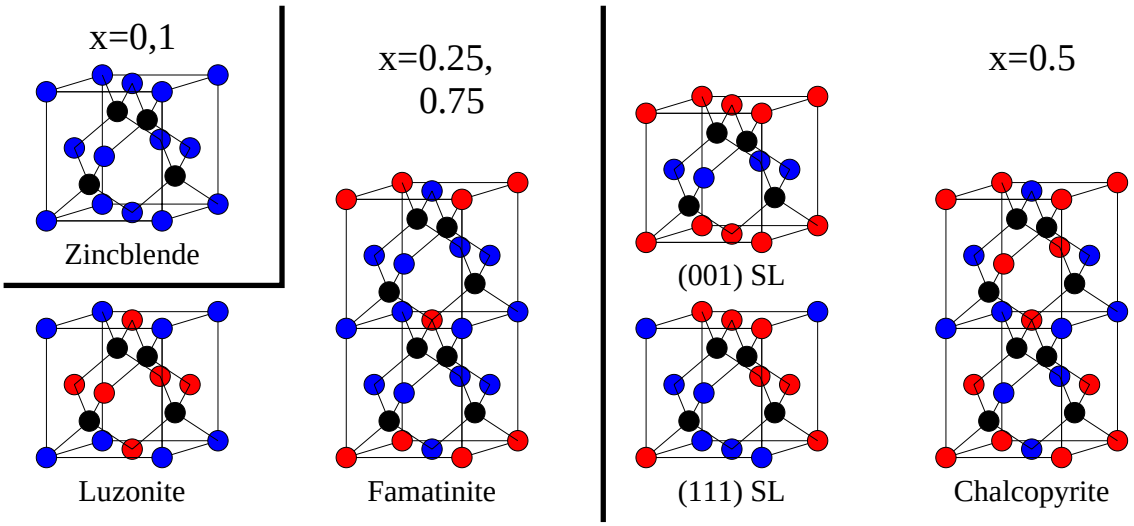

Figure 4.1 (color): Selected ordered pseudobinary structures, with cationic disorder, for different values of the concentration.

longer-ranged [40], but they can be calculated by interpolating the short-range terms.

The most significant check of the validity of the approach is given by the comparison between the DFPT formation energies of a number of ordered structures, and the corresponding fully self-consistent relaxed results. The ordered structures shown in Fig. 4.1 have been considered. These structures share the same lattice of the zincblende phase, and their symmetry group is a ZB subgroup. The Brillouin zone sampling has been performed with sets of $\mathbf{k}$-points equivalent to the 10-points-set we used in the zincblende structure, in order to avoid systematic numerical errors. All calculations are performed at a lattice constant $a_0 = 10.69$ a.u., that is the average among those of the pure constituents, and which is also the equilibrium lattice constant of the virtual crystal. The resulting formation energies are displayed in Table 4.1. In these results the elastic term is included, according to Eqs. 2.49-2.50. The formation energies are all positive, as shown in the Table 4.1, and this is an indication of the tendency of the system to segregate at low temperature, rather than to order. The maximum error of the perturbative expansion is 8.0 meV, and the mean square

	Chem+Relax			Chem+Relax	
Structures	**DFT**	**DFPT**	Structures	**DFT**	**DFPT**
$ZnMgS_2$ 001	82.0	78.1	$ZnMgSe_2$ 001	83.8	86.1
$ZnMgS_2$ 111	100.0	96.8	$ZnMgSe_2$ 111	101.1	104.8
$Zn_2Mg_2S_4$ Ch	64.9	60.6	$Zn_2Mg_2Se_4$ Ch	65.0	68.6
Zn_3MgS_4 L	164.2	159.3	Zn_3MgSe_4 L	34.8	33.8
$ZnMg_3S_4$ L	29.9	28.7	$ZnMg_3Se_4$ L	165.7	170.1
Zn_3MgS_4 F	154.8	150.5	Zn_3MgSe_4 F	24.0	25.0
$ZnMg_3S_4$ F	22.3	19.9	$ZnMg_3Se_4$ F	157.9	161.3
Zn_2SSe 001	118.5	112.0	Mg_2SSe 001	110.1	117.7
Zn_2SSe 111	123.0	116.7	Mg_2SSe 111	114.9	122.4
$Zn_4S_2Se_2$ Ch	112.4	104.9	$Mg_4S_2Se_2$ Ch	102.6	110.6
Zn_4S_3Se L	189.6	184.4	Mg_4S_3Se L	52.1	56.7
Zn_4SSe_3 L	59.5	55.0	Mg_4SSe_3 L	187.5	194.2
Zn_4S_3Se F	186.9	180.8	Mg_4S_3Se F	48.3	53.1
Zn_4SSe_3 F	56.2	51.4	Mg_4SSe_3 F	183.9	190.6

Table 4.1: Formation energy (meV/atom-pair) of 28 pseudobinary ordered structures. All calculation are performed at $a_0 = 10.69$ a.u..

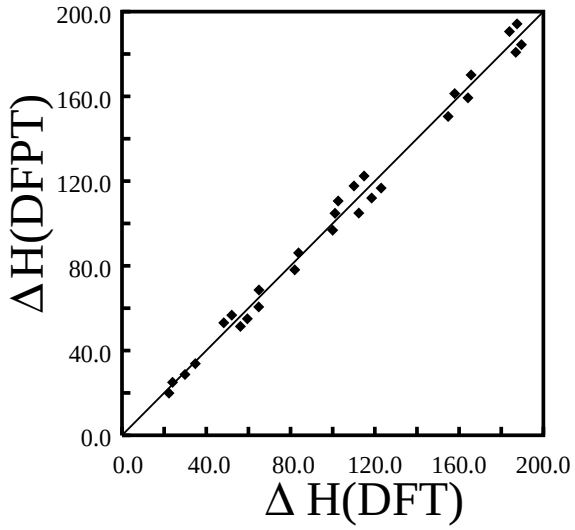

Figure 4.2: DFPT *vs.* DFT formation energies of 28 pseudobinary structures. The straight line corresponds to the perfect agreement. Energies are given in meV/2 atoms.

error (m.s.e.) is 5.0 meV. This discrepancy is larger for the structures with anionic disorder, where the virtual cation is replaced by pure zinc or pure magnesium, and this could have been expected being Zn – Mg chemical difference larger than that between sulphur and selenium. This level of accuracy, with errors smaller than 10%, is rather satisfactory, as shown in Fig. 4.2, but it is possible to obtain an even better accuracy with a rather modest effort, as explained in the next subsection.

4.1.1 Three-body terms

Three-body contributions can be included in the perturbative expansion in principle, by calculating explicitly the third-order derivatives of the total energy, by generalizing the DFPT approach. This strategy, involving complicate and cumbersome mathematical expressions, is however not very practical. We assume that three-body terms are short-ranged. In this hypothesis, it is quite convenient to adopt the RIM approach mentioned in the previous chapter [33] that calculates many-body terms on the same footing of 2-spins contributions.

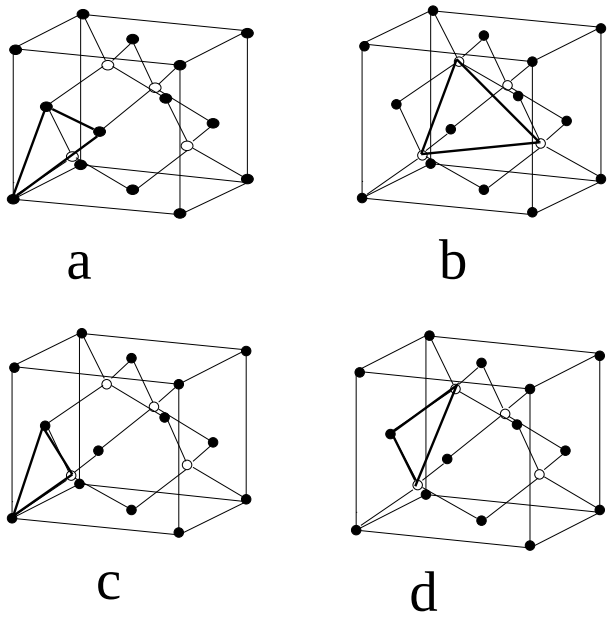

Figure 4.3: Three-body terms included in our calculations. In the upper panels we show the three-cations (a), three-anions (b), and "mixed" (c,d) contributions.

As we previously discussed, the RIM method can be safely adopted only when interactions are short-range, since the ordered structure used in the fit are rather small and contain $8 \div 16$ atoms. It is therefore not adequate for the second order interaction that we find to be long-ranged, but we expect it to be accurate for the small third order corrections.

In our expansion we include only a very small number of three-spin terms, which are illustrated in Fig. 4.3. The interaction parameters corresponding to these four clusters have been determined by fitting the difference among the second-order and the self-consistent energies of the ordered phases. This has been done for three different volumes, fitting the 3-body interaction constants to the 28 pseudobinary ordered structures shown in Fig. 4.1 and in Table 4.1, that are placed on the borders of the square of the compositions.

The maximum error is thus reduced to 2.1 meV and the m.s.e. to 0.8 meV, to be compared with 8.0 meV and 5.0 meV, respectively, obtained without the three-body terms. To test the predictivity of the correction we considered 39 *other* quaternary ordered structures, obtaining a maximum error of 1.5 meV and a m.s.e. of 0.6 meV. As can be seen in Fig. 4.4,

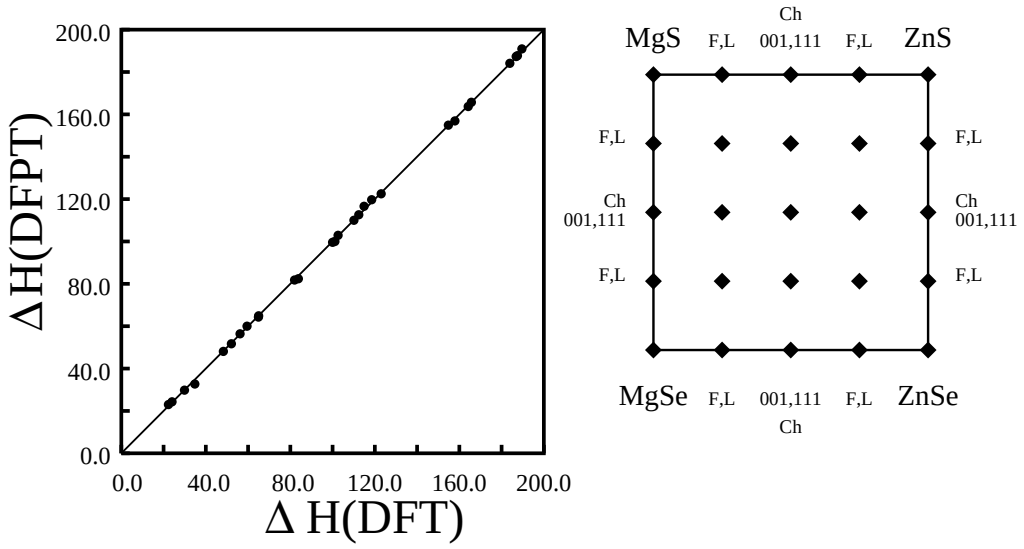

Figure 4.4: Left panel: DFPT energies corrected with four 3-body terms *vs.* DFT results. Right panel: square of the compositions. The 28 pseudobinary structures concentrationsare placed on the borders, while the 39 quaternary structures stay inside the square. Energies are given in meV/2 atoms.

this kind of agreement can be considered very satisfactory and the two-body and three-body interaction constants may be confidently used for the study of the high temperature properties of $Zn_xMg_{1-x}S_ySe_{1-y}$.

4.2 Pseudobinary alloys

Our calculations show that the formation enthalpies of the simplest ordered structures are positive. This implies that the system has a strong tendency to segregate in its constituents at low temperatures. At high T, disordered configurations are expected to become favored, because of the increasing importance of the entropic term. Our aim is to determine the behavior of the alloy between such limits, and to understand the interplay between segregation and clustering as functions of temperature.

	Chem+Relax				Chem+Relax		
Structures	**DFT**	**DFPT**	3rd	Structures	**DFT**	**DFPT**	3rd
$ZnMgS_2$ 001	82.0	78.1	81.8	$ZnMgSe_2$ 001	83.8	86.1	82.4
$ZnMgS_2$ 111	100.0	96.8	99.6	$ZnMgSe_2$ 111	101.1	104.8	100.0
$Zn_2Mg_2S_4$ Ch	64.9	60.6	64.3	$Zn_2Mg_2Se_4$ Ch	65.0	68.6	64.9
Zn_3MgS_4 L	164.2	159.3	163.7	Zn_3MgSe_4 L	34.8	33.8	32.7
$ZnMg_3S_4$ L	29.9	28.7	29.8	$ZnMg_3Se_4$ L	165.7	170.1	165.7
Zn_3MgS_4 F	154.8	150.5	154.9	Zn_3MgSe_4 F	24.0	25.0	24.3
$ZnMg_3S_4$ F	22.3	19.9	23.0	$ZnMg_3Se_4$ F	157.9	161.3	156.9
Zn_2SSe 001	118.5	112.0	119.7	Mg_2SSe 001	110.1	117.7	110.0
Zn_2SSe 111	123.0	116.7	122.5	Mg_2SSe 111	114.9	122.4	116.6
$Zn_4S_2Se_2$ Ch	112.4	104.9	112.6	$Mg_4S_2Se_2$ Ch	102.6	110.6	102.9
Zn_4S_3Se L	189.6	184.4	190.9	Mg_4S_3Se L	52.1	56.7	51.7
Zn_4SSe_3 L	59.5	55.0	60.0	Mg_4SSe_3 L	187.5	194.2	187.7
Zn_4S_3Se F	186.9	180.8	187.3	Mg_4S_3Se F	48.3	53.1	48.1
Zn_4SSe_3 F	56.2	51.4	56.4	Mg_4SSe_3 F	183.9	190.6	184.1

Table 4.2: Formation energy (meV/atom-pair) of the 28 pseudobinary ordered structures with self-consistent calculations, DFPT, and DFPT with the third-order corrections. All calculations are performed at $a_0 = 10.69$ a.u..,

4.2.1 ZnS_xSe_{1-x}: structural properties

The ZnS_xSe_{1-x} alloy is by far the most widely studied of the four pseudobinaries, both from the theoretical and experimental point of view. This alloy has already been extensively used for designing opto-electronic devices being, for $x = 0.06$, lattice-matched to GaAs.

The interaction constants previously computed are used to carry out lattice-gas Monte-Carlo simulations from which we calculate the finite-temperature properties of the system. Such simulations are performed using a supercell of 1024 atoms, at constant temperature, pressure, and chemical potentials. To this end, we attempt two different types of Monte-Carlo moves: the reversal (flipping) of the spin attached to each particle and a variation of the volume of the supercell. The trial move is accepted with the Metropolis probability:

$$p = \min\Big\{\exp\Big[-\beta(\Delta H - \mu\Delta N)\Big], 1\Big\}, \tag{4.1}$$

where ΔH is the enthalpy variation associated to the move, ΔN is the variation of the number of particles, $\mu = \mu_S - \mu_{Se}$ is the difference between the chemical potentials of S and Se species and $\beta = (k_B T)^{-1}$, where T is the temperature and k_B is the Boltzmann constant. The single-spin-flipping-based algorithm is known in literature as *Glauber dynamics* [67].

For each fixed temperature we perform the simulations starting with very large and positive values of the chemical potential for which ZnS is clearly more stable than ZnSe, and then decreasing it slowly towards a Se-rich region. For every value of μ we perform a large number ($1000 \div 5000$) of MonteCarlo trial moves per site, to be sure that thermal equilibrium is actually reached and to lower the statistical error. Each constant μ simulation starts with the last configuration of the previous one (with a slightly different chemical potential). Then we sample the configurational space of the system moving in the opposite direction, beginning with a large and negative value of μ and increasing it with small steps.

The simulations performed in the Glauber dynamics scheme are thus developed in a

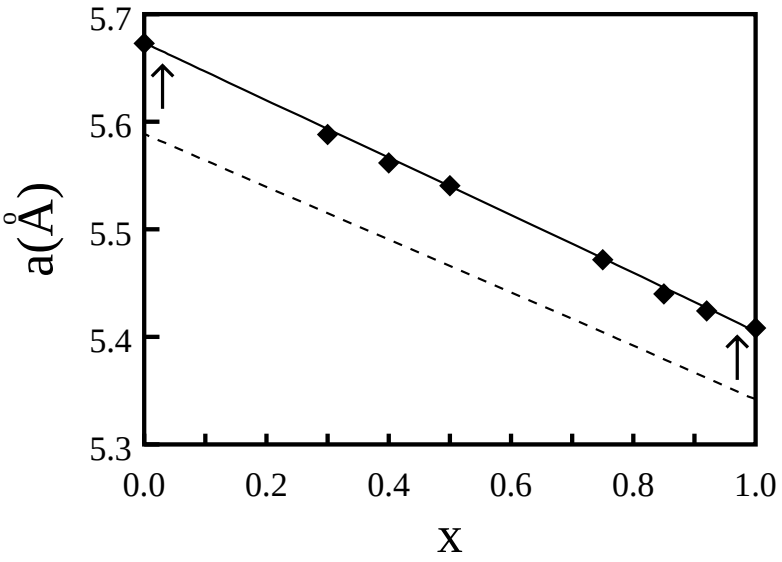

Figure 4.5: Theoretical (dashed line), "corrected" theoretical (solid line) and experimental (diamonds) lattice parameter of ZnS_xSe_{1-x} as function of the concentration.

"quasi grand canonical" ensemble, in the sense that the total number of particles is fixed, but the equilibrium concentration of any chemical species is determined by the value of its conjugate potential. In this ensemble the concentrations of the atomic species are not fixed, and their equilibrium values are subject to fluctuations even at fixed chemical potentials if the temperature is slightly changed. With this procedure any segregating tendency of the alloy comes out even in smaller supercells with the appearance of hysteresis cycles.

Before discussing the theoretical predictions on the thermodynamic stability of the alloy, it is interesting to compare our results on the structural properties of Zn(S, Se) with available experimental data. In Fig. 4.5 we display the theoretical *vs.* experimental [68] lattice parameter of the solution. We see that the discrepancy is of the order of 1-2%. However, as it has been discussed before, this is the typical accuracy of LDA calculations, and if we "correct" our results by rigidly shifting our predictions in such a way as to recover the experimental values in the pure constituents limit ($x = 0, 1$) ZnSe and ZnS, we obtain a very good agreement for *every* value of the concentration. In other words, our calculations

Δd(S-Zn)		N(S)		N(Se)	
th.	exp.	th.	exp.	th.	exp
1.1%	0.7%	0.7	0.7	11.3	11.3

Table 4.3: Theoretical and experimental structural parameters for $ZnS_{0.06}Se_{0.94}$. In the first column we display the per cent variation of the $S-Zn$ bond-length, with respect to the bulk-like value. The second and the third columns refer to the average number of S and Se atoms in the shell of second-nearest neighbors of a sulphur atom.

are very good in catching the relative values and, in particular, the almost perfect linear behavior of the lattice constant with composition (Vegard's law [69]), rather typical of semiconductor alloys.

A more detailed information on the microscopic distortions of the crystal lattice can be obtained by analyzing the bond-length distribution of the alloy. In semiconductor alloys, it is typically found, both in theoretical [38, 39] and experimental works [70], that despite the fact that Vegard's law is followed, the atoms are able to readjust themselves in such a way as to maintain bond-lengths very similar to those found in the pure materials. In Table 4.3 we compare a few theoretical structural parameters with EXAFS data [13]. In particular, we accordingly observe a very small per cent variation of the zinc-sulphur bond-length with respect to its bulk-like value.

For what concerns the short-range order in the anionic sublattice, whose indication is the average number of like atoms in the first shell(s) of nearest-neighbors, the agreement is perfect: for the alloy grown at a temperature of about 550 K the ratio between the number of S atoms and the number of Se atoms in the second shell of neighbors of a *sulphur* atom (the first is completely occupied by Zn atoms) is very close to the value of the concentration, and this indicates that, at least at such temperatures, the tendency to clusterization is very

small. In a perfectly homogeneous alloy, in fact, the average number of like atoms does not depend on the distance and, thus, on the particular shell of neighbors, but only on the average concentration.

4.2.2 ZnS_xSe_{1-x} and other pseudobinaries: the phase diagrams

From the MonteCarlo simulations performed for ZnS_xSe_{1-x}, MgS_xSe_{1-x}, $Zn_xMg_{1-x}S$ and $Zn_xMg_{1-x}Se$ at various different temperatures, it is possible to extract the equilibrium concentration as a function of the corresponding chemical potential. In Fig. 4.6 we display the results of three simulations referring to temperatures above, around and below the critical temperature T_c, for each one of the alloys.

Above T_c the concentration is a continuous and univocal function of the chemical potential, thus indicating a complete miscibility for any composition. Decreasing the temperature, a hysteresis cycle appears, signalling the opening of a miscibility gap: the system behaves differently according to the initial state of the simulation. The relative stability and concentrations of the two phases in which the system decomposes when its average composition is inside the forbidden region can be determined by comparing the free energy F of the two phases. This may be done via thermodynamic integration of the chemical potential with respect to the concentration, since $\mu = \partial F/\partial x$. To this end, the dependence of the chemical potential upon the concentration is fitted by:

$$\mu(x) = k_B T \log\left(\frac{x}{1-x}\right) + \frac{dP(x)}{dx} + \Delta E, \tag{4.2}$$

where the first term is the entropy of a perfectly random solution, $P(x)$ is a fourth- or sixth-order polynomial constrained to vanish for $x = 0, 1$, and ΔE is the energy difference between the pure materials (corresponding to the same limits). The miscibility gap occurs between the two values of the concentration having the same free energy, that is found by the common tangent (Maxwell) construction (see Fig. 4.7). From a geometrical point of

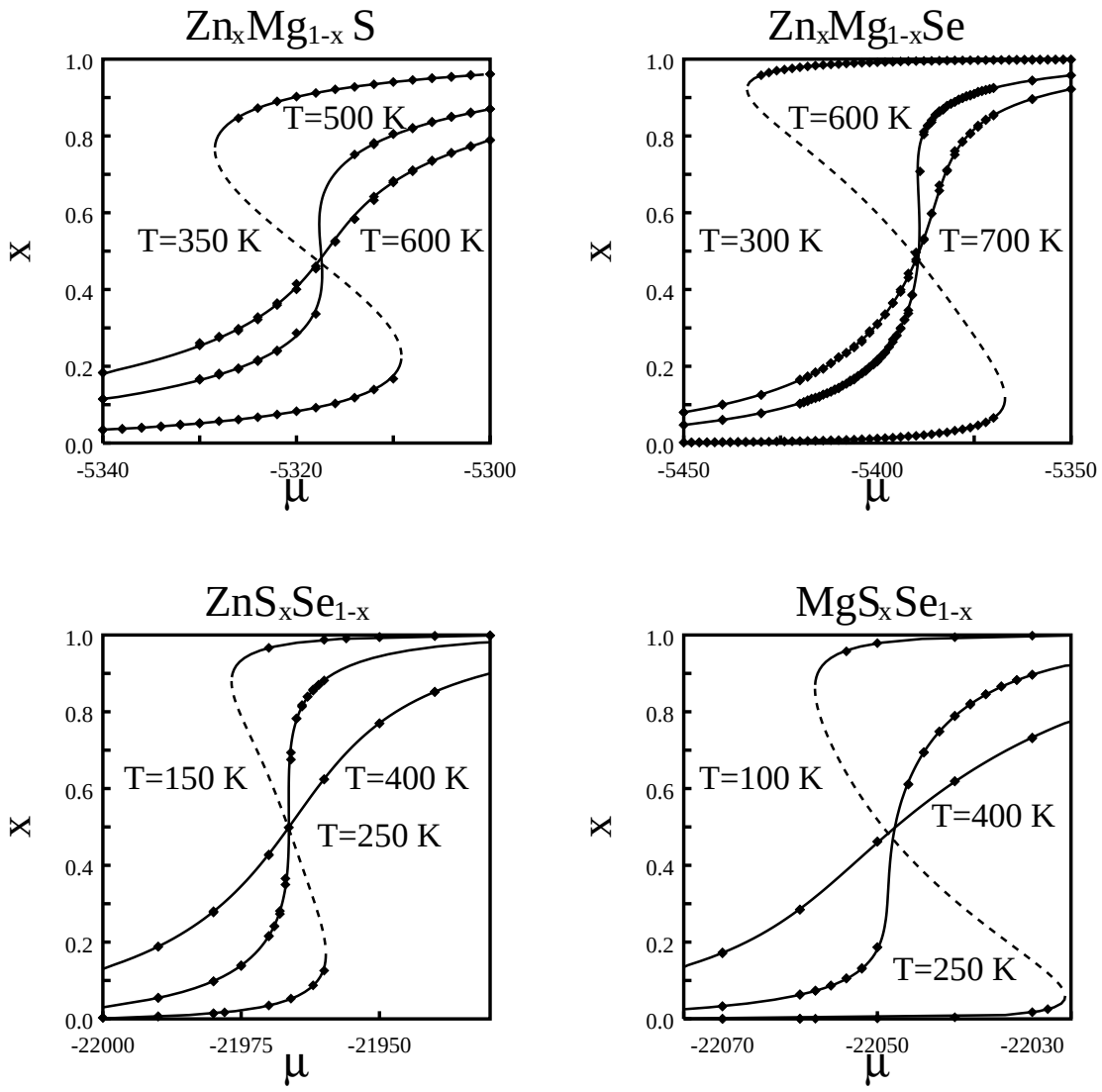

Figure 4.6: Results of the simulations (diamonds) and polynomial fits (lines) of the concentration *vs.* the chemical potential in the 4 pseudobinary alloys at different temperatures, above and below T_c.

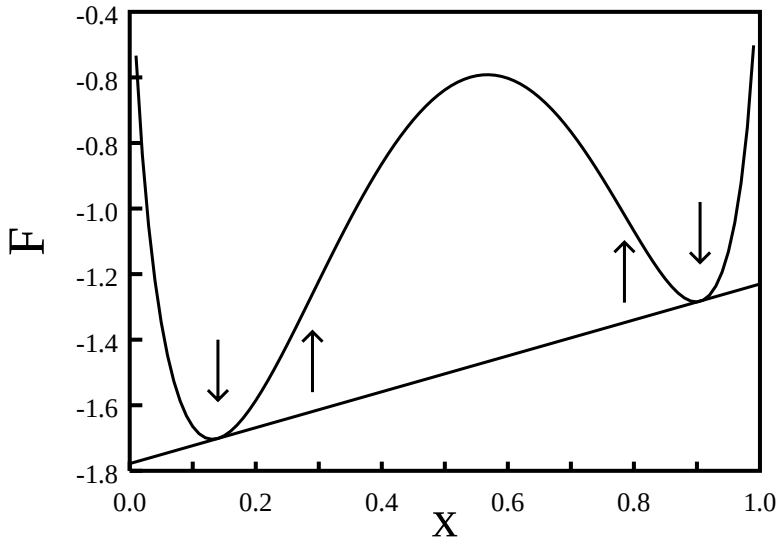

Figure 4.7: Free energy as function of the concentration in Zn(S, Se) at T=200 K. The down arrows indicate the common-tangent points (miscibility gap) while the up ones refer to the flex points of the free energy (spinodal curve).

view, the thermodynamically stable concentrations are all those whose tangent line is a lower bound to the free energy in any other point. The spinodal line is located instead in correspondence of the maximum and the minimum of the chemical potential (flex points of F). The region between the edges of the miscibility gap and the spinodal line is metastable: the system is stable with respect to local fluctuations of the composition but unstable with respect to global segregation. The region between the two spinodal lines is, due to the concavity of the free energy, completely unstable.

In Fig. 4.8 we show the resulting phase diagrams of the pseudobinary alloys. The critical temperatures are higher for the two solutions with cationic disorder than for those with anionic disorder: T_c in the formers is around the typical growth temperatures, while the latter are completely miscible down to T=300 K. Again, this result was expected, since the chemical difference between the cation is larger, and the tendency to segregation consequently is stronger. Such results about the critical temperatures are in agreement

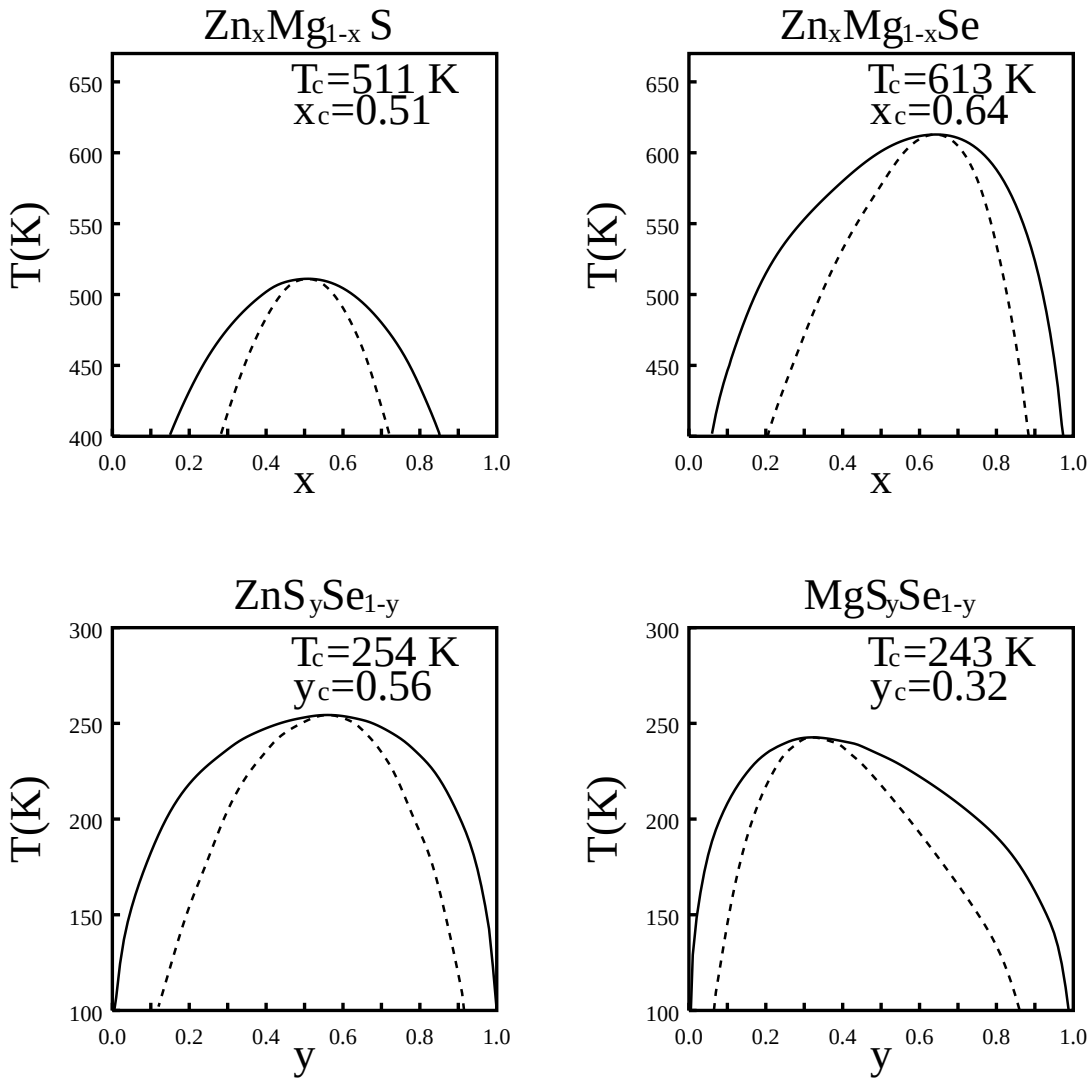

Figure 4.8: Miscibility gaps (full lines), spinodal curves (dashed lines), critical temperatures and concentrations of the 4 pseudobinary alloys. Note the different temperature scales of the upper and lower pictures.

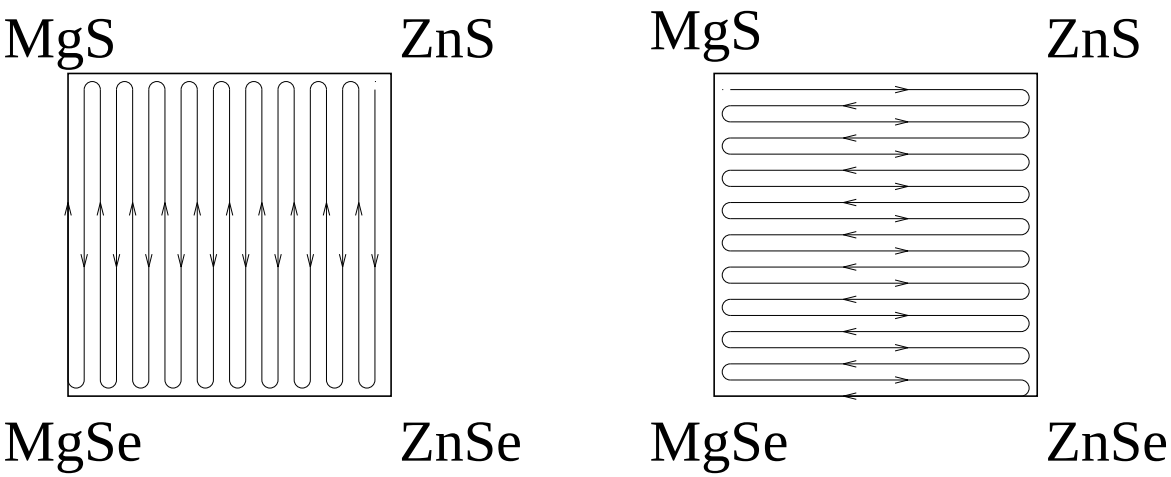

Figure 4.9: MonteCarlo simulation paths for the quaternary alloy.

with the few available experimental findings on the coexistence curves of such alloys, and indicate the complete miscibility of Zn(S, Se) at room temperature.

4.3 Quaternary alloy

The determination of the phase diagram in the case of the quaternary (Zn, Mg)(S, Se) alloy can be obtained by generalizing the MonteCarlo approach used for the pseudobinaries. Each MonteCarlo simulation has been performed at fixed temperature and chemical potentials; as explained in Section 4.2.1, the starting configuration is taken from the last configuration of the previous simulation.

The sampling of the entire space of the compositions requires the independent variation of the two chemical potentials. Our chosen paths in that space are displayed in Fig. 4.9. We start the sequence of the simulations in a region close to one of the pure constituents (near one corner in the square of the compositions), *i.e.* ZnS, fixing the value of μ_x and varying, with the same quasi-adiabatic approach used for the pseudobinary alloys, μ_y until the region close to ZnSe has been reached, and then coming back to the ZnS-rich corner. Then we change a little μ_x and restart the simulations varying μ_y so as to move from the

top side of the square towards the bottom side and then to the top again. This way, little by little, the system moves from the right part (Zn-rich region) towards the left, Mg-rich part of the diagram, as can be seen in the left panel of Fig. 4.9. The last simulations start from almost pure MgS, bring the system close to MgSe (left-bottom corner) and then back in the region of magnesium sulfide. Then we have performed the simulations fixing μ_y and varying μ_x, going forth and back from the right side of the square to the left one, and slowly moving from the top part (S-rich) of the diagram towards the bottom side (Fig. 4.9, right panel).

4.3.1 Phase diagram

The two different ways of sampling the configurational space of the quaternary alloy give the same results for high temperatures, when the system is completely miscible: to each pair of values of the chemical potentials (μ_x, μ_y) correspond a unique pair of values of the concentrations (x, y), independently of the chosen path and, thus, of the starting configuration.

It could be in principle quite difficult to perform simulations close to or below T_c, when a miscibility gap opens. The basic requirement needed to perform the MonteCarlo simulations is that the limiting points (in correspondence of the limiting values of the chemical potentials) must be thermodynamically stable points, depending just on μ_x and μ_y and not on the path or on the starting configuration. In our case, however, the fact that there is a stronger tendency to segregate in the cation sublattice than in the anionic one, as shown by the critical temperatures of the pseudobinary alloys, makes the sampling procedure quite easier. For a wide range of temperatures below T_c the vertical sides of the square of compositions correspond in fact to thermodynamically stable concentrations. In practice, we may use in this range the sampling paths displayed in the right panel of Fig. 4.9,

being the anionic species completely miscible at such temperatures and thus depending the concentration y simply on the value of its conjugate chemical potential μ_y and not on the initial conditions.

The determination of the regions of stability and metastability, at each temperature, may be done generalizing the procedure used for the determination of the free energy of the system in the unidimensional cases. In the present it was necessary to fit at the same time μ_x and μ_y to the derivatives of a two-dimensional function describing the free energy:

$$\begin{aligned} F(x,y) &= k_B T[x\ \log\ x + (1-x)\log(1-x) + y\ \log\ y + (1-y)\log(1-y)] + P(x,y) \\ &+ xyE(\mathrm{ZnS}) + x(1-y)E(\mathrm{ZnSe}) \\ &+ (1-x)yE(\mathrm{MgS}) + (1-x)(1-y)E(\mathrm{MgSe}), \end{aligned} \tag{4.3}$$

$$\begin{aligned} \mu_x(x,y) &= \frac{\partial F(x,y)}{\partial x} = k_B T \log\left(\frac{x}{1-x}\right) + \frac{\partial P(x,y)}{\partial x} + [E(\mathrm{ZnSe}) - E(\mathrm{MgSe})] \\ &+ [E(\mathrm{ZnS}) - E(\mathrm{ZnSe}) - E(\mathrm{MgS}) + E(\mathrm{MgSe})]y, \end{aligned} \tag{4.4}$$

$$\begin{aligned} \mu_y(x,y) &= \frac{\partial F(x,y)}{\partial y} = k_B T \log\left(\frac{y}{1-y}\right) + \frac{\partial P(x,y)}{\partial y} + [E(\mathrm{MgS}) - E(\mathrm{MgSe})] \\ &+ [E(\mathrm{ZnS}) - E(\mathrm{ZnSe}) - E(\mathrm{MgS}) + E(\mathrm{MgSe})]x, \end{aligned} \tag{4.5}$$

where the first term in the right-hand side of the formulae comes again from the hypothesis of regular solution and independent concentrations that holds for x, y close to 0 or 1. The polynomials are chosen in such a way as to have the pseudobinary-alloys coefficients on the borders of the square, while the last "trivial" terms account for the total-energy differences among the pure constituents.

The regions of *spinodal* (local) stability correspond to those concentrations for which the Hessian matrix is positive definite. The thermodynamically stable concentrations (binodal

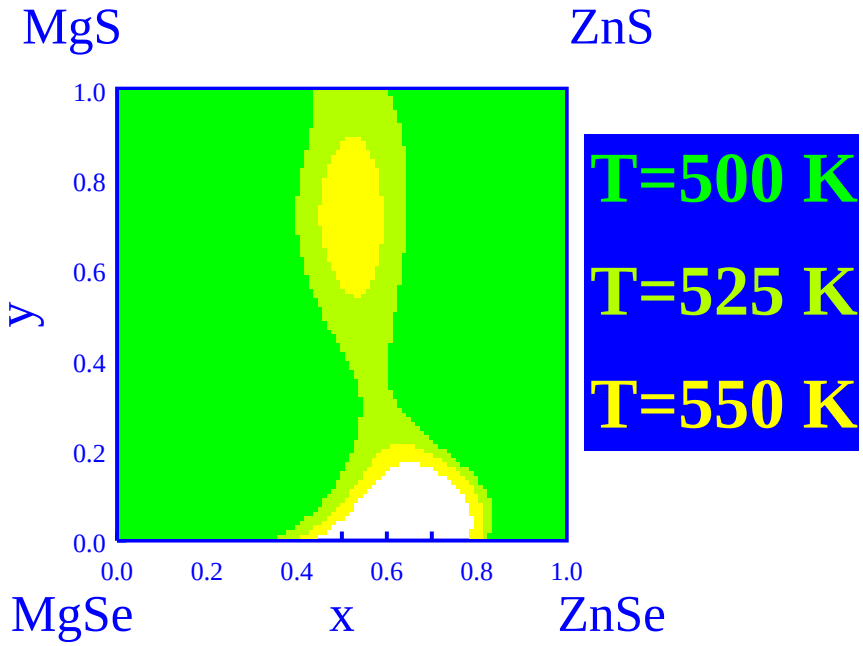

Figure 4.10 (color): Spinodal stability regions at different temperatures.

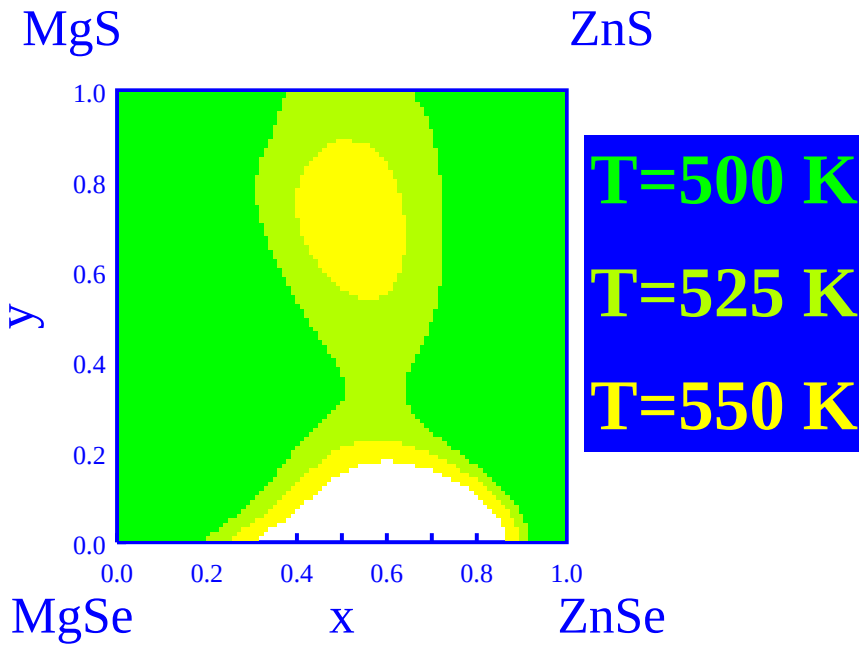

Figure 4.11 (color): Regions of thermodynamic stability in zincblende structure at different temperatures.

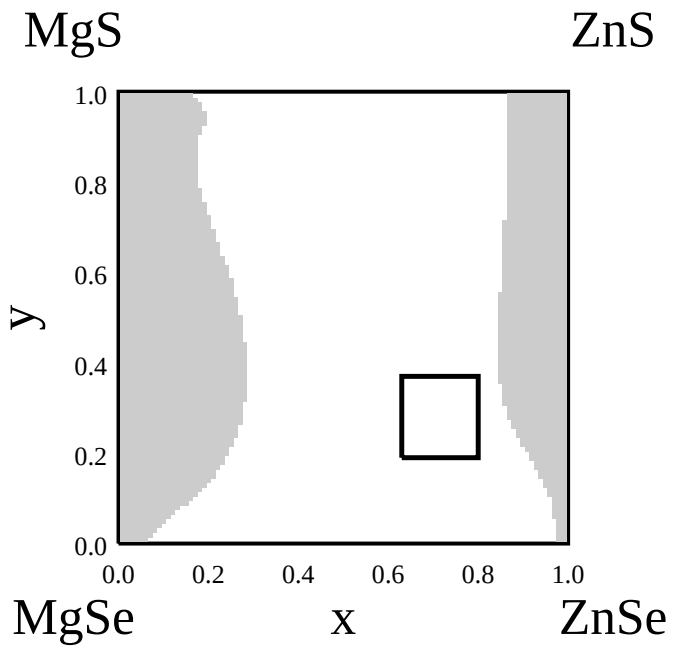

Figure 4.12: Regions of thermodynamic stability in zincblende structure at $T = 400\ K$ (gray) and the "minimum" experimental miscibility gap (empty rectangle).

regions), and thus the miscibility gaps, are determined with a generalization of the common-tangent Maxwell construction previously mentioned for the pseudobinary case. The stable points are those whose tangent plane is a lower bound of the free energy surface. In Fig. 4.10 we display the locally stable portions of the square of compositions, at three different temperatures. For $T = 550\ K$, the disordered alloy is stable at all the compositions but for a small island close to the $Zn_xMg_{1-x}Se$ pseudobinary alloy, whose critical temperature is of about 613 K. Decreasing the temperature this island becomes larger and a forbidden region appears inside the square of compositions, close to the middle point $x, y = \frac{1}{2}$. Cooling down to $T = 500\ K$, the Mg-rich and the Zn-rich regions are separated by a "corridor" in which the disordered alloy is not locally stable.

In Fig. 4.11 we show the corresponding binodal regions for the same temperatures. In this case we remark that the indicated thermodynamic stability refers only to the zincblende structure. In the Mg-rich region other phases, namely the rocksalt and the wurtzite structures, become favored. It is interesting to notice that an experimental estimate [13] of the

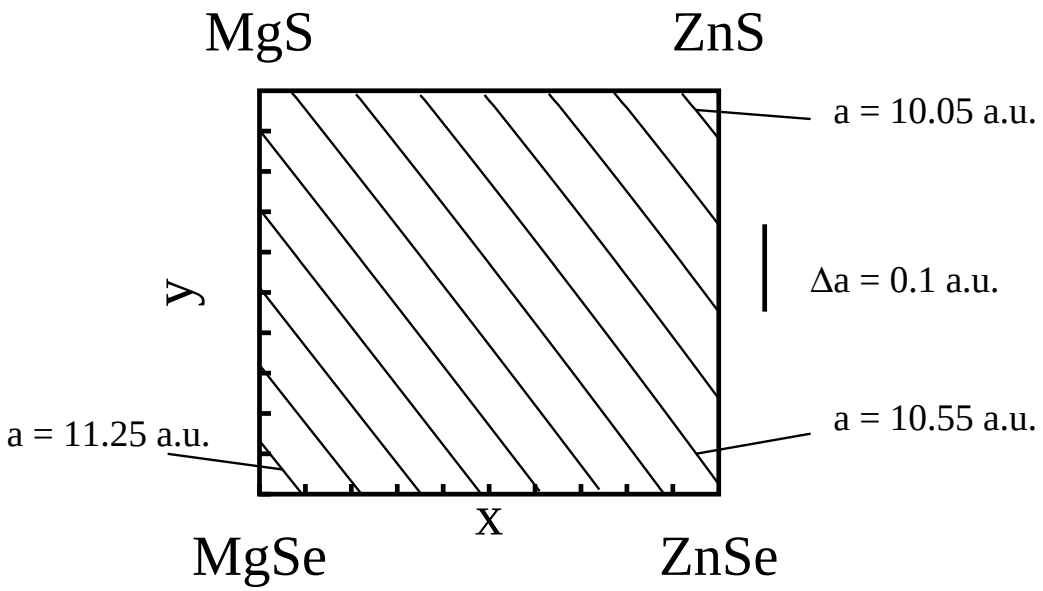

Figure 4.13: Theoretical lattice parameter as functions of the compositions, at $T = 800\ K$, given in atomic units.

critical temperature, obtained fitting a delta-lattice parameter model [71] to experimental lattice constants, locates T_c between 525 K and 625 K. Our results are in very good agreement with this estimate.

Due to the low diffusity of atoms, it is always difficult to determine experimentally the miscibility gaps in semiconductor alloys. In the only experimental measure [9] we are aware of, a miscibility gap is observed to occur, at room temperature, *at least* in the region indicated by the rectangle in Fig. 4.12. Our calculations accordingly predict that in that portion of the square a miscibility gap opens already at $T = 400\ K$.

4.3.2 Structural properties

The MonteCarlo simulations give access also to relevant information on the structural properties of the quaternary $Zn_xMg_{1-x}S_ySe_{1-y}$ alloy.

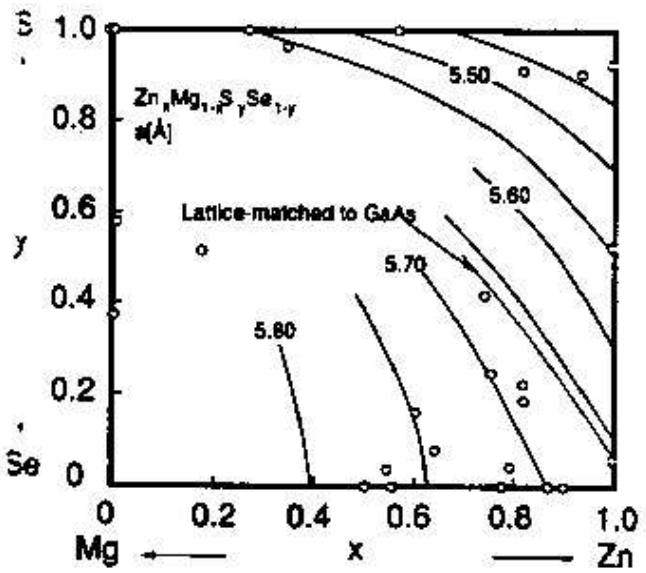

Figure 4.14: Experimental lattice parameter as functions of the compositions.

In Fig. 4.13 we report our prediction about the equilibrium lattice parameter of the alloy at $T = 800\ K$, well above the critical temperature of the system. The results show a strong linear dependence upon compositions, following Vegard's law. This result, if compared with the experiments (see Fig. 4.14), show a good agreement in the Zn-rich region, especially in proximity of pure ZnSe, while the agreement is poor in the magnesium-rich region, where the instability of the system makes it very difficult to measure with the same precision the concentrations. There are in fact very few experimental points, so that the drawn fitting lines are broken in that region. Furthermore, our results are appropriate in conditions of thermodynamic equilibrium, which is not necessarily reached in semiconductor growth processes, being the diffusion coefficients usually very small in solid semiconductors.

The above result refers to the average lattice constant of the alloy in the experimental sample or in the simulations supercell. It is interesting to detect in more detail the occurrence of local distortions due to presence of different chemical species. To this end, we studied, for different values of the concentrations, the bond-length distributions in the disor-

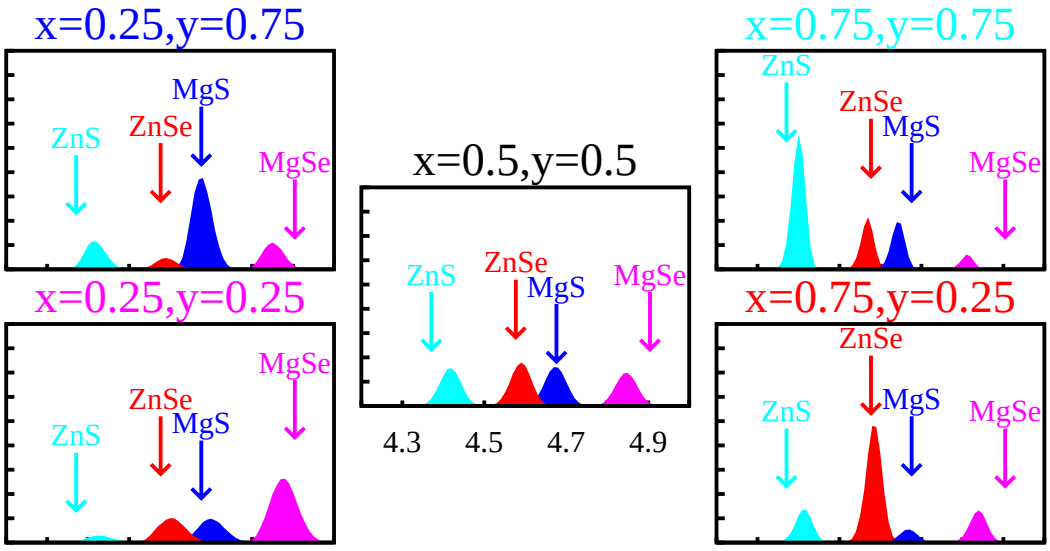

Figure 4.15 (color): Bond-length distributions (in atomic units) for $(x, y) = (0.5, 0.5)$, $(x, y) = (0.25, 0.25)$, $(x, y) = (0.25, 0.75)$, $(x, y) = (0.75, 0.25)$ and $(x, y) = (0.75, 0.75)$. The arrows indicate the bulk-like bond-lengths of the pure compounds.

dered alloy. The results are displayed in Fig. 4.15 where 4 separate peaks, corresponding to $Zn - S$, $Zn - Se$, $Mg - S$ and $Mg - Se$ bond lengths, are observed. In the same pictures the ideal (bulk) bond lengths are reported with arrows. It is evident that, at any concentration, the bond-lengths are very close to the values they have in the pure constituents. This result is in agreement with EXAFS measurements reported in Ref. [13]. In particular, this is true for $Zn - Se$ and $Mg - S$, whose ideal lattice parameters are close to the lattice constants of the alloy at the different concentrations. The largest deviations are smaller than 2%.

4.3.3 Short-range order

From our calculations, the quaternary solid solution is found to be stable as a disordered alloy above $T \approx 520 - 550\ K$, that is, in the range of the typical growth temperatures. It is interesting to study the clustering tendency of the system also before the segregation transition at T_c, in order to understand if the appearance of nucleation of the pure constituents is important also at high temperature.

In order to clarify this issue we have calculated the two-body correlations of the system at temperatures of complete miscibility. The correlation function is defined as:

$$C_{ss'}(\mathbf{R}) = \langle \sigma_{s\mathbf{R}'} \sigma_{s'\mathbf{R}+\mathbf{R}'} \rangle - \langle \sigma_{s\mathbf{R}'} \rangle \langle \sigma_{s'\mathbf{R}'} \rangle; \tag{4.6}$$

therefore, $C_{ss'}(\mathbf{R}) = 0$ in the perfectly random alloy, and $C_{ss'}(\mathbf{R}) = \pm 1$ for the pure materials.

The determination of the thermodynamic properties of the system has been obtained by adopting the Glauber dynamics method discussed in Section 4.2.1. The correlation functions of the system, that we study above the critical temperature, are instead better determined at fixed compositions, avoiding fluctuations of the average concentrations that occur in MonteCarlo simulations performed at fixed chemical potentials and at different temperatures. To this end, we perform simulation in a canonical ensemble, in the sense that we fix the concentrations and our trial move is no more a spin-flipping, but an exchange of spins between a randomly chosen pair of cations or anions. This scheme is commonly referred to as *Kawasaki dynamics* [67]. The number of particles of each chemical species does not vary and so the results do not depend on the chemical potential. In this way the energetically most favored dispositions of the atoms on the lattice is obtained and it is easier to analyze the possible nucleation of clusters of pure materials.

In order to obtain the true minimum energy configuration and to avoid that the system remained trapped in metastable configurations, it has been necessary to use a simulated annealing technique, starting the simulations from very high temperatures and then cooling down slowly the system. Every annealing cycle begins from the last configuration of the previous run, with a slightly lower temperature. The temperature step, ΔT, between the simulations was 25 K in the high-temperature runs, and reduced to 5 K in proximity of T_c. The number of simulation steps was of the order of 10^4 in the high-T simulations, and increased, in the lower-temperature runs, up to 10^5.

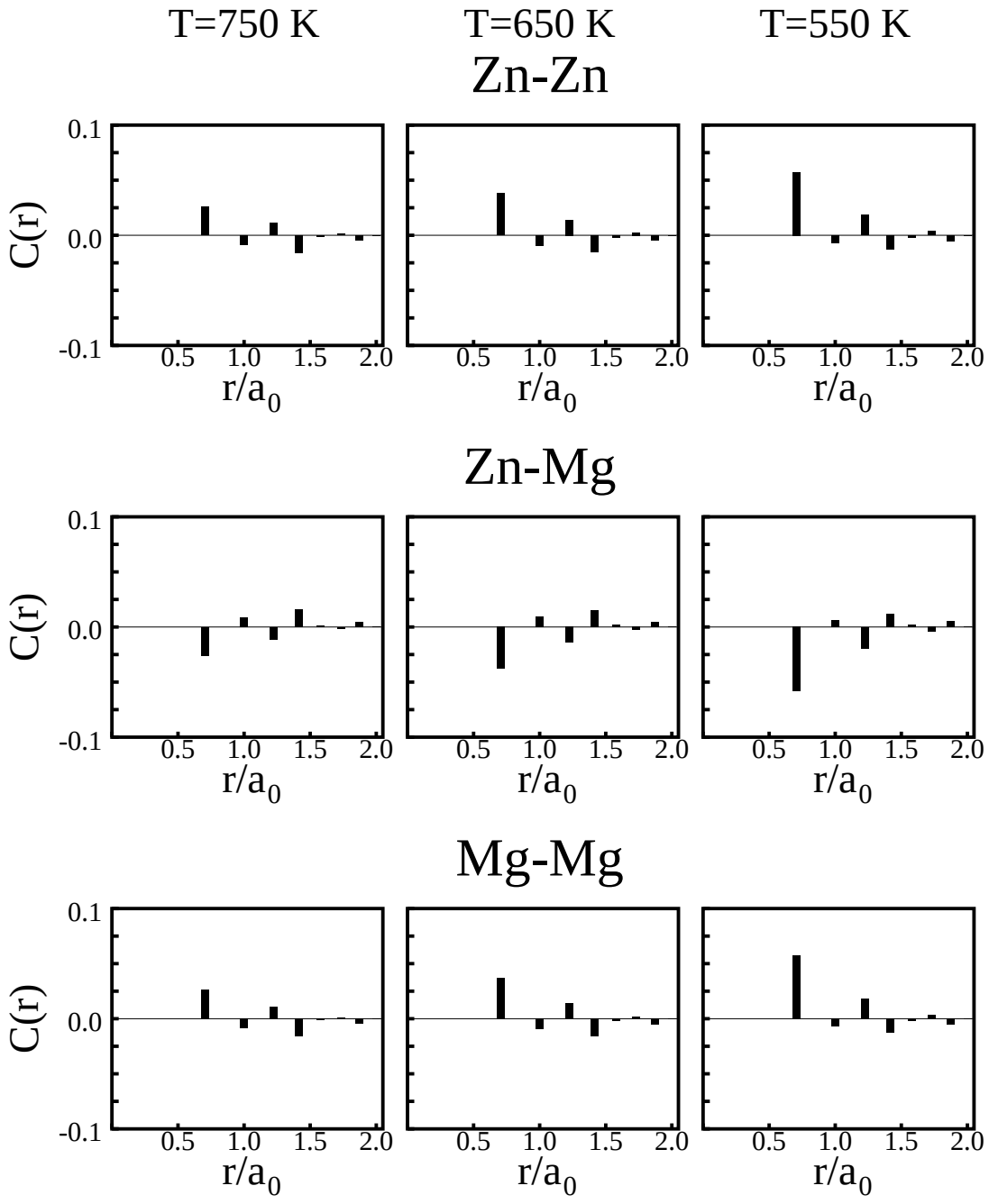

Figure 4.16: Two-body correlations of $Zn_{\frac{1}{2}}Mg_{\frac{1}{2}}S_{\frac{1}{2}}Se_{\frac{1}{2}}$ in the cationic sublattice at three different temperatures.

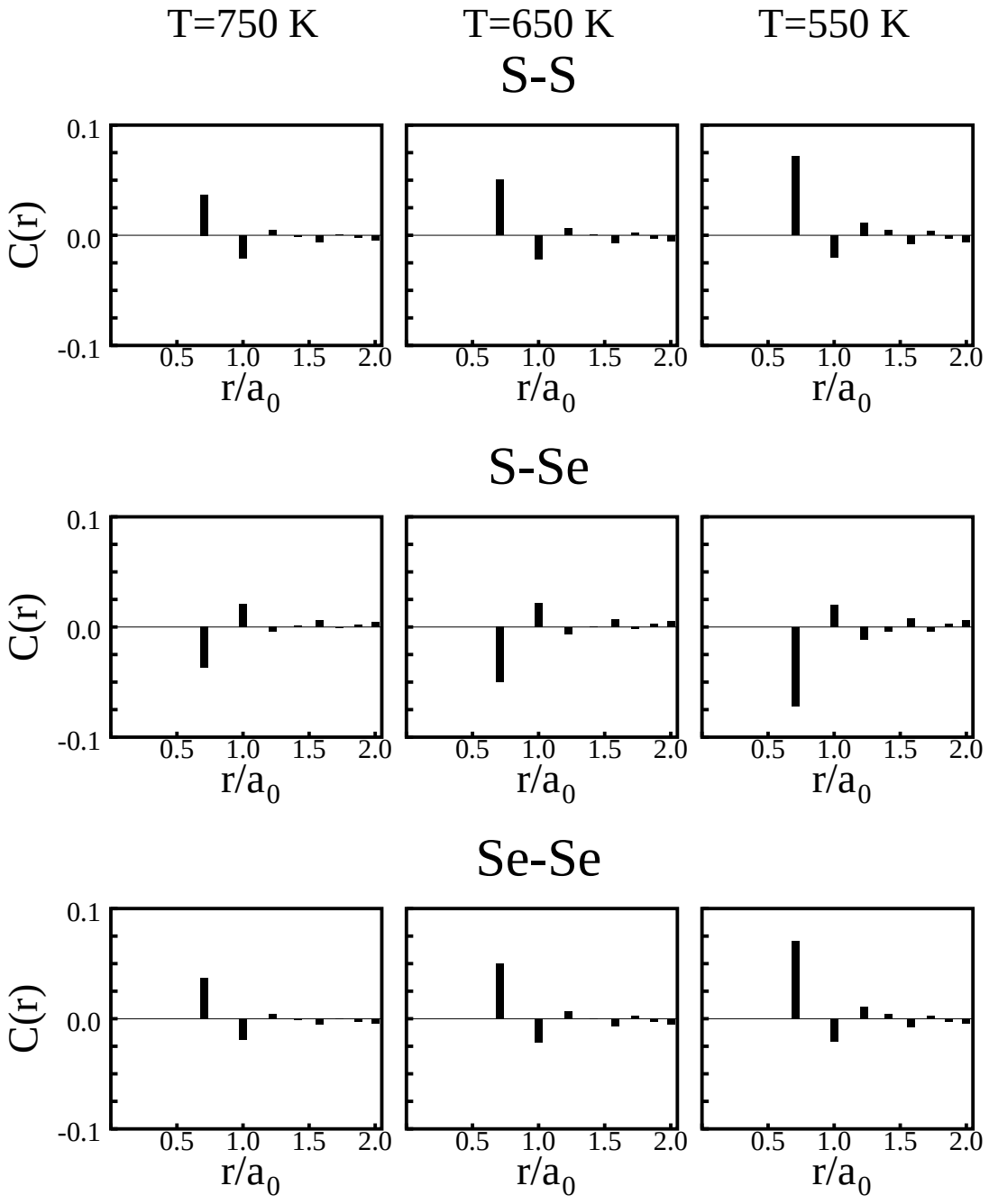

Figure 4.17: Two-body correlations of $Zn_{\frac{1}{2}}Mg_{\frac{1}{2}}S_{\frac{1}{2}}Se_{\frac{1}{2}}$ in the anionic sublattice at three different temperatures.

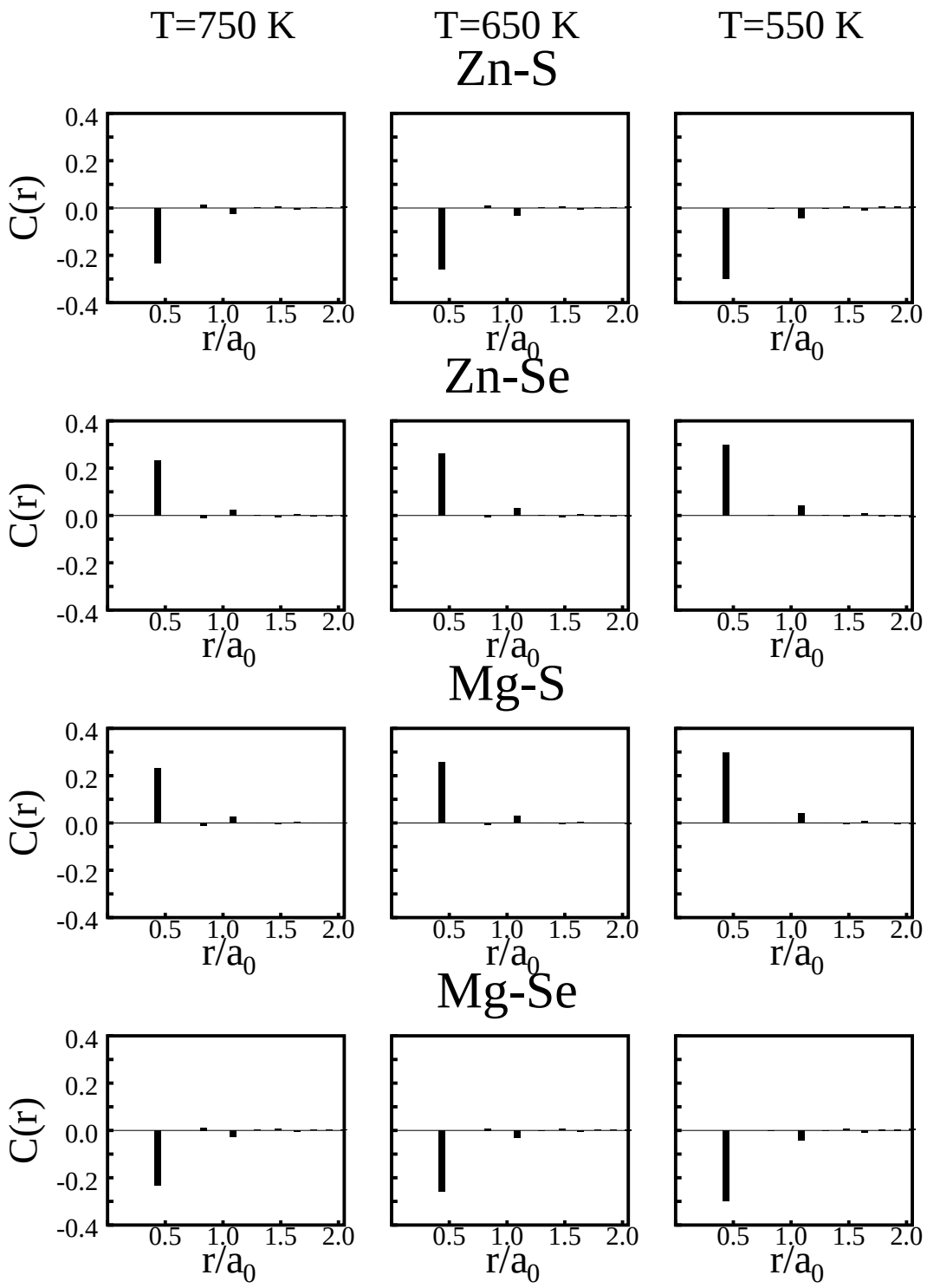

Figure 4.18: Two-body "mixed" cation-anion correlations of $Zn_{\frac{1}{2}}Mg_{\frac{1}{2}}S_{\frac{1}{2}}Se_{\frac{1}{2}}$ at three different temperatures. Note that the order of magnitude is larger than in the previous pictures.

In Fig. 4.16 we show the two-body correlations of $Zn_{\frac{1}{2}}Mg_{\frac{1}{2}}S_{\frac{1}{2}}Se_{\frac{1}{2}}$ alloy in the cationic sublattice, *i.e.* zinc-zinc, zinc-magnesium and magnesium-magnesium. In the first shell of nearest-neighbors of the sublattice the Zn – Zn and the Mg – Mg correlation functions have a positive signs, and their value increases going down in temperature, while, as counterpart, the first Zn – Mg peak has negative sign. This indicates a tendency to clusterization of like-cations. The same behavior is found, in Fig. 4.17, in the anionic sublattice, where the sulphur-sulphur and the selenium-selenium first peaks are positive and become larger and larger as the temperature decreases, while the S – Se first-shell correlations is negative, indicating also in the anionic sublattice a clusterization of like atoms.

In Fig. 4.18 we display the two-body cation-anion correlations. Note that in this case the scales are expanded, being the correlations peaks much stronger. We observe that for the first nearest-neighbors shell the correlation function is very large and positive for Zn – Se and Mg – S even at high temperature, while it is large and negative for Zn – S and Mg – Se. This is the signal of a strong tendency to clusterization of the former compounds, while the latter are unfavored especially because of the large elastic cost that they have to pay at the lattice constant of the alloy at this concentration [$a_0(Zn_{\frac{1}{2}}Mg_{\frac{1}{2}}S_{\frac{1}{2}}Se_{\frac{1}{2}}) \approx 10.68$ a.u.].

The relevance of short-range correlations to the electronic properties of the alloy will be examined in the next chapter.

5 Electronic properties of the alloy

As discussed in the Introduction, the technological interest in the $(Zn, Mg)(S, Se)$ solution is related to its optical properties: the fundamental band gap of such alloy ranges from the green-blue up to the ultraviolet wavelength regions. The study of the electronic properties should be performed in three step: *i)* the determination of the equilibrium structural properties, obtained and discussed in the previous chapter; *ii)* an efficient approach in dealing with the compositional disorder; *iii)* the inclusion of electronic correlations. It is however very hard to combine such many-body terms with a proper description of disorder. In the following part of the work, we will thus assume that disorder and quasi-particle effects act separately: we will deal explicitly with compositional disorder at LDA level, and many-body terms will be added as semi-empirical corrections.

5.1 Special quasi-random structures

The special quasi-random structures (SQS) approach to the study of the electronic properties of alloys, described in Section 2.6, relies on the hypothesis that the band structure of a (bulk or disordered) material is affected mainly by the local environment. The chemical nature of the atoms beyond the fourth or fifth shells of neighbors seems to have little or negligible effects on the electronic properties of the system [20, 72]. A disordered solution can thus be mimicked by using rather small supercells that reproduce as better as possible

the alloy short-range order (SRO).

In the present work, a threefold generalization to the SQS method, as described in the original formulation by Zunger and co-workers [20], has been carried out: *i)* it has been extended to the quaternary alloy case; *ii)* several different concentrations has been considered; *iii)* short-range order effects have been included. For any fixed concentration(s), we have considered the correlation functions $C_{ss'}(\mathbf{R})$ (see Eq. 4.6) taken at $T = 550\ K$, close to typical growth temperatures. This is a reasonable choice in the purpose of studying the alloy properties even at lower temperatures, since the low diffusivity of atoms in semiconductor alloys "freezes" them in the initial configuration, determined by the experimental growth conditions, even when the external temperature is decreased down to room temperature or below.

We have generated three families of SQS's, whose crystal lattice are respectively: a 64-atom simple cubic cell (SC64), a 128-atom fcc supercell (FCC128), and a 216-atom simple cubic cell (SC216). The determination of the most appropriate atomic configurations in the SQS's has been carried out with a simulated annealing technique. Given a structure belonging to one of the three families, and a correlation function $C_{ss'}(\mathbf{R})$ as obtained from the MonteCarlo simulations, the purpose is to find a distribution $\{\sigma\}$ of the atoms on the lattice whose associated (supercell) correlation function $\bar{C}_{ss'}(\mathbf{R})$, is as similar as possible to the MonteCarlo-determined one. To this end, we define a *cost function* as:

$$W[\{\sigma\}] = \sum_{ss'\mathbf{R}} g(\mathbf{R}) |C_{ss'}(\mathbf{R}) - \bar{C}_{ss'}(\mathbf{R})|^2, \tag{5.1}$$

where $g(\mathbf{R})$ are weights assigned to each shell of neighbors. The arbitrariness in their choice is exploited to obtain a better description of short-range order in the nearest shells. The recipe we have followed reads:

$$g(\mathbf{R}) \propto \frac{1}{\mathbf{R}^n} \theta(\bar{\mathbf{R}} - \mathbf{R}), \tag{5.2}$$

where $1 \leq n \leq 4$, and the step function limits the summation in Eq. 5.1 to distances smaller than a cutoff radius $\bar{\mathbf{R}}$. Through the choice of different values of n and/or of a cutoff radius, a number of different SQS's may be generated.

To minimize the cost function avoiding being trapped in local minima, we performed a MonteCarlo simulated annealing by introducing a fictitious temperature and a related Boltzmann probability, whose expression has the standard form:

$$P[\{\sigma\}] = e^{-\beta W[\{\sigma\}]}. \tag{5.3}$$

The starting configuration of the MC annealing cycles is chosen by disposing all the particles around the central atom according to the probability related to the two-body correlation and with the appropriate concentration of the alloy to mimic. A Kawasaki dynamics is developed [67]: at each iteration, two particles belonging to the same sublattice are randomly chosen and their spin are exchanged. The trial move is accepted or rejected according to a Metropolis algorithm. During the simulation, the fictitious temperature is lowered very slowly, until the system reaches the minimal error configuration.

To test the effectiveness of the method to reach the true minimum, we have used the correlation functions of highly-ordered configurations, as for instance a $(ZnS)_1(MgSe)_1$ (001)-oriented superlattice. Despite the high inhomogeneity of such a configuration, the technique rapidly drives the system in the correct minimum and we can expect it to be successful also in the more homogeneous case of a disordered alloy. In Fig. 5.1 we compare, as an example, the MonteCarlo Zn – Se two-body correlation function of the $Zn_{\frac{1}{2}}Mg_{\frac{1}{2}}S_{\frac{1}{2}}Se_{\frac{1}{2}}$ alloy at $T = 550\ K$ with the analogous correlation function obtained for a 128-atom SQS. The accuracy of the SQS approach is very good in the first four cation-anion shells (that correspond to eight shells of cationic and anionic neighbors), while at larger distances a few spurious peaks, due to the periodicity of the supercell, appear. The effect of such distant neighbors on the electronic bands is very small. In fact, we have compared the band energies of

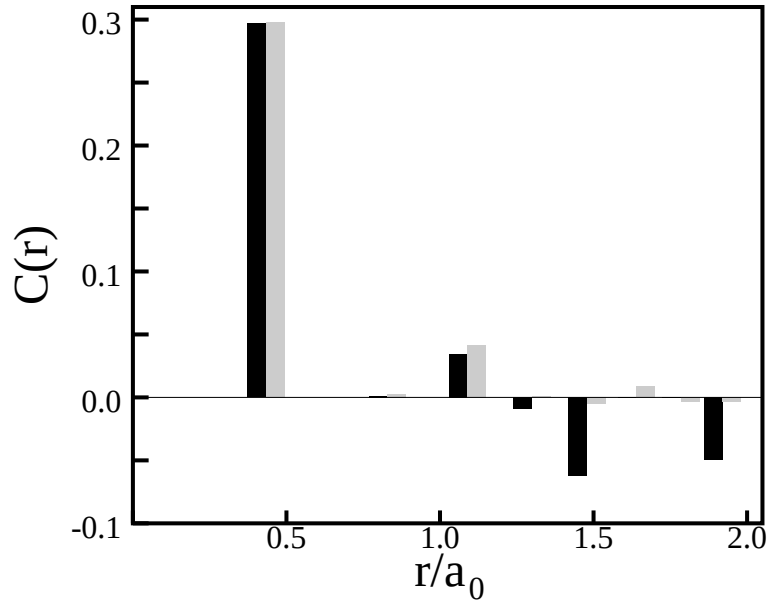

Figure 5.1: Comparison between 1024-atom-MonteCarlo (gray) and 128-atom-SQS (black) $Zn-Se$ two-body correlation function of $Zn_{\frac{1}{2}}Mg_{\frac{1}{2}}S_{\frac{1}{2}}Se_{\frac{1}{2}}$ at $T = 550\ K$.

SQS's, determined with different choices of the weights $g(\mathbf{R})$, whose correlation functions were different only far from the origin, obtaining the same results within the precision of the calculations ($0.01\ eV$).

As discussed above, a number of equivalent SQS's is obtained for any concentration. The choice of the structures to be actually used for the electronic bands calculations, among those ones given by the previously discussed approach, is then made on the basis of first- and second-nearest-neighbors distributions: as shown in Fig. 5.2, we choose the supercells whose distributions are the most similar to the MonteCarlo ones, which, in turn, are very close to binomial distributions. Through this recipe we obtain SQS's better describing the details of the local environment with respect to the original formulation [20], in which only the mean values of the distribution functions are used. This difference seems however to affect very little the electronic bands of the system.

Given a configuration, in order to calculate the band structure it is necessary to know the relaxed position of the atoms in the cell. The computational effort needed for the *ab-*

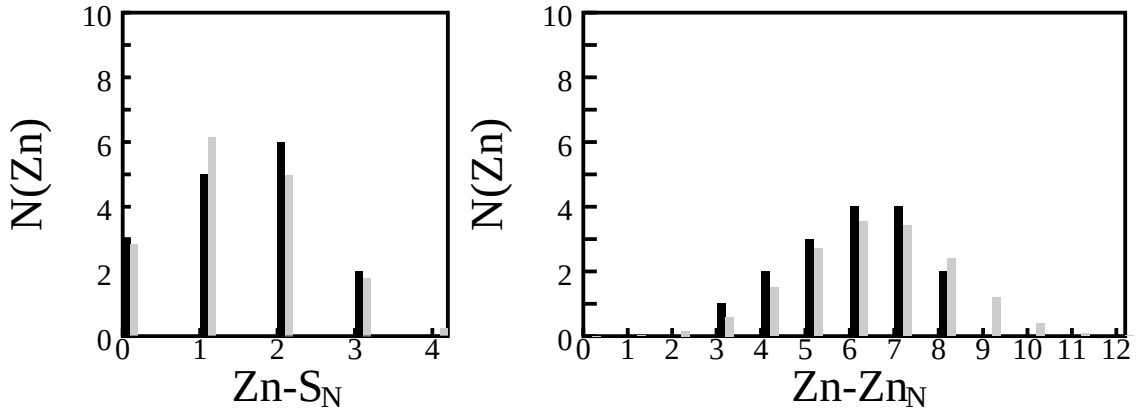

Figure 5.2: Comparison between MonteCarlo (gray) and 64-atom-SQS (black) atomic distributions of particles in the first and second shells of neighbors. In the left panel we display on the horizontal axis the five possible numbers of S atoms tetrahedrally bonded to a Zn atom and on the vertical axis the number of such different clusters present in the cell (normalized to 32 also for the MonteCarlo distribution). In the right panel we analogously show the $Zn - Zn_N$ cluster distribution in the cationic sublattice.

initio calculation of the relaxed geometry of up to 64-atom supercell is still reasonable with modern computers and parallel codes. For the larger cells such calculations are possible but not very practical. We use for the calculation of the electronic properties of such larger supercells the relaxed positions obtained in the DFPT framework through Eq. 2.40. The validity of such approximation is confirmed by the comparison of the electronic density of states (DOS) obtained using the relaxed positions of DFPT and those ones coming from DFT-self-consistent calculations.

In Fig. 5.3 we display the electronic density of states in the gap region, calculated at the Γ point of the SC64 supercell with ideal, fully relaxed, and DFPT-relaxed positions of atoms. It is evident that the two latter curves are almost indistinguishable, while the DOS with ideal lattice positions is very different. This indicates that the effect of ionic relaxation is accurately accounted for within the perturbative approach which we therefore decide to adopt in the following.

In a disordered system the meaning of the band picture commonly used for bulk materials

is weaker, due to the lack of translational invariance. The band-structure picture is however still valid, and observed experimentally. It is interesting to construct the pseudo-band structure of the alloy by projecting SQS eigenfunctions, calculated on a set of $\mathbf{k}$ points of the supercell Brillouin zone, onto the corresponding refolded $\mathbf{k}$ points of the zincblende structure. This is important in determining the direct or indirect nature of the fundamental band gap.

The projected electronic density of states of the alloy is obtained from the wavefunctions of the supercells by the simple expressions:

$$n_{\mathbf{k}_{ZB}}(\epsilon) = \sum_i \delta(\epsilon - \epsilon_i) \sum_{\mathbf{k}_{SQS}} |\langle \psi_{i,\mathbf{k}_{SQS}} | P_{\mathbf{k}_{ZB}} | \psi_{i,\mathbf{k}_{SQS}} \rangle|^2, \tag{5.4}$$

where $\mathbf{k}_{ZB}$ and $\mathbf{k}_{SQS}$ are the reciprocal-space points corresponding to the elementary cell and to the supercell respectively, $\psi_{i,\mathbf{k}_{SQS}}$ is the i-th eigenfunction of the SQS calculated in $\mathbf{k}_{SQS}$ and ϵ_i is the corresponding eigenvalue, and $P_{\mathbf{k}_{ZB}}$ is the projector on the elementary cell $\mathbf{k}$-points:

$$P_{\mathbf{k}_{ZB}} = \sum_{\mathbf{G}} |\mathbf{k}_{ZB} + \mathbf{G}\rangle\langle \mathbf{k}_{ZB} + \mathbf{G}|, \tag{5.5}$$

where $\mathbf{G}$ are the reciprocal-space vectors.

Analogously, it is possible to project the superlattice eigenvectors onto the atomic pseudo-wavefunction, in order to get information about the contributions of the different kinds of atoms to the total DOS. This may be useful in understanding the main features of alloy band structure and energy gaps in terms of the electronic properties of the pure constituents.

We have also tested the dependence of the fundamental band gap as function of the number of particles present in the SQS supercell. We display in Fig. 5.4 the band gap of three $Zn_{\frac{1}{2}}Mg_{\frac{1}{2}}S_{\frac{1}{2}}Se_{\frac{1}{2}}$ structures containing 64, 128 and 216 atoms, and we see that with such SQS's this quantity is well converged, within 0.01-0.02 eV.

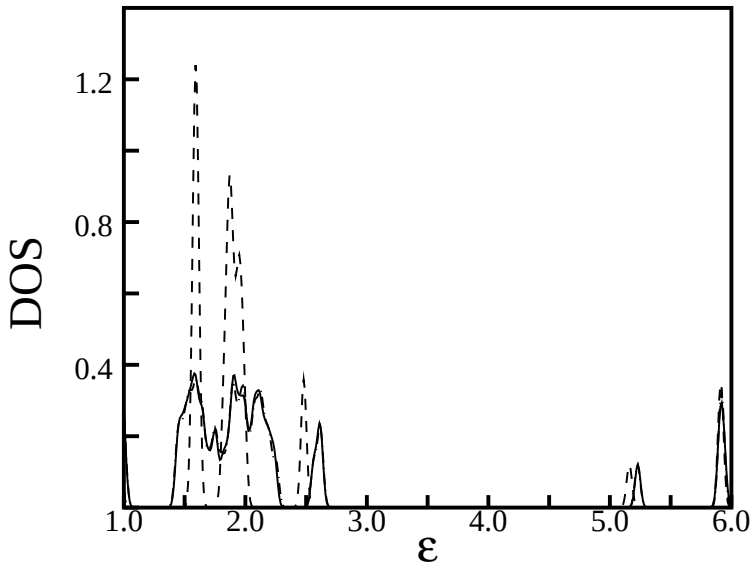

Figure 5.3: Electronic density of states, in a energy range that includes the fundamental gap, of a 64-atom-SQS, calculated for the Γ point of the supercell, with ideal (dashed), relaxed according to DFPT (dotdashed) and fully relaxed (solid) atomic positions. Energies are given in eV, while the DOS is in arbitrary units.

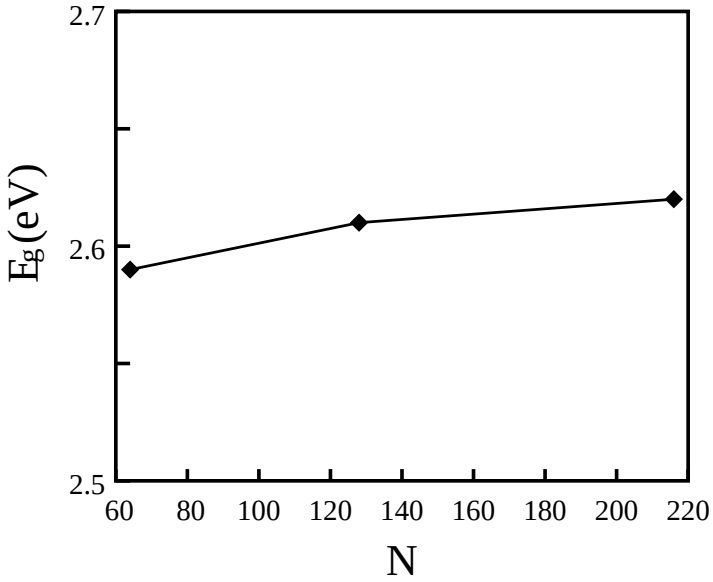

Figure 5.4: Fundamental energy gap in the $Zn_{\frac{1}{2}}Mg_{\frac{1}{2}}S_{\frac{1}{2}}Se_{\frac{1}{2}}$ alloy as function of the number of particles contained in the supercell. The diamonds refer to 64-, 128- and 216-atom-SQS.

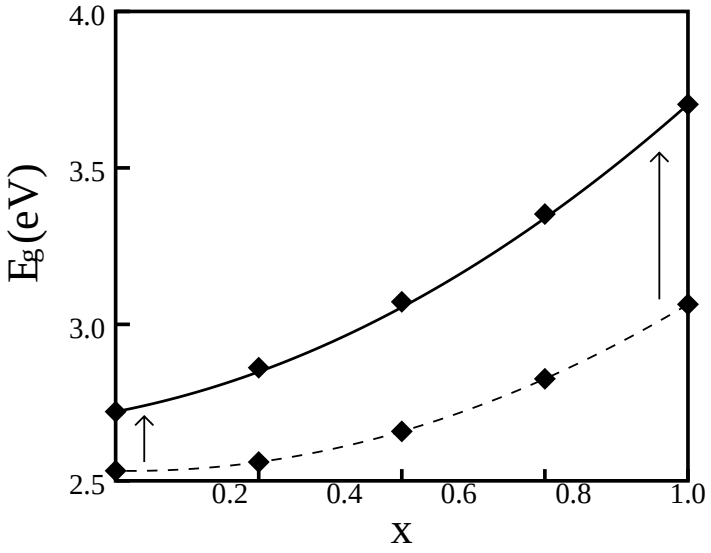

Figure 5.5: Energy gap of the Zn(S, Se) pseudobinary alloy as function of the composition. Experimental findings are represented by the solid line; the theoretical results are shown with diamonds, and the dashed line is a quadratic fit to them. The diamonds close to the experimental line are the "corrected" theoretical gaps.

5.2 ZnS_xSe_{1-x}: energy gap *vs.* composition

The electronic properties of the Zn(S, Se) pseudobinary alloy, which are well characterized experimentally, have been studied by the techniques expounded above, at three different concentrations, *i.e.* $x = 0.25, 0.50, 0.75$, using SC64 supercells.

In Fig. 5.5 we display our results on the fundamental band gap of the alloy and compare them with available experimental data. As previously discussed, LDA calculations systematically underestimate the optical gap. Adding a simple linear interpolation of the errors done at the pure-compound extremes, brings our theoretical predictions in very good agreement with experiments.

Our data so corrected can be accurately interpolated by the formula:

$$E_g = E_g(\mathrm{ZnSe}) + bx + cx^2, \tag{5.6}$$

where the curvature, commonly known as *bowing parameter*, is $c \approx 0.56eV$. Experiments

accordingly report $0.41eV \leq c \leq 0.63eV$ [73, 74]. It is worth noting that the virtual crystal bowing parameter is small and *negative*: $c \approx -0.1eV$.

The accuracy by which the theoretical calculations catch the non-linear dependence of the band gap upon the composition in the pseudobinary ZnS_xSe_{1-x} alloy indicates an almost linear dependence of quasi-particle effects on the concentration; the hypothesis that they act separately from the disorder is thus satisfactorily fulfilled. This is encouraging for the study of the quaternary alloy electronic properties, for which the available experimental data are less precise.

5.3 Electronic properties of $Zn_xMg_{1-x}S_ySe_{1-y}$

We report results on the electronic properties of the alloy along the line of lattice-matching to GaAs, which is the typical substrate on which such alloys are grown and whose lattice constant is $a_0 = 10.68$ a.u.. In particular, we have studied three different concentrations along that line, chosen among the discrete set of compositions compatible with our finite (64-atom) supercell and close to the ZnSe-rich region: $(x, y) = (\frac{1}{2}, \frac{1}{2}); (\frac{3}{4}, \frac{1}{8}); (\frac{27}{32}, 0)$.

5.3.1 Band structure and energy gap

It is interesting to compare the results obtained using different levels of approximations to the true alloy, in order to understand, and possibly to isolate, the different contributions to the physical properties of the system. In Fig. 5.6 we display the energy gap as a function of the cationic composition, as obtained from calculations performed *i)* on the appropriate virtual crystal, *ii)* on supercells describing the perfectly random alloy, and *iii)* on SQS's that reproduce the SRO correlations obtained from the MonteCarlo simulations.

We see that virtual-crystal is a bad approximation of the real system, while the effects of SRO show up in a slight opening of the fundamental band gap, as shown also in Table 5.1.

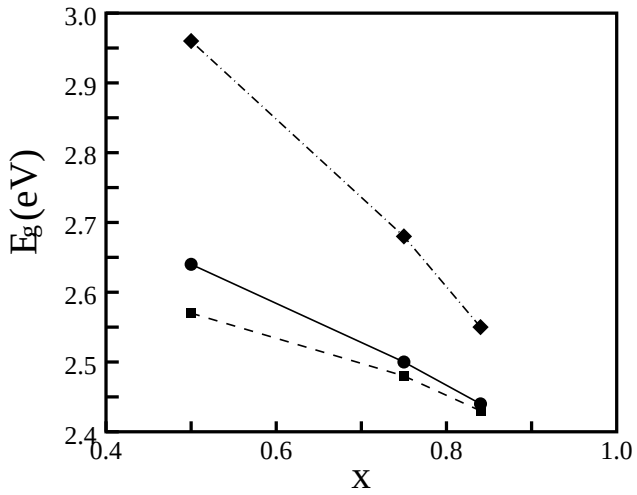

Figure 5.6: Energy gap of the (Zn, Mg)(S, Se) pseudobinary alloy as function of the x composition, indicated with the diamonds. The corresponding y composition is given in the text. The dotdashed line refers to virtual crystal calculations, the dashed one to perfectly-random-alloy SQS results and the solid line to the short-range-ordered alloy band gaps.

As expected, such differences are larger for $(x, y) = (\frac{1}{2}, \frac{1}{2})$, where the system is the farthest from the pure-materials limit. The discrepancies become smaller moving towards the pure-compounds corners, where the three different situations merge in the same.

It is interesting to analyze how the bulk-like states are refolded in the reduced Brillouin zone of the supercell. In Fig. 5.7 we project, according to Eq. 5.4, the electronic density of states of the $Zn_{\frac{1}{2}}Mg_{\frac{1}{2}}S_{\frac{1}{2}}Se_{\frac{1}{2}}$ alloy on the Γ point of the zincblende structure BZ. The eigenvectors at the top of the valence and at the bottom of the conduction bands actually have a strong Γ character. The direct-gap nature of the pure materials is thus conserved also in the alloy.

	Energy gap		
x	SRO	Random	Virtual
0.50	2.64	2.57	2.96
0.75	2.50	2.48	2.68
0.84	2.44	2.43	2.55

Table 5.1: Energy gap *vs.* composition for the alloys in which SRO effects are taken into account, for the perfectly random solutions, and for the virtual-crystal. Energies are in eV.

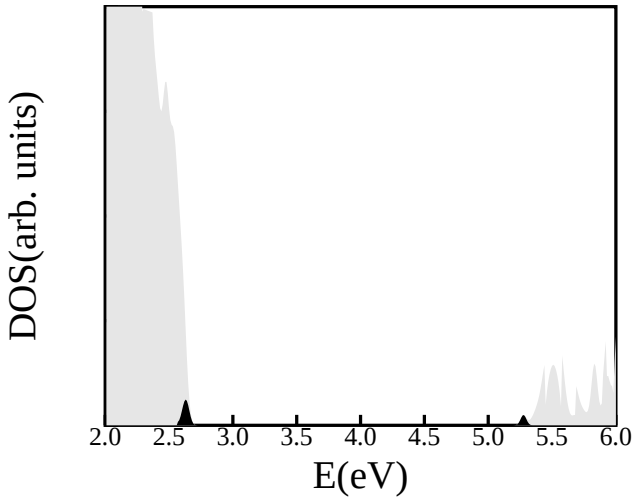

Figure 5.7: Electronic density of states of $Zn_{\frac{1}{2}}Mg_{\frac{1}{2}}S_{\frac{1}{2}}Se_{\frac{1}{2}}$ in the gap window (gray) and its projection on the Γ point of the zincblende structure (black).

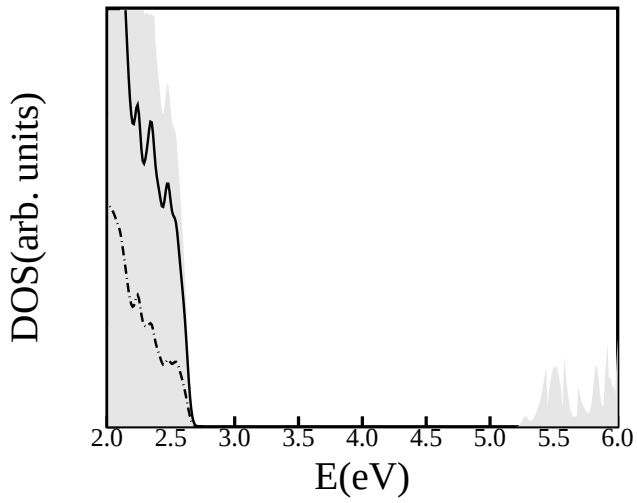

Figure 5.8: Electronic density of states of $Zn_{\frac{1}{2}}Mg_{\frac{1}{2}}S_{\frac{1}{2}}Se_{\frac{1}{2}}$ in the gap window (gray) and its projection on the Se (full line) and S (dotdashed line) atoms.

5.3.2 Analysis of the short-range-order effects

The effects of SRO on the electronic properties of the system have been studied on the $Zn_{\frac{1}{2}}Mg_{\frac{1}{2}}S_{\frac{1}{2}}Se_{\frac{1}{2}}$ solution. We have used FCC128 or SC216 SQS's, being the details of the electronic density of states more sensitive to the supercell size, with respect to the fundamental gap which appears to be well converged already with SC64 cells.

The first step of such study consists in the analysis of the different atomic contribution to the electronic density of states of the alloy. This has been done by projecting the SQS eigenfunctions on the orthogonalized atomic orbitals. In Fig. 5.8 we show the total DOS of the $Zn_{\frac{1}{2}}Mg_{\frac{1}{2}}S_{\frac{1}{2}}Se_{\frac{1}{2}}$ *non-random* alloy and its projection onto the anionic valence orbitals. It is evident that the anions give by far the larger contribution to the states at the top of the valence band, and this is consistent with the common picture of polar semiconductors, in which the valence states have a strong anionic character, while the conduction states are essentially cation-like. In particular, the contribution of Se orbitals to the electronic DOS

		ψ_v				ψ_c			
	E_g	Zn	Mg	S	Se	Zn	Mg	S	Se
SRO	2.63 eV	0.05	0.01	0.26	0.67	0.28	0.33	0.21	0.17
Rand.	2.56 eV	0.04	0.02	0.23	0.70	0.27	0.33	0.25	0.14

Table 5.2: Energy gap and projection of the top-valence and of the bottom-conduction states on the anions for the SRO and the perfectly random alloys and for the virtual-crystal.

appears to be of the order of $\approx$ 70 %, while the projection on sulphur atoms is slightly above 20 %. Such effects may be actually understood in terms of the electronic properties of the pure materials. Using Harrison's tight-binding tables [75], we find that the top of the valence band states of S-compounds lie about 0.5 eV below the analogous states of the corresponding Se-compounds.

In Table 5.2 we compare the energy gap and the projection onto the anions of the top of the valence (ψ_v) and of the bottom of the conduction (ψ_c) bands states for the SRO and the perfectly random alloy. We see from this table that to the slight difference in the band gap between the short-range-ordered and the random $Zn_{\frac{1}{2}}Mg_{\frac{1}{2}}S_{\frac{1}{2}}Se_{\frac{1}{2}}$ alloys corresponds a slight difference in the contribution of the anions to the states that determine the gap. The Zn and Mg contributions appear to be practically independent of the local environment. The difference between the two gaps is due to a different energy value of ψ_c, being the energy of ψ_v equal in the two cases. Analyzing the projection of ψ_c on the anionic states, we see that the conduction state is rather delocalized on the four atomic species. In the true, non-random, alloy the selenium-orbitals character is slightly stronger and that the contribution of the sulphur atoms appear instead to be smaller than in the random case.

This difference can be qualitatively understood in terms of pure materials properties: in Fig. 5.9 we display again the electronic DOS of the short-range-ordered $Zn_{\frac{1}{2}}Mg_{\frac{1}{2}}S_{\frac{1}{2}}Se_{\frac{1}{2}}$

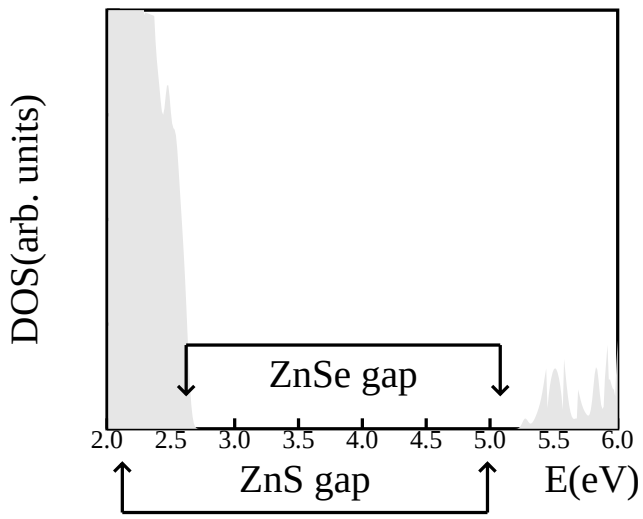

Figure 5.9: Electronic density of states of $Zn_{\frac{1}{2}}Mg_{\frac{1}{2}}S_{\frac{1}{2}}Se_{\frac{1}{2}}$ in the gap window (gray), and the fundamental band gaps of Zn-chalcogenides, with the valence-band-offset predicted by Harrison's model.

solution near the fundamental gap, and we report the band gaps of the pure Zn chalcogenides, aligned with the Harrison's handbook valence-band-offset. The energy gaps of the Mg compounds are larger, and in this simplified picture we assume their effect on the alloy electronic properties to be less important. In such a qualitative analysis, the bottom of the conduction states of ZnS and ZnSe are very close in energy, and in particular the zinc-sulfide level appear to be slightly lower. The closeness of such levels may explain the delocalization of the ψ_c state, at variance with ψ_v that appears to be much more localized, being the energy top-valence levels of the Zn compounds quite distant.

The fact that the state at the bottom of the conduction band of ZnSe is higher than the corresponding level of ZnS could explain the larger gap of the non-random alloy, being in this case the bottom-conduction state more localized on Se than in the random solution. In the random alloy there is another effect that should contribute to lower the energy level of ψ_c and, thus, the fundamental band gap. In such alloy the Zn – S bonds are slightly more stretched than in the true non-random solution. The effect of a small stretching of the

bonds in the bulk ZnS shows up in a reduction of the $\Gamma - \Gamma$ direct gap of the material, and we expect a similar behavior to occur qualitatively also in the alloy. The $Zn - Se$ bond-lengths are instead practically unaffected, being in both cases very close to their bulk values. As a consequence, the difference between ZnS- and ZnSe-like levels is larger in the random alloy with respect to the non-random solution. This may explain the stronger localization of the bottom state of the conduction band in the former case, and is consistent with the gap reduction occurring in the random alloy.

6 Conclusions

In this thesis we have extensively studied the structural, thermodynamic and electronic properties of the quaternary $(Zn, Mg)(S, Se)$ solid solutions and of the pseudobinary alloys related to it. This work has been motivated by a collaboration with the MBE group of the TASC-INFM Labs. in Trieste. From the theoretical point of view, the *ab-initio* perturbative scheme of Density-Functional Perturbation Theory, successfully applied in the past to the study of binary or pseudobinary alloys [38–42], has been generalized to the case of quaternary solid solutions.

The $Zn_xMg_{1-x}S_ySe_{1-y}$ alloy appears to be very promising for opto-electronic applications in the blue-green optical range. At variance with most $II-VI$ alloys, this solution allows one to modulate almost independently the optical gap and the lattice parameter. This property is very important in the purpose of growing solutions, lattice-matched to GaAs, whose optical gaps range in the entire blue-green window.

Our calculations provide the equilibrium structural properties of the alloy. The theoretical lattice constant of the quaternary solution as a function of the compositions is in agreement with experimental data in the ZnSe region of the square of the concentrations, while the agreement is poor in the Mg-rich portion, where strong deviations from the Vegard's law of linearity are claimed in experimental literature. However, the available data in that region are scarce, being the Mg chalcogenides not stable in the zincblende phase; we

believe that non-linear behaviors, if any, occur far from thermodynamic equilibrium. As it is usually found in semiconductor alloys, the lattice constant is an almost linear function of the concentration in spite of the fact that the bond lengths are very close to their bulk-like values, as shown, for the present case, in EXAFS experiments [13].

The large difference among the lattice parameters of the constituents of the alloy is a potential problem, because strain effects induce local clusterizations and, consequently, possible instabilities of the alloy with respect to segregation and a higher density of defects (threading dislocations) in the optical devices. The experimental determination of miscibility gaps and thermodynamically forbidden regions is very difficult. Alternative solutions that overcome the segregation problem have been recently proposed [3, 4], and are based on the MBE growth of superlattices rather than of the homogeneous solutions.

We actually find that the large elastic energies due to the very different equilibrium lattice parameters of the constituents of the alloy induce a significant short-range-order even at very high temperatures. As expected, the ZnSe and MgS local clusterizations are more likely to occur, being their lattice parameter close to the average lattice constant of the alloy for $x = y = \frac{1}{2}$. We report the first *ab-initio* calculation of the phase diagram of a quaternary alloy, that is in agreement with the estimates of T_c based on empirical models and with the few existing experimental data on the miscibility gap. We predict that a separation, below $T = 500\ K$, of a Zn-rich and a Mg-rich phases occur, while the anionic disorder persists also about 50 K below room temperature.

The system is thus thermodynamically stable as a disordered alloy at the typical MBE temperatures, despite the important short-range order effects. Further theoretical investigations are however needed in order to clarify the role of defects in the stability of this material and of the optical devices based on it.

It is worth noting that the growth of the homogeneous solution should be even more

allowed with respect to theoretical predictions: MBE processes occur very far from thermodynamic equilibrium, that is hardly reached by the system due to its low diffusivity. The very nature of the experimental problem is not related to thermodynamic instability, but more probably to the strong—and poorly known—dependence of the sticking coefficient of sulphur atoms on temperature [5]. The inclusion of Be atoms in the alloy has been recently proposed as a solution of such a problem [76].

Our study of the electronic properties of the alloy shows that short-range order effects are important: the optical gap is strongly affected by the local environment, and mean-field approximations are inadequate in the description of the electronic band structure of the solution. The interplay of disorder and quasi-particle effects, not included in our calculations, is verified to be sufficiently small to justify our perturbative approach in the study of optical properties.

Acknowledgments

It is a very hard task to summarize my three-year-experience at SISSA in few lines, as well as to acknowledge all the people that have contributed to make this period of my life so fruitful and pleasant, both from the scientific and from the human points of view.

First, I want to thank my supervisors, Stefano de Gironcoli and Stefano Baroni, that introduced me in this field of research. Both of them, in a different manner, have continuously and very patiently encouraged and helped me with precious suggestions, teaching me a lot of physics and the right way to face physics research. Nonetheless, they have been and are friends, with whom I've shared a lot of nice (not-so-scientific) experiences.

I owe special thanks to the TASC group headed by prof. Alfonso Franciosi, and in particular to Silvia Rubini, always so nice and patient in answering my many questions and in giving me "the latest news" about experimental findings.

I would like to acknowledge Erio Tosatti, for the pleasant and friendly atmosphere he has created in the Condensed Matter sector, and for the important advice he gave me; Sandro Scandolo, always ready to solve small and big problems in office 107 and always joining the *drawing-room conversations* with people continuously coming in the room; Guido Chiarotti, so often the very soul of such conversations. I want to thank also all the staff and secretariat members and system managers, always kind and efficient, and, in particular, the "jokers" Riccardo Iancer & Andrea Parma.

Sabrina Gustin, kind and efficient as INFM secretary, is one of the best person I know and one of my dearest friends, that I will enjoy very much to see again every time I will

come back to Trieste.

There is a huge number of people, not directly involved in my work, that have been very important for me, making my years at SISSA unforgettable. I do not regard Daniele Passerone as a house-mate or a friend, but definitely as a brother, missed a lot in "Villa Elena" during this last year, but "virtually" close to me through the Net. Alice Ruini has been the wonderful companion in all the experiences I've had through these years, the fundamental support, in bad or good mood, and whenever I've needed a friend. Barbara Montanari is SPS and I've enjoyed her true and deep friendship in Trieste and I'm enjoying it now that she lives so far. Franz "Robin Hood" Di Tolla is an elder brother, a great friend and a source of very precious advice, the "booming" Matteo probably is the most pleasant and friendly person I've ever met, Stefano "Tex" Martinelli is a friend on whom I can always rely. I want also to acknowledge the friendship of the "page-boy" Lorenzo and the "page-girl" (one-shot) Antonella, of the sunny Valentina, of the voracious Marco & Alessandro, of my housemates Claudio and Carlo (and Chiara), of Cecilia and Giovanni, of the "New Yorkers" Stefano Serra and Franck Celestini, of Claudia Bungaro, Paolo De Los Rios, Cristina Lavini, Silvia, "Giallo", Catia, Stefano Liberati, Stefano Giovanazzi and many more.

I owe my gratitude to all those people living so far from Trieste, but that have been always so close to me. I thank my parents, my brothers Veronica and Giuliano, and Maria, whose cooking art is now worldwide famous, for the marvellous moral support they have been giving me; Guglielmo, Paolo and Alessandro, and my colleagues Giuliana, Franz, Dino, and Nino that made me continuously feel their friendship; my graduation thesis supervisors Paolo Giaquinta and Franco Buda, that urged me to try this experience, never grudging their encouragement.

My last thanks are devoted to Antonella, for her infinite love and trust in me.

Bibliography

[1] D. Hervé, E. Molva, L. Vanzetti, L. Sorba, and A. Franciosi, IEEE Lett. **31**, 459 (1995).

[2] S. Rubini, A. Franciosi, TASC-INFM, private communication.

[3] J.-S. Kim, S.-H. Suh, C.-H. Kim, and S.-J. Chung, Solid State Commun. **100**, 817 (1996).

[4] B. J. Wu, L. H. Kuo, J. M. DePuydt, G. M. Haugen, M. A. Haase, and L. Salamanca-Riba, Appl. Phys. Lett. **68**, 379 (1996).

[5] J. Han and R. L. Gunshor, in *II-VI Blue/Green Light Emitters: Device Physics and Epitaxial Growth*, ed. by R. L. Gunshor and A. V. Nurmikko, Semiconductor and Semimetals **44**, Academic Press, (1997), p. 17.

[6] S. Fujita, Y. Kawakami, and S. Fujita, Physica B **191**, 57 (1993).

[7] H. Okuyama, K. Nakano, T. Miyajima, and K. Akimoto, Jpn. J. Appl. Phys. **30**, L1620 (1991); J. Cryst. Growth **117**, 139 (1992).

[8] H. Okuyama, F. Hiei, and K. Akimoto, Jpn. J. Appl. Phys. **31**,340 (1992); H. Okuyama, Y. Morinaga, and K. Akimoto, J. Cryst. Growth **127**,335 (1993).

[9] B. J. Wu, J. M. DePuydt, G. M. Haugen, G. E. Höfler, M. A. Haase, H. Cheng, S. Guha, J. Qiu, L. H. Kuo, and L. Salamanca-Riba, Appl. Phys. Lett. **66**, 3462 (1995).

[10] B. Jobst, D. Hommel, U. Lunz, T. Gerhard, and G. Landwehr, Appl. Phys. Lett. **69**, 97 (1996); J. Suda, Y. Kawakami, S. Fujita, and S. Fujita, Jpn. J. Appl. Phys. **33**, 290 (1994); U. Lunz, B. Jobst, S. Einfeld, C. R. Becker, D. Hommel, and G. Landwehr, J. Appl. Phys. **77**, 5377 (1995); M. Ikeda, A. Ishibashi, and Y. Mori, J. Vac. Sci. Technol. A **13**, 683 (1995); E. Oh, S. D. Lee, H. D. Jung, J. R. Kim, M. D. Kim, B. J. Kim, J. K. Ji, H. S. Park, T. I. Kim, S. V. Ivanov, A. A. Toporov, and T. V. Shubina, J. Appl. Phys. **80**, 5951 (1996); A. Toda, T. Asano, K. Funato, F. Nakamura, and Y. Mori, J. Cryst. Growth **145** 537 (1994).

[11] S. Taniguchi, T. Hino, S. Itoh, K. Nakano, N. Nakayama, A. Ishibashi, and M. Ikeda, Electron. Lett. **32**, 552 (1996).

[12] J. M. Gaines, J. Petruzzello, and B. Greenberg, J. Appl. Phys. **73**, 2835 (1993); J. M. Gaines, R. R. Drenten, K. W. Haberrem, T. Marshall, P. Mensz, and J. Petruzzello, Appl. Phys. Lett. **62**, 2462 (1993); D. C. Grillo, Y. Fan, L. He, J. Han, R. L. Gunshor, M. Hagerott, H. Jeon, A. Salokatve, A. V. Nurmikko, G. C. Hua, and N. Otsuka, Appl. Phys. Lett. **63**, 2723 (1993); S. Itoh, H. Okuyama, S. Matsumoto, N. Nakayama, T. Ohata, T. Miyajima, A. Ishibashi, and K. Akimoto, Electron. Lett. **29**, 766 (1993); M. A. Haase, P. F. Baude, M. S. Hagedom, J. Qiu, J. M. DePuydt, H. Cheng, S. Guha, G. E. Hofler, and B. J. Wu, Appl. Phys. Lett. **63**, 2315 (1993).

[13] T. Maruyama, T. Ogawa, K. Akimoto, Y. Kitajima, S. Itoh, and A. Ishibashi, Jpn. J. Appl. Phys. **34**, 539 (1995); T. Maruyama, T. Ogawa, K. Akimoto, Y. Kitajima, S. Itoh, and A. Ishibashi, J. Cryst. Growth **159**, 41 (1996).

[14] S. Guha, J. M. DePuydt, M. A. Haase, J. Qiu, H. Cheng, Appl. Phys. Lett. **63**, 3107 (1993); S. Guha, H. Munekata, and L. L. Chang, J. Appl. Phys. **73**, 2294 (1993); G. C. Hua, N. Otsuka, D. C. Grillo, Y. Fan, M. D. Ringle, J. Han, R. L. Gunshor, M.

Hovinen, and A. V. Nurmikko, Appl. Phys. Lett. **65**, 1331 (1994).

[15] L. H. Kuo, L. Salamanca-Riba, J. M. DePuydt, H. Cheng, and J. Qiu, Philosoph. Mag. **A69**, 301 (1994); L. H. Kuo, L. Salamanca-Riba, B. J. Wu, J. M. DePuydt, G. M. Haugen, S. Guha, and M. A. Haase, Appl. Phys. Lett. **65**, 1230 (1994); C. C. Chu, T. B. Ng, J. Han, G. C. Hua, R. L. Gunshor, E. Ho, E. L. Warlick, L. A. Kolodziejski, and A. V. Nurmikko, Appl. Phys. Lett. **69**, 602 (1996).

[16] P. Hohenberg and W. Kohn, Phys. Rev. **136**, B864 (1964).

[17] W. Kohn and J. L. Sham, Phys. Rev. **140**, A1133 (1965).

[18] W. E. Pickett, Comp. Phys. Rep. **9**, 115 (1989).

[19] S. Baroni, P. Giannozzi, and A. Testa, Phys. Rev. Lett. **58** , 1861 (1987).

[20] A. Zunger, S.-H. Wei, L. G. Ferreira, and J. E. Bernard, Phys. Rev. Lett. **65**, 353 (1990); S.-H. Wei, L. G. Ferreira, J. E. Bernard, and A. Zunger, Phys. Rev. B **42**, 9622 (1990); K. C. Hass, L. C. Davis, and A. Zunger, Phys. Rev. B **42**, 3757 (1990).

[21] R. Kikuchi, Phys. Rev. **81**, 988 (1951); J. A. Barker, Proc. R. Soc. London **216**, 45 (1953); T. Morita, J. Phys. Soc. Jpn. **12**, 753 (1957).

[22] R. O. Jones and O. Gunnarsson, Rev. Mod. Phys. **61**, 689 (1989).

[23] J. P. Perdew in *Electronic structure of solids '91*, edited by P. Ziesche and H. Eschrig (Akademie Verlag, Berlin, 1991); J. P. Perdew and Y. Wang, unpublished; A. D. Becke, Phys. Rev. A **33**, 3098 (1988); C. Lee, W. Yang, and R. G. Parr, Phys. Rev. B **37**, 785 (1988).

[24] C. Filippi, C. J. Umrigar, and M. Taut, J. Chem. Phys. **100**, 1290 (1994); C. J. Umrigar and X. Gonze, Phys. Rev. A **50**, 3827 (1994); C. J. Umrigar and X. Gonze, Proceedings

of the Conference on Concurrent Computing in the Physical Science 1993.

[25] A. Baldereschi, Phys. Rev. B **7**, 5212 (1973); D. J. Chadi and M. L. Cohen, Phys. Rev. B **8**, 5747 (1973); H. J. Monkhorst and J. P. Pack, Phys. Rev. B **13**, 5188 (1976).

[26] D. R. Hamann, M. Schlüter, and C. Chiang, Phys. Rev. Lett. **43**, 1494 (1979); G. B. Bachelet, D. R. Hamann, and M. Schlüter, Phys. Rev. B **26**, 4199 (1982).

[27] L. Kleinman and D. M. Bylander, Phys. Rev. Lett. **48**, 1425 (1982).

[28] X. Gonze, P. Käckell, and M. Scheffler, Phys. Rev. B **41**, 12264 (1990).

[29] L. Nordheim, Ann. Phys. (Leipzig) **9**, 607 (1931).

[30] P. Soven, Phys. Rev. **156**, 809 (1967); D. W. Taylor, *ibid.* **156**, 1017 (1967); U. Onodera and Y. Toyozawa, J. Phys. Soc. Jpn. **24**, 341 (1968); B. Velicky, S. Kirkpatrick, and H. Ehrenreich, Phys. Rev. **175**, 747 (1968).

[31] D. de Fontaine, in *Solid State Physics*, edited by H. Ehrenreich, F. Seitz, and D. Turnbull (Academic, New York, 1979), **34**, 73.

[32] J. W. D. Connolly and A. R. Williams, Phys. Rev. B **27**, 5169 (1983).

[33] L. G. Ferreira, S.-H. Wei, and A. Zunger, Phys. Rev. B **40**, 3197 (1989); S.-H. Wei, L. G. Ferreira, and A. Zunger, Phys. Rev. B **41**, 8240 (1990).

[34] S. Baroni, P. Giannozzi, and A. Testa, Phys. Rev. Lett. **59** , 2662 (1987).

[35] S. de Gironcoli, S. Baroni, and R. Resta, Phys. Rev. Lett. **62**, 2853 (1989), S. de Gironcoli, S. Baroni, and R. Resta, Ferroelectrics **111**, 19 (1990).

[36] P. Giannozzi and S. Baroni, J. Chem. Phys. **100**, 8537 (1994).

[37] P. Giannozzi, S. de Gironcoli, P. Pavone, and S. Baroni, Phys. Rev. B **43**, 7231 (1991).

[38] S. de Gironcoli, P. Giannozzi, and S. Baroni, Phys. Rev. Lett. **66**, 2116 (1991).

[39] N. Marzari, S. de Gironcoli, and S. Baroni, Phys. Rev. Lett. **72**, 4001 (1994).

[40] S. de Gironcoli, Ph. D. thesis; N. Marzari, graduation thesis.

[41] S. Baroni, S. de Gironcoli, and P. Giannozzi, Phys. Rev. Lett. **65**, 84 (1990).

[42] S. de Gironcoli, and S. Baroni, Phys. Rev. Lett. **69**, 1959 (1992).

[43] S. de Gironcoli, Phys. Rev. (RC) B **51**, 6773 (1995); C. Bungaro, S. de Gironcoli, and S. Baroni, Phys. Rev. Lett. **77**, 2491 (1996).

[44] M. Buongiorno Nardelli, P. Giannozzi, and S. Baroni, Phys. Rev. Lett. **69**, 1069 (1992); M. Buongiorno Nardelli, P. Giannozzi, and S. Baroni, Phys. Rev. B **51**, 8060 (1995); A.M. Saitta, D. Alfè, S. de Gironcoli, and S. Baroni, Phys. Rev. Lett. **78**, 4958 (1997).

[45] H. Hellmann, *Einführung in die Quantenchemie* (Deuticke, Leipzig, 1937); R. P. Feynman, Phys. Rev. **56**, 340 (1939).

[46] X. Gonze and J. P. Vigneron, Phys. Rev. B **39**, 13120 (1989); A. Debernardi and S. Baroni, Solid State Commun. **91**, 813 (1994); A. Dal Corso and F. Mauri, Phys. Rev. B **50**, 5756 (1994); A. Debernardi, S. Baroni, and E. Molinari, Phys. Rev. Lett. **75**, 1819 (1995).

[47] M. H. Cohen, J. Phys. Radium **23**, 643 (1962).

[48] H. Kanzaki, J. Phys. Chem. Solids **2**, 24 (1952); H. Kanzaki, J. Phys. Chem. Solids **2**, 107 (1952).

[49] R. M. Dreizler and E. K. U. Gross, *Density Functional Theory*, Springer, Berlin; J. P. Perdew and M. Levy, Phys. Rev. Lett. **51**, 1884 (1983); L. J. Sham and M. Schlüter,

Phys. Rev. Lett. **51**, 1888 (1983); L. J. Sham and M. Schlüter, Phys. Rev. B **32**, 3883 (1983).

[50] D. R. Hamann, Phys. Rev. Lett. **42**, 662 (1979).

[51] V. Fiorentini, Phys. Rev. B **46**, 2086 (1992); V. Fiorentini and A. Baldereschi, J. Phys.: Condens. Matter **4**, 5967 (1992).

[52] G. B. Bachelet and N. E. Christensen, Phys. Rev. B **31**, 879 (1985).

[53] M. S. Hybertsen and S. G. Louie, Phys. Rev. Lett. **55**, 1418 (1985); M. S. Hybertsen and S. G. Louie, Phys. Rev. B . **34**, 5390 (1986); R. W. Godby, M. Schlüter, and L. J. Sham, Phys. Rev. Lett. **56**, 2415 (1986); R. W. Godby, M. Schlüter, and L. J. Sham, Phys. Rev. B **35**, 4170 (1987); R. W. Godby, M. Schlüter, and L. J. Sham, Phys. Rev. B **36**, 6497 (1987); R. W. Godby, M. Schlüter, and L. J. Sham, Phys. Rev. B **37**, 10159 (1988); F. Gygi and A. Baldereschi, Phys. Rev. Lett. **62**, 2160 (1989).

[54] M. Rohlfing, P. Krüger, and J. Pollmann, Phys. Rev. Lett. **75**, 3489 (1995).

[55] D. H. Vanderbilt, Phys. Rev. B **41**, 7892 (1990).

[56] U. von Barth and R. Car, unpublished.

[57] A. Dal Corso, S. Baroni, R. Resta, and S. de Gironcoli, Phys. Rev. B **47**, 3588 (1993).

[58] S. G. Louie, S. Froyen, and M. L. Cohen, Phys. Rev. B **26**, 1738 (1982); G. E. Engel and R. J. Needs, Phys. Rev. B **41**, 7876 (1990); A. Qteish and R. J. Needs, Phys. Rev. B **43**, 4229 (1991).

[59] D.M. Ceperley, and B.J. Alder, Phys. Rev. Lett.**45**, 566 (1980).

[60] J. Perdew and A. Zunger, Phys. Rev. B **23**, 5048 (1981).

[61] F. D. Murnaghan, *Deformation of an elastic solid*, (John Wiley, New York 1951), chapt. 4.

[62] S.-G. Lee and K. J. Chang, Phys. Rev. B **52**, 1918 (1995); R. Pandey and A. Sutjianto, Solid State Commun. **91**, 270 (1994).

[63] J. Bergsma, Phys. Lett. **32A**, 324 (1970); L. A. Feldkamp, D. K. Steinman, N. Vagelatos, J. S. King, and G. Venkataraman, J. Phys. Chem. Solids, **32**, 1573 (1971).

[64] M. Cardona and G. Harbeke, Phys. Rev. A **137**, 1467 (1965); M. Balkanski and Y. Petroff, 7th Intern. Conf. on the Physics of Semiconductors, Dunod, Paris (1964); J. W. Baars, Proc. Int. Conf. II-VI Semiconducting Compounds, ed. by D. G. Thomas, W. A. Benjamin, New York (1967); C. J. Vesely and D. W. Langer, Phys. Rev. B **4**, 451 (1971).

[65] A. Ebina, M. Yamamoto, and T. Takahashi, Phys. Rev. B **6**, 3786 (1972); J. L. Freeouf, Phys. Rev. B **7**, 3810 (1973); D. Theis, Phys. Status Solidi B **79**, 125 (1977); D. E. Eastman, W. D. Grobman, J. L. Freeouf, and M. Erbudak, Phys. Rev. B **9**, 3473 (1974); L. Ley, R. A. Pollak, F. R. McFeely, S. P. Kowalczyk, and D. A. Shirley, Phys. Rev. B **9**, 600 (1974); A. Ebina, T. Unno, H. Suda, H. Koinuma, and T. Takahashi, J. Vac. Sci. Technol. **19**, 301 (1981).

[66] P. Bellon, J. Chevalier, E. Augarde, J. P. André, and G. P. Martin, J. Appl. Phys. **69**, 2388 (1989); T. A. Gant, M. Dutta, N. A. El-Masry, S. M. Bedair, and M. Stroscio, Phys. Rev. B **46**, 3834 (1992); T. S. Kuan, T. F. Kuech, W. I. Wang, and E. L. Wilkie, Phys. Rev. Lett. **54**, 201 (1985); C. Bocchi, P. Franzosi, and C. Ghezzi, J. Appl. Phys. **57**, 4533 (1985).

[67] A. D. Sokal, *Monte Carlo Methods in Statistical Mechanics: Foundations and New*

Algorithms, Cours de Troisième Cycle de la Physique an Suisse Romande, Lausanne (1989), pp. 19-20.

[68] L. Ozawa and Y. Nagashima, J. Electrochem. Soc. Jpn. **32**, 26 (1964); A. Scharmann, D. Schwabe, and D. Weyland, J. Lumin. **18/19**, 833 (1979).

[69] L. Vegard, Z. Phys **5**, 17 (1921).

[70] J. C. Mikkelsen Jr. and J. B. Boyce, Phys. Rev. B **28**, 7130 (1983); J. C. Woicik, C. E. Bouldin, M. I. Bell, J. O. Cross, D. T. Tweet, B. D. Swanson, T. M. Zhang, L. B. Sorensen, C. A. King, J. L. Hoyt, P. Pianetta, and J. F. Gibbons, Phys. Rev. B **43**, 2419 (1991); H. Kajiyama, S. Muramatsu, T. Shimada, and Y. Nishino, Phys. Rev. B **45**, 14005 (1992).

[71] G. B. Stringfellow, J. Cryst. Growth **27**, 21 (1974); *ibid.* **65**, 454 (1983).

[72] A. P. Sutton, *Electronic structure of materials*, (Oxford Science Publications, Oxford, 1993).

[73] L. G. Suslina, D. L. Fedorov, S. G. Konnikov, F. F. Kodzhespirow, A. A. Andreev, and E. G. Shariai, Fiz. Tekh. Poluprovodn. **11**, 1934 (1977)[Sov. Phys. Semicond. **11**, 1132 (1977)]; A. Ebina, E. Fukunaga, and T. Takahashi, Phys. Rev. B **10**, 2495 (1974); L. Soonckindt, D. Etienne, J. P. Marchand, and L. Lassabatere, Surf. Sci. **86**, 378 (1979); D. Etienne, M. de Murcia, and G. Bougnot, Thin Solid Film **70**, 285 (1980).

[74] R. Mach, P. Flogel, L. G. Suslina, A. G. Areshkin, J. Maege, and G. Voigt, Phys. Status Solidi B **109**, 607 (1982); A. A. El Shazly, M. M. H. El Naby, M. A. Kenawy, M. M. El Nahass, H. T. El Shair, and A. M. Ebrahim, Appl. Phys. A **36**, 51 (1985).

[75] W. A. Harrison, *Electronic structure and the properties of solids*, Dover Publishing, New York, (1989).

[76] A. V. Nurmikko and A. Ishibashi, in *II-VI Blue/Green Light Emitters: Device Physics and Epitaxial Growth*, ed. by R. L. Gunshor and A. V. Nurmikko, Semiconductor and Semimetals **44**, Academic Press, (1997), p. 234.